Enhancing the complexity of neural tissue engineering platforms for repair of neurological injury

Alan Peter Weightman

Thesis submitted for degree of Doctor of Philosophy

June 2015

Keele University

SUBMISSION OF THESIS FOR A RESEARCH DEGREE

Degree for which thesis being submitted: Doctor of Philosophy

Title of thesis: **Enhancing the complexity of neural tissue engineering platforms for repair of neurological injury**

This thesis contains confidential information and is subject to the protocol set down for the submission and examination of such a thesis? NO

Date of submission	02/04/2015
Original registration date	01/10/10
Name of candidate	Alan Peter Weightman
Research Institute	Institute for Science and Technology in Medicine
Name of Lead Supervisor	Prof. Divya Chari

I certify that:

(a) The thesis being submitted for examination is my own account of my own research

(b) My research has been conducted ethically. Where relevant a letter from the approving body confirming that ethical approval has been given has been bound in the thesis as an Annex

(c) The data and results presented are the genuine data and results actually obtained by me during the conduct of the research

(d) Where I have drawn on the work, ideas and results of others this has been appropriately acknowledged in the thesis

(e) Where any collaboration has taken place with one or more other researchers, I have included within an 'Acknowledgments' section in the thesis a clear statement of their contributions, in line with the relevant statement in the Code of Practice (see Note overleaf).

(f) The greater portion of the work described in the thesis has been undertaken subsequent to my registration for the higher degree for which I am submitting for examination

(g) Where part of the work described in the thesis has previously been incorporated in another thesis submitted by me for a higher degree (if any), this has been identified and acknowledged in the thesis

(h) The thesis submitted is within the required word limit as specified in the Regulations

Total words in submitted thesis (including text and footnotes, but excluding references and appendices) ……40,063

Signature of candidate ……Date ……

Abstract

The extent of regeneration is often limited after spinal cord injury (SCI), due to the post-injury microenvironment that is unsupportive of nerve fibre regeneration and the limited intrinsic reparative capacity of neurons. Current mainstream clinical therapies focus on reducing the extent of damage in the early stages of injury, rather than promoting regenerative mechanisms in sites of pathology. In this context, one promising biomedical engineering strategy emerging globally to promote repair following SCI is the reconstruction of neural circuitry in injury sites via the implantation of polymer scaffolds, or 'structural bridges.' To date, the development of such synthetic bridges has faced two major challenges: an overwhelming reliance on basic 2-D scaffolds functionalised with single cell types (which therefore fail to mimic the complex circuitry of the neural lesion environment); and heavy dependence on live animal models of neurological injury for functional screening and developmental testing, in the absence of *in vitro* injury models that mimic the complex pathological sequelae of neurological injury *in vivo*.

To this end, this thesis demonstrates an enhancement of the spatial and cellular complexity of both nanofibre-based scaffolds for spinal cord repair and *in vitro* SCI models for screening efficacious scaffold formulations. Nanofibre-hydrogel constructs containing aligned glial cell co-cultures (derived from primary sources) were successfully developed by systematically optimising the assembly protocol and construct design features. Further, protocols were developed to demonstrate the feasibility of increasing the number of constituent nanofibre layers in constructs with astrocyte mono-cultures, for further processing of constructs into an implantable form.

A safe and effective method of inducing complete transecting lesions in organotypic spinal cord slice cultures was developed following the production of a prototype double-bladed lesioning tool. The development of quantitative image-based assays of fluorescently labelled astrocyte, microglial and neuronal cell populations within slice lesion sites showed mimicry of multiple cardinal features of neurological injury *in vivo*. Finally, a method was developed to coat portable frames of aligned nanofibres with therapeutic biomolecules and incorporate frames into lesioned slices. Patterns of nanotopography induced outgrowth/alignment of astrocytes and neurons in the *in vitro* model were strikingly similar to that induced by comparable materials in related studies *in vivo*. This demonstrates the predictive utility of the model and the potential to reduce and refine the use of lower-throughput live animal models for screening applications.

Contents

List of tables and figures

Abbreviations

2-D	Two dimensional
3-D	Three dimensional
ASIA	American Spinal Injury Association
ANOVA	Analysis of variance
BDNF	Brain-derived neurotrophic factor
BBB	Basso, Beattie and Bresnahan
CNS	Central nervous system
CSPG	Chondroitin sulphate proteoglycan
ChABC	Chondroitinase ABC
DAPI	4', 6-diamidino-2-phenylindole
DRG	Dorsal root ganglion
DMEM	Dulbecco's modified Eagle's medium
DIV	Days *in vitro*
EBSS	Earle's balanced salt solution
ECM	Extracellular matrix
EGF	Epidermal growth factor
FDA	Food and Drug Administration
FITC	Fluorescein isothiocyanate
FTIR	Fourier transform infrared
GFAP	Glial fibrillary acidic protein
$GFAP^+$	GFAP-positive

IMS	Industrial methylated spirits
Lectin^{+}	Lectin-positive
MASCIS	Multicenter Animal Spinal Cord Injury Study
MBP	Myelin basic protein
MBP^{+}	Myelin basic protein-positive
NDS	Normal donkey serum
NT-3	Neurotrophin-3
OD	Optical density
OPC	Oligodendrocyte
P#	# post natal days
PBS	Phosphate buffered saline
PHEMA	Poly(2-hydroxyethyl methacrylate)
PFA	Paraformaldehyde
PLA	Poly-lactic acid
PLLA	Poly-L-lactic acid
PLGA	Poly-lactic-co-glycolic acid
PNS	Peripheral nervous system
PTFE	Polytetrafluoroethylene
rhNT-3	Recombinant human neurotrophin-3
RT	Room temperature
SANP	Self assembling nanofibre peptides
SCI	Spinal cord injury
S.E.M.	Standard error of the mean

SEM	Scanning electron microscopy
SWOT	Strengths weaknesses opportunities threats
TUJ-1^{+}	TUJ-1-positive

Acknowledgements

I would like to express my utmost gratitude to my supervisors Dr. Divya Chari and Dr. Ying Yang, for their expertise, insight and support in the completion of this thesis. Their guidance and training has been invaluable to me. In this regard, I also wish to thank Dr. Mark Pickard, who trained me in most of the techniques that I used and always made time for me. I also thank Dr. Stuart Jenkins and Dr. Ian Wimpenny, for teaching me how to prepare mixed glial cultures and perform electrospinning, respectively. Their knowledge helped me throughout my time in the laboratory. Thanks are also due to Karen Walker, for patently teaching me to use the field emission scanning electron microscope.

I would like to acknowledge the contributions of my advisor, Dr. Paul Roach, who conducted the Fourier transform infrared spectroscopic analysis and in general, provided useful insight whenever it was called upon.

I am grateful to Ian Wright Nigel Bowers, Ron Knapper and Chris Bain at Keele University School of Life Sciences, and Dave Bosworth, Zoe Bosworth and Debbie Adams at the animal facility, whom have facilitated my completion of the laboratory work for this project.

I would also like to thank the following people from the School of Life Sciences and the Guy Hilton research centre for their friendship and moral support: Dr. Amy Judd, Dr. Alinda Fernandes, Dr. James Edwards-Smallbone, Ashley Jordan, Munya Kamudzandu, Dr. Deepak Kumar, Dr. Sammy Wilson, Sandhya Moise, Mike Rotherham, Dr. Hareklea Markides, and Daniel Weinberg. Special thanks go to Jacki Tickle and Lady Síle Griffin for being thoughtful desk buddies and great craic. Extra special thanks go to my housemates Chris Adams, Rupert

Wright, James Everett, Natalie Fisher, Josh Price and Nipper, for much hilarity and debate.

I would like to thank everyone from the DTC in regenerative medicine, including students and past mini-project supervisors. I am grateful to the EPSRC for funding my research.

Finally, I thank my family for the endless support and encouragement they have given me. I dedicate this thesis to my grandfather, who passed away during its preparation.

Chapter 1: General introduction

1.1. An overview of spinal cord injury (SCI)

In the UK there are an estimated 40,000 individuals with traumatic SCI, with a prevalence of approximately 10-15 people per million in the population each year.[1] The economic burden of SCI in the UK is estimated to be over £500 million every year.[2] In addition to many detrimental effects that the injury has on patient quality of life, many years of patient care and medical treatment have profound socioeconomic consequences. The spinal cord and its spinal nerves are responsible for transmitting information between the brain and the body and therefore hold great functional importance because these pathways essentially enable animals to interact with the environment they are in. Furthermore, the inability of the adult central nervous system (CNS) to undergo significant functional repair following neurological injury (a trait common with all mammals) often results in paralysis of tissue below the injury site. Indeed, the most debilitating injuries are those that occur at the level of the neck, between the first and fourth cervical nerve, because they can result in the complete paralysis of the four limbs (quadriplegia). The initial damage to the spinal cord can arise from one or more mechanisms, including non-penetrating insults.[3] Current methods of treatment are limited in their ability to regenerate the spinal cord and hence, finding a cure is currently the subject of intensive biomedical research globally. In this context, results from the field of neural tissue engineering have shown promise in promoting regeneration across spinal cord lesions. However, the heavy use of *in vivo* SCI screening models that have significant drawbacks is necessitating the development of higher-throughput *in vitro* models of SCI. The above topics pertaining to spinal cord anatomy, injury pathology, modelling SCI and neural tissue engineering are discussed below.

1.1.1. Anatomy of the spinal cord

The nervous system is divided into the CNS, which consists of the brain and spinal cord, and the peripheral nervous system (PNS) that consists of the cranial nerves and the nerves that project between the spine and the body. CNS tissue can be divided into the grey matter, which consists of neural cell bodies, dendrites and synaptic contacts and white matter, which consists of ascending and descending nerve fibre tracts. With regards to the latter, these are commonly grouped according to their origin, course and projection (**Figure 1**). Promoting the regeneration of these essential tracts represents a major therapeutic goal in the restoration of motor and sensory function after SCI.

The spinal cord contains multiple cell populations that mediate highly specialised functions. The basic structural and functional unit of the nervous system is a neuron, which transmits electrical signals along its axon to neighbouring cells. The neuroglial cells are the other major cellular components of the CNS that act to support the function of neurons. Astrocytes have numerous roles crucial for the optimal function of the nervous system, which include the formation and control of the blood-brain barrier, the regulation of neuronal development, removal of neuronal waste and regulation of CNS pH.[4] Microglial cells constitute an immunocompetent cell population that essentially form the immune system of the CNS. In the mature CNS they may appear as resting, activated or phagocytotic microglia, depending on the surrounding environment.[5] Oligodendrocytes form the myelin sheath surrounding axons in the CNS and can myelinate as many as 30-50 separate axons.[6] They arise from oligodendrocyte precursor cells (OPCs) that populate the brain and spinal cord in waves during development,[7] with subpopulations remaining into adulthood for the migration and replacement of damaged oligodendrocytes in injury.[8] A myelin sheath

is a section of membrane wrapped spirally around the axon that extends out from the soma via thin projections. The myelin insulates the axons and markedly increases the propagation rate of action potentials by reducing the conductive surface area to small gaps that lie in between consecutive myelin sheaths (nodes of Ranvier).[9]

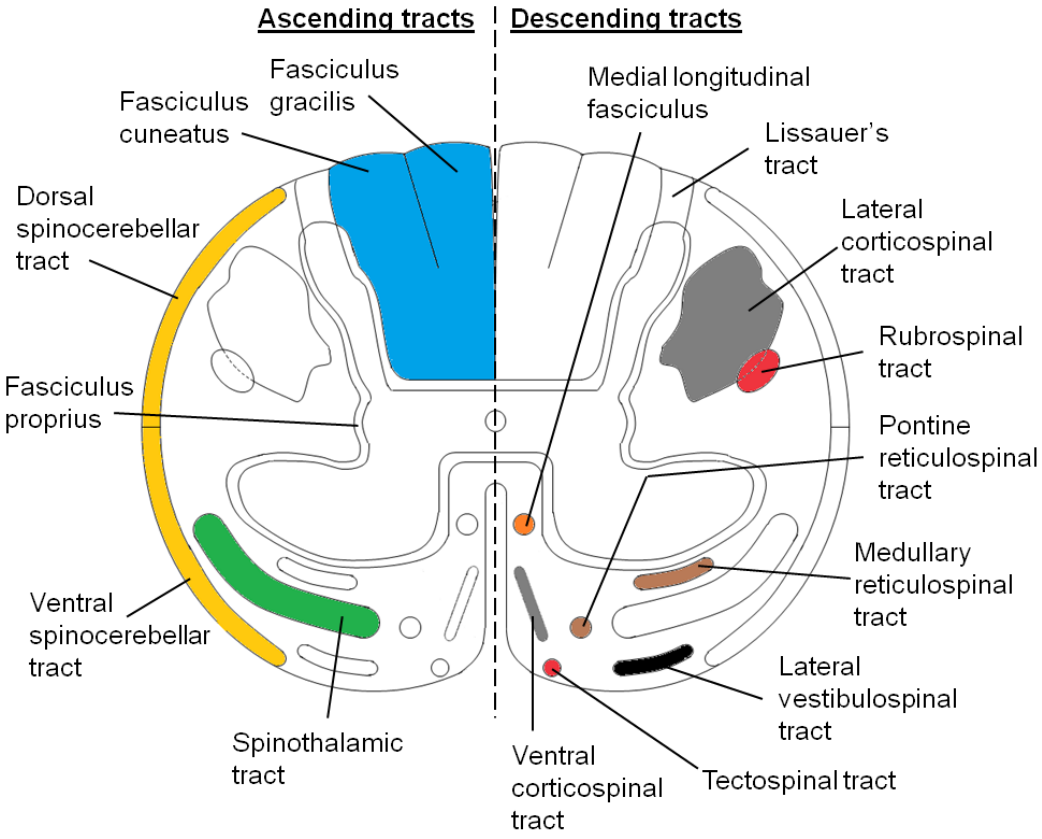

Figure 1. Ascending and descending pathways of the spinal cord essential for neurological function (adapted from Crossman & Neary, 2005).[10]

1.1.2. Pathology of SCI

SCIs can be characterised according to the type of injury and resultant damage caused. Possible mechanisms of injury include shear or compressive forces; dislocation; compression; fracture; and laceration.[11] These can be caused by extrinsic objects or bone fragments that penetrate the cord, haematoma formation, a local shock wave at the time of impact, or a combination of these.[3] The injuries that either completely or partially transect the spinal cord cause the greatest neurological damage, commonly resulting in loss of sensory or motor function (depending on the tracts affected) below the site of injury. However, compressive, non-penetrating injuries are more common and some level of neural function is preserved below the site of injury.[12] The acute injury occurs in the initial minutes to days after the initial impact.[13] The extent of damage that occurs during this period determines the severity of the pathological processes that develop in the following weeks to months, resulting in a chronic injury that can last for many years after the initial injury.

1.1.2.1. Acute injury

The extent of the initial structural damage inflicted during the initial mechanical insult is dependent on the particular mechanism, but can include the severing of axons, disruption to the vascular system (leading to wider-spread swelling and ischemia) and the necrosis of neurons and glia. As a result, the acutely traumatized spinal cord experiences: significant neurotoxicity from the excessive release of glutamate neurotransmitter and free radicals from cellular apoptosis; ionic fluxes; and alterations in blood flow, resulting in ischaemia.[3,14] The necrosis of oligodendrocytes releases myelin debris into the surrounding extracellular

environment, within which are several known inhibitors of nerve fibre growth, such as Nogo-A,[15] myelin-associated glycoprotein[16] and oligodendrocyte myelin glycoprotein.[17] Microglia are also activated following damage, resulting in rapid migration towards the lesion site.

1.1.2.2. Chronic injury

A range of pathophysiological changes occur at the injury site, which progresses in both rostral and caudal directions from the lesion epicentre over the following days to months, termed the secondary injury.[18] The chronic injury manifests as ischemia, micro-vascular damage, glutamatergic excitotoxicity, oxidative stress, and inflammation.[19] Cord swelling and a reduction in blood flow causes the apoptosis of oligodendrocytes and subsequent degeneration of axonal tracts due to a loss of trophic support.[20] Under the conditions of prolonged damage and cellular death in the lesion environment activated microglia further transform into phagocytotic microglia.[9] They have been shown to release pro-inflammatory cytokines such as tumour necrosis factor-α and infiltrate into lesion sites, where they are responsible for the breakdown and phagocytosis of cellular debris and toxic substances.[21,22] Their activation can be a significant barrier to the development of efficacious interventions as there is evidence implicating them as inhibitors of axonal regeneration via expression of inhibitory guidance molecules such as Netrin-1 and repulsive guidance molecules.[23,24] These environmental factors stimulate astrocytes surrounding the damaged, necrotic area to undergo a complex response called 'reactive astrogliosis.' This response is characterised by a hypertrophy and likely proliferation of the astrocytes immediately surrounding the damaged, necrotic area.

Reactive astrocytes upregulate expression of the astrocyte specific glial fibrillary acidic protein (GFAP) within and adjacent to lesions, to form a glial scar,[25] which constitutes a critical physical barrier to axonal regeneration.[26] The glial scar functions to 'seal' lesion sites and the blood-brain barrier, to protect the remaining functional tissue from injury mechanisms.[27] Reactive astrocytes and other neural cell types in the area of glial scarring also produce chondroitin sulphate proteoglycans (CSPG), such as neurocan and brevican,[28] which are potent inhibitors of neurite outgrowth and contribute to the establishment of an environment non-permissive to axonal growth.[29] The final manifestation of chronic injury is the formation of a fluid-filled cavity at the lesion site, a major obstacle for the regeneration of host tissue.[30]

1.1.3. Current treatments and challenges

There are two major pathological causes for a lack of axonal regeneration in the CNS; the limited intrinsic regeneration capability of the injured neurons *per se* and the non-permissive environment to axonal growth that surrounds the lesion.[31] However, when injured neurons are exposed to permissive signals, some have been shown to regenerate, although this regenerative capability differs between neuronal types,[32] the neuronal age[33] and distance from the site of injury.[34] Current repair strategies to treat SCI are centred on neural protection during the acute phase of SCI. They do not initiate regeneration *per se* but act to reduce the onset and extent of the secondary, more permanent damage as a result of glial scar formation. This strategy aims to preserve and optimise any neurological function remaining by maintaining axonal function and preventing apoptotic cell death. Repair strategies include: (i) the induction of systemic hypothermia in the patient to slow the onset of inflammation,

local oxidative stress and the metabolic rate;[14] (ii) drugs that either antagonise or breakdown inhibitory molecules to axonal regeneration e.g. Nogo-A inhibitors;[35] and (iii) therapies that deliver growth factors to the injury site.[36] Whilst these treatments have been reported to reduce the extent of injury in animal models and human studies,[14] significant improvements in axonal regeneration have thus far been elusive, highlighting the limited ability of current treatments to promote regeneration of the spinal cord. However, there is a general consensus that a more effective way of promoting repair and functional recovery is the use of multiple strategies within the same treatment to reverse multiple facets of the complex response to injury. In this regard, combinatorial strategies from the field of neural tissue engineering aim to simultaneously breakdown the glial scar and reverse the environment inhibitory to nerve fibre outgrowth, whilst supporting and guiding any regenerative events that occur from spared host tissue at the lesion margins. These strategies will be discussed later.

1.1.4. Models of SCI

The two main transection models available to study axonal regeneration (and thus transecting SCIs) are complete and partial transection.[11] Complete transection is regarded to be the better of the two as the injury is complete and does not introduce questions regarding the axonal regeneration of specific nerve fibre tracts that can differ in their regenerative potential. Partial transection models attempt selective injury of particular tracts and are widely used because animal care is easier post-surgery. Another advantage is that these lesioned tracts can be compared with the contralateral uninjured side, although it is harder to determine how complete the

transection is in severing all the nerve fibres of the tract and whether any functional improvement in the animal observed is because of compensatory mechanisms occurring from other functional systems.[19] Axonal regeneration is harder to verify anatomically in non-penetrating, contusion force models because of the incomplete nature of this injury. However, this type of SCI is more prevalent in the population and these models more accurately reflect the patho-physiology encountered. The most commonly used model is the New York University (or NYU) impacter that drops a 10g weight from various heights onto the exposed dorsal surface of the spinal cord and reproducibly creates spinal cord lesions.[37] Others, for example, look to more consistently evaluate the impact delivered[38] or simulate ongoing compression.[39,40]

Animal models are extremely important for studying SCI in the laboratory setting and as a testing platform, enable the development of experimental therapeutic strategies and facilitate their validation before use in humans. Live SCI models in animals are most commonly used because they represent a living system able to mimic the human body to a greater extent than more simplistic *in vitro* models. However, there are many associated drawbacks associated with their use including their cost and high associated animal usage for screening purposes. *In vitro* reductionist models such as microfluidic devices are useful for isolating specific aspects of the response to injury and examining regenerative processes in a higher-throughput screening system, [41,42] although in general they suffer from a lack of spatial and cellular complexity compared to *in vivo* injury models, which limits their predictive utility.

Alternatively, organotypic slice culture has been used to culture thin sections of animal brain and spinal cord tissue for many years[43] and its use in generating SCI

models has only recently been realised. Organotypic spinal cord slice cultures represent an *in vitro*, 3-D, multicellular model of tissue that can be maintained at the air-medium interface for several weeks. Numerous slices can be produced in the parasagittal plane from each spinal cord and they have been successfully lesioned to form a SCI model.[44] This model has the potential to reduce and refine the use of live animal SCI models for screening novel treatments that promote regeneration, in accordance with the 3 R's principle (reduction, refinement and replacement), because animal SCI models have a much lower throughput. The use of this 3-D, *in vitro* model alternative as a testing platform for the evaluation of promising strategies to enhance spinal cord repair may increase the throughput of initial therapeutic testing and ultimately help to develop better designed, more efficacious treatments. However, there have not been many published reports using this model to evaluate the efficacy of new therapies to promote spinal cord regeneration. Thus there remains an unexplored potential for translatable *in vitro* animal models of SCI that can model the injury in 3-D and provide a more rapid assessment of promising strategies for spinal cord repair, such as nanofabricated polymer scaffolds produced within the field of neural tissue engineering.

1.2. Principles of tissue engineering for spinal cord repair

Tissue engineering has been extensively described as '*an interdisciplinary field that applies the principles of engineering and life sciences towards the development of biological substitutes that restore, maintain, or improve tissue function or a whole organ*.'[45] Tissue engineering strategies attempt to support the development of new tissue, according to the structural, chemical and cellular

requirements of the injured tissue. One of the major focuses within the field is the production of scaffolds, which are implanted into injury sites to fill the lesion cavity. Scaffold design strategies in the context of spinal cord repair include: (i) extracellular matrix (ECM) mimicry, to facilitate the attachment and proliferation of cell populations within and/or into the scaffolds;[46] (ii) interactions with spared host tissue on a macro- and micro-cellular level to direct regeneration of nerve fascicles[47] and individual axons[48] across the injury site along their specific neuronal pathways; (iii) the incorporation of therapeutic cell populations e.g. neural stem cells[49] to repopulate the injury site and/or release growth factors at basal or enhanced levels (transfected cells) to stimulate axonal growth; and (iv) the incorporation of biomolecules e.g. chondroitinase ABC (ChABC), to make the environment more permissive to axonal outgrowth (**Figure 2**).[50] These strategies aim to promote regeneration of the tissue and restore lost function, in comparison with current treatments that aim primarily to reduce the onset of chronic injury, and will be discussed individually in the following sections.

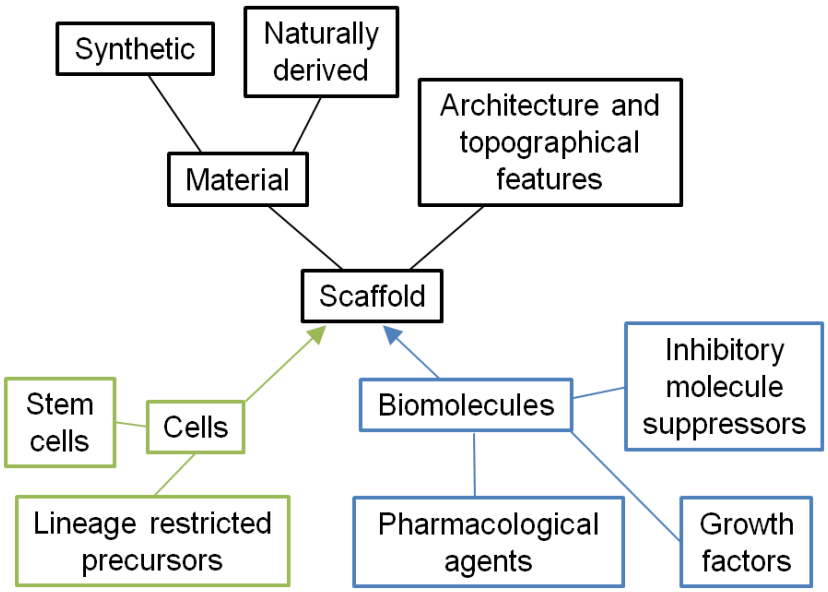

Figure 2. The strategic approaches to tissue repair that form the basis of tissue engineering. *Scaffolds can be implanted into injury sites in isolation, or together with various combinations of cells and/or biomolecules. Combinatorial strategies aim to address multiple aspects of injury pathology to maximise the reparative processes occurring at the injury site.*

1.3. Scaffolds for spinal cord repair

Tissue engineering strategies utilising scaffolds to form micro-environments for tissue regeneration present a promising alternative for future, more-efficacious treatment options for spinal cord repair. General scaffold design considerations include: (i) biodegradability to remove the requirements for further post-operative surgery; (ii) biocompatibility with the host (including non-toxic degradation products) to prevent an adverse immune response;[51] (iii) sufficient mechanical properties to withstand the mechanical loads applied in the injury site of the particular tissue (for the spinal cord a stabilising structure has been shown to

improve scaffold performance);[52] and (iv) adequate porosity to provide sufficient blood flow, neuronal attachment and outgrowth.[53]

1.3.1. Scaffold materials

The choice of material for the scaffold can have a large influence on the overall design, the combination of strategies utilised and the efficacy following introduction into relevant injury models. Many different polymers have been used to produce scaffolds, which may be grouped according to their natural or synthetic derivation. However, no material has emerged as a clear favourite. Overall, the main consideration is the extent that the scaffold mimics the ECM environment found *in vivo*, to maximise the interaction of the scaffold with injured host tissue.

Natural polymers represent a class of naturally occurring materials that are biocompatible. They include hyaluronic acid, agarose, alginate, gelatin, fibronectin, fibrin, chitosan and collagen.[54] The latter four are perhaps the most promising polymers for use in tissue engineered scaffolds for spinal cord repair, since they can support orientated axonal growth and sequester growth factors.[55] Type I collagen is one of the most common natural materials used,[56] due to its abundance in the ECM of connective tissues in animals and its natural fibre morphology.[57] Additionally its gellation at physiological temperatures allows it to be used as an injectable delivery device supporting cell attachment and release of bound growth factors upon implantation.[58] Hydrogels such as collagen and gelatin have been widely used to form the internal matrix of scaffolds, to help prevent their collapse following implantation and to mimic the ECM for improved neural cell attachment.[59] However, the hydrogels do not possess aligned topographical cues, unless the fibrils are

aligned prior to use,[60] and the adhesion of cells can be limited e.g. unmodified alginate scaffolds.[61] It has been recognised that the use of hydrogels in combination with another material (e.g. aligned nanofibres) to form a composite can overcome limitations inherent with using either material alone and produce scaffolds that mimic both the fibrous protein network and the ground substance of the ECM.[62]

Synthetic polymers are generally cheaper to produce than natural polymers and in general use more controlled and reproducible synthesis techniques.[59] However, a considerable subset are non-degradable so there is an ongoing risk of inflammation, scaffold displacement and nerve compression, which may necessitate additional surgery for scaffold removal.[63] Poly(2-hydroxyethyl methacrylate) (or PHEMA) is an example of a more commonly used non-degradable synthetic material, due to tuneable mechanical properties, cell permeability and synthesis without the use of solvents, facilitating the incorporation of bioactive compounds into the scaffold.[64] However, possible toxicity, mechanical issues and relatively simple scaffold designs have limited its potential use for SCI.[63] Aliphatic polyesters represent a class of biocompatible synthetic materials, which are food and drug administration (FDA) approved and produce endogenous metabolic degradation products that can be readily resorbed.[65] The aliphatic polyesters consist of lactide, caprolactone and glycolide monomers or there combinations e.g. poly-lactic acid (PLA) and poly-lactic-co-glycolic acid (PLGA).[56] However, they are often hydrophobic and non-adhesive to cells, thus failing to mimic the ECM. As a result they are often combined with natural materials e.g. peptides to produce biosynthetic scaffolds that display better cellular attachment than the synthetic polymer alone e.g. polycaprolactone with chitosan,[66] gelatin[67] or collagen.[68] A common technique is to immobilise a cell adhesive peptide (GRGDY) onto the surface of the scaffold.[69] The results showed

that the modified nanofibre scaffolds were a preferable environment for cellular attachment, proliferation, and differentiation, compared to unmodified control scaffolds.

1.3.2. Scaffold architecture

Scaffolds have been fabricated to give a number of various structural features, ranging from simple injectable hydrogels to arrays of fibres fabricated at the nanoscale. They can have an entirely random orientated structure or are constructed with an aligned configuration at either the macro- or microscale. Termed 'contact-guidance', scaffolds with aligned features are able to guide attached outgrowing neurons along features on the surface e.g. microgrooves, or along the surface itself e.g. micro- or nanofabricated fibres, or a combination of both.[70] The topographical cues may be presented to the host tissue at two different scales, representing different strategies for repair.

The macro-structure of the spinal cord refers to the organisation of the spinal cord and the nerve fibre tracts that run in both rostral and caudal directions with diameters of between 100-1000 μm. Scaffolds with multiple aligned channels reflecting this organisation have been created to optimise the regeneration of axons in their fascicular groups.[47,71,72] The channel diameter appears to affect the number of regenerating axons in scaffolds when implanted with Schwann cells into transected rat spinal cords, as smaller channel diameters of approximately 450μm promoted greater regeneration than larger diameter channels.[73]

Larger axons have a diameter of between 15-20μm,[55] so micro-engineered scaffolds e.g. fibrous scaffolds try to promote more specific outgrowth at the cellular level towards the corresponding separated fascicular bundles. Overall, the total cross-sectional area of the topographical cues is the most important determinant for the extent of host cellular attachment to the scaffold and the potential of the scaffold to direct tissue regeneration by contact-guidance. Various scaffolds have been produced that incorporate this aligned topography,[59] but nanofibrous scaffolds produced by electrospinning have arguably produced the most promising to date.

1.3.3. Cell sources for spinal cord transplantation

One hallmark of SCI is a disruption to the intricate supporting circuitry of glial cells in the lesion site, which are necessary for the function and integration of spontaneously regenerating nerve fibres with host neuronal networks.[74] One strategy for repair is the replacement of the injured/dying cells in the injury site with immature populations of glial cells, to replace those lost and to create a pro-regenerative niche in the normally inhibitory environment to axonal outgrowth.[28,75] There are many candidate transplant cell types identified to-date as cell sources for spinal cord repair.

Stem cells are characterised by two key features: their ability to self-renew and their ability to generate a wide range of progeny (i.e. multipotentiality).[76] They can be obtained from embryonic, foetal, or adult tissue. Embryonic stem cells have great potential as a cell source. The first cellular regenerative therapy to undergo clinical trials was the human ESC-derived oligodendrocyte progenitor, named GRNOPC1 (developed by Geron).[77] In general however, the current challenges of differentiating

them to more specific progenitor and primary cell types with a high degree of efficiency make other cell types more attractive for current tissue engineering applications. Other stem or progenitor cells that are relatively more lineage-restricted may be more translatable into clinical therapies in the short term. For example, neural stem cells (NSC),[78] Wharton's Jelly-derived, human umbilical mesenchymal stem cells,[79] olfactory ensheathing cells[80] and Schwann cells[81] have shown positive results following testing in live animal models of SCI. Furthermore, they have both been shown to express therapeutic concentrations of growth factors which may stimulate nerve fibre outgrowth.[79,82,83]

1.3.4. Biomolecule delivery

Growth factors are polypeptide signalling molecules synthesised by cells. These signals can induce growth, proliferation and differentiation, both positively and negatively in the cells that they act upon, thus guiding cellular growth and development. They have the potential to augment the regenerative capacity of CNS neurons through the stimulation of many regeneration-associated genes (RAGs), whose expression profiles are either upregulated or constitutively active during development and regeneration.[19] Many growth factors have been discovered thus far, but only a few of the main growth factors for the specific tissue to be repaired have been incorporated into scaffolds, with an uncertainty over their multiple (therefore unwanted) effects on different tissues.[84] Growth factors that promote neuronal survival, axonal growth and remyelination are most important for SCI. These include nerve growth factor, brain-derived neurotrophic factor (BDNF), glial cell line-

derived neurotrophic factor, neurotrophic factor-3 and -4 (NT-3 and -4); and basic fibroblast growth factor.[85]

A further strategy exists to suppress the activity of molecules inhibitory to nerve fibre growth found in the environment of the lesion site. For example, CSPGs are intensely upregulated following SCI and associated with the ECM of the neuroglial scar.[86] The bacterial enzyme ChABC is able to break the glycosaminoglycan chains from the core of the protein, attenuating its inhibition of axonal growth.[87] Furthermore, the administration of ChABC in a rat SCI model was found to promote regeneration and functional repair, including the recovery of locomotor and proprioceptive function. An additional example of a molecule inhibitory to axonal regeneration is Nogo-A,[35] a constituent of CNS myelin that has been shown to activate the Rho intracellular signalling pathway.[88] Anti-Nogo antibodies have been tested in rat[89] and primate[90] models of SCI following intrathecal application. Results showed an increase in the sprouting of axons into lesion sites and improvements in behavioural tests. Further, Novartis have recently conducted a human clinical trial to assess the safety and pharmacokinetics of the antibody in patients, demonstrating the interest surrounding this strategy to promote regeneration (ClinicalTrials.gov identifier: NCT00406016). A further strategy is to use antagonists or pharmacological agents that specifically target the Rho signalling pathway, which regulates axonal growth and cellular apoptosis following activation by multiple inhibitory components of CNS myelin.[91,92] Preclinical findings from transecting SCI models in mice show improved behavioural recovery following treatment[93] and phase II clinical trials have shown no major adverse effects, with some improvements to the American spinal injury association (or ASIA) scores in a quarter of patients (ClinicalTrials.gov identifier: NCT00500812).

1.4. Current scaffold design strategies for spinal cord repair

An assessment of different scaffold design strategies reported in the literature is given below, in the context of scaffold complexity, combination with multiple treatment strategies and the potential of nanofibre-based scaffolds to direct the regeneration of neural tissue.

1.4.1. Channelled scaffolds

Multiple or single channelled scaffolds represent a relatively basic scaffold design, capable of guiding axonal growth in fascicles or at a more macro scale. Studies have shown them to promote contact-guidance of axonal regeneration, although a combinatorial approach has improved regeneration above what would otherwise be possible. For example, Silva, *et al.* (2010) report the fabrication of single channelled, tubular structured scaffolds produced by rapid prototyping followed by post-processing thermal treatment.[94] Rapid prototyping represents a highly reproducible fabrication technique permitting the precise control of the 3-D architecture of the scaffold. The produced scaffolds were 2-3 mm in diameter and consisted of a starch/PCL blend, containing encapsulated human oligodendrocyte cell line MO3-13 within a gellan gum hydrogel in the central space. They were shown to elicit minimal inflammation and integrate well within a rat hemisection SCI model. Further characterisation of this scaffold is needed *in vivo* with regards to axonal regeneration and the incorporation of inhibitory molecule suppressors and/or growth factors may improve scaffold efficacy further. The major disadvantage to this

scaffold design is the level of guidance possible on a local cellular level due to the limited surface area of the aligned channels available for the contact-guidance of spared host tissue.

More promising multiple channelled scaffolds have been produced, incorporating a combinatorial approach into their design. Templated agarose scaffolds were produced with multiple channels at a diameter of 200μm each.[95] The axons of the ascending dorsal column sensory pathways in rat models were transected at the C4 level and the extent of regeneration was assessed following a combination of: (i) scaffold implantation; (ii) delivery of bone marrow stromal cells within scaffolds transfected with NT-3; (iii) lentiviral vectors expressing NT-3 injected at sites adjacent to the lesion; and (iv) the compression of the sciatic nerve to induce a growth state in the injured neuron. Animals with all four treatments continued to grow 83% (±13%) of their axons along the full length of the lesion (greater than 2 mm) to distal scaffold areas. Unfortunately axonal growth into the opposite side of the lesion was prevented by the formation of a reactive cell layer. A different PLGA polymer scaffold with seven parallel channels has been fabricated by injection moulding-solvent evaporation.[96] Seven wires (508 or 660 μm in diameter) were uniformly spaced as an array inside a mold with 3 mm internal diameter. A PLGA polymer solution was injected into the mold to fill the empty space and subsequently vacuum-dried for at least 24 hours to remove solvent from the polymer solution. Finally the wires were removed, leaving a porous multiple channelled scaffold. Schwann cells were loaded into the channels and the scaffolds transplanted into completely transected rat spinal cords at the T9 level. ‘Fast Blue’ fluorescent dye was used to trace the source of regenerating axons and they were found to have regenerated through the scaffold and up to 14 mm into the distal cord.

Scaffolds with smaller channel diameters have been produced that focus on the outgrowth of single/multiple axons in a spatially orientated manner.[97] In this study the scaffold was fabricated from alginate and the capillary channels formed by copper nitrate addition, creating multiple parallel channels with an average diameter of 27 μm. Produced scaffolds were initially screened to analyse the effect of scaffold coating with laminin, collagen, poly-L-ornithine and fibronectin ECM components on the linearly orientated regrowth of axons in completely transected entorhino-hippocampal organotypic slice cultures. The *in vitro* study showed that there was no improvement with coated scaffolds and thus proved to be a valuable tool for initial scaffold screening and avoiding unnecessary animal experimentation. The most promising scaffold was subsequently transplanted into a rat dorsal column transection model with NSCs to assess the capacity of the scaffold to support a population of viable cells. The scaffold was shown to possess more regenerative capacity with the NSCs and mediated the guidance of axons. Scaffolds with these smaller, much more numerous channels may offer a better solution to directed axonal outgrowth than macro-scale channel scaffolds but more combinatorial strategies are required to validate this hypothesis.

Finally, PLGA scaffolds have been produced incorporating both multiple channels and significant porosity by injection moulding, thermally induced phase separation and particulate leaching.[98] Scaffolds were transplanted into completely transected rat thoracic spinal cords either in isolation or with a dose of recombinant human neurotrophin-3 (rhNT-3) applied dorsally to the scaffold. The high porosity and channel interconnectivity facilitates the entry of neurotrophin-3 and the drainage of waste from the scaffold, which is more limited in the multichannel scaffolds listed above that do not contain such porosity. The animals displayed a significant

functional improvement when administered with the scaffold and rhNT-3, supporting this hypothesis.

1.4.2. Porous scaffolds

Porous scaffolds have been produced with less uniaxial directionality than channelled scaffolds, but the results have been promising due to a more diverse set of combinatorial approaches employed. Highly porous PLGA scaffolds mimicking the structure of the spinal cord have been fabricated using a thermal-induced phase separation technique.[99] The central portion of the scaffolds (representing grey matter) were seeded with either NSCs or NSCs and Schwann cells and the outer part of the scaffolds consisted of orientated pores for axonal growth (representing white matter tracts). The scaffolds were transplanted into a 3 mm gap in the right hemicord of rats, with the scaffolds incorporating both cell types showing greater axonal regeneration and functional improvement than acellular scaffolds or those with just one cell type. Hyaluronic acid hydrogels[100] with pore sizes of 100 μm were constructed incorporating poly-L-lysine to permit the attachment of cells and antagonists to the Nogo-66-receptor to help lessen glial scar formation. This receptor becomes activated upon binding to myelin-derived molecules that inhibit axonal regeneration, such as Nogo-A, myelin associated glycoprotein and oligodendrocyte myelin glycoprotein.[101] Results from scaffolds implanted into rats after lateral hemisection found that there were more cells and myelinated axons in scaffolds with the antagonists than in those without.

Overall, the channelled and porous scaffolds produced thus far were generally more successful in permitting axonal regeneration and functional recovery

when they were administered with growth factors, molecular antagonists and cells, supporting the theory that more complex scaffolds simultaneously utilising a combination of strategies can address multiple facets of the injury response. While results have been promising, the designs of the scaffolds mentioned above do not fully exploit the benefits offered by fibrous scaffolds, including a higher surface area to volume ratio for increased cellular attachment and contact-guidance of regenerating axons.

1.4.3. Fibrous Scaffolds

Overall, scaffolds with a fibrous topography possess greater mimicry of spinal cord cellular architecture. Fibrous scaffolds with a fibre diameter at the micrometer scale have been published, composed of linearly ordered collagen fibres bundled together. [102] The fibre diameters were less than 200µm. BDNF was fused with a collagen binding domain and bound to the collagen fibres, as well as covalently cross-linked epidermal growth factor (EGF) receptor neutralising antibody. The EGF receptor has been identified as a downstream target of the molecules inhibitory to axonal regeneration (mentioned above).[103] This scaffold was inserted into 6 mm complete transecting lesions in rat models and was shown to bridge the cavity, promote axonal outgrowth into the scaffold, significantly neutralise the growth inhibitors present at the injury sites and show signs of functional improvement in animals.

Poly-L-lactic acid (PLLA) nano- and microfibres were both produced by electrospinning with a high degree of alignment and their ability to induce contact-guidance and differentiation in NSCs *in vitro* was evaluated.[104] Their results show

that NSC elongation and neurite outgrowth both occurred, parallel to the direction of nanofibre scaffold alignment, and that NSC differentiation occurred at faster rates for the nanofibres compared with microfibres. This was the first published evidence for the important role that the nanofibre scaffolds can play to promote the contact guidance of neural cell populations and justifies their subsequent use in neural tissue engineering for spinal cord repair. Nanoscale fibres more strongly mimic the ECM and thus can control the sub-cellular processes, such as differentiation, to a greater degree.[105]

Nanofibrous scaffolds can be produced by template synthesis, drawing, self-assembly or phase-separation.[56] The disadvantages of these production techniques include: discontinuous fibre production and therefore unsuitability for large scale production;[106] the use of viscoelastic materials and inconsistencies in the fibres formed;[107] slow reaction rates and difficult larger scale production;[108] and more complicated, time-consuming production than electrospinning,[109] respectively. Electrospinning is an inexpensive, fast, relatively easy, larger scale production method for the collection of highly aligned and randomly orientated nanofibres as small as 3 nm in diameter.[110] The principle is simple but the optimisation and control of many processing parameters is required for accurate and reproducible fibre fabrication. Through the subsequent manipulation of various setup parameters and conditions, including grounded collector design, many aligned fibrous structures may be formed with varying arrangements, fibre diameters and densities.[111] More common published collector set-ups for aligned nanofibre fabrication include a rotating drum,[112] parallel electrodes,[113] rotating wire drum[114] and rotating tube collector with knife-edged electrodes underneath.[115] However, difficulties exist in post-collection processing for the 3-D scale-up of nanofibre scaffolds that permit

significant cellular infiltration following implantation *in vivo*.[116] Furthermore, the number of studies published testing nanofibre scaffolds as the principle topographical cue across the cross-sectional area is limited, given the potential of the strategy to direct cellular growth *in vitro*.[104,117] These *in vivo* studies also use scaffolds that are relatively simple in spatial design and cellular complexity.

1.5. Aims and objectives of the project

In the preceding sections I have attempted to highlight the benefits of a range of tissue engineering strategies for the repair of SCI. This thesis aims to address three specific issues that I have identified in preceding sections.

Clinically relevant live animal injury models show the potential of implanted nanofibre scaffolds to promote regeneration of the injured spinal cord, in contrast to the majority of current treatment strategies that rely on minimising early damage post-injury. The capacity to maximally exploit the benefits of such scaffolds requires a few major issues to be addressed.

The first aim of this thesis is to address the lack of spatial and glial cell complexity in implantable constructs reported so far using aligned nanofibre scaffolds, with a view to more efficient and neuromimetic constructs for CNS repair. This will be addressed by developing a methodology to fabricate nanofibre-collagen hydrogel composites, for the co-culture and alignment of multiple neuroglial cell populations. A method of scaling-up the number of constituent nanofibre layers will be developed, to aid the production of more complex bridges that facilitate the infiltration of host tissue and transplanted cells throughout the depth of the structure.

The second aim is to develop and optimise a more complex model of SCI *in vitro* (compared with systems currently available to the neural tissue engineering community) based on the use of organotypic cultures of spinal cord tissue. The mimicry of multiple cardinal features of injury *in vivo* will be assessed by developing quantitative image-based assays of fluorescently labelled cell populations in the slice lesions.

Finally, a method to safely deliver frames of aligned nanofibres into lesioned spinal cord slice cultures will be developed, in order to test the utility of the slice injury paradigm for screening efficacious, pro-regenerative neural tissue engineering strategies, towards the reduction and refinement of live animal experimentation (according to the 3'Rs principles) for SCI research.

More detailed descriptions of the chapter objectives follow:

Chapter 2: Alignment of multiple glial cell populations in 3D nanofibre scaffolds - toward the development of multicellular implantable scaffolds for repair of neural injury

This chapter will follow the development and optimisation of methodologies to assemble nanofibre-hydrogel constructs with increased spatial and cellular complexity. The compatibility of nanofibre-hydrogel constructs to support the growth, alignment and elongation of neural cells will be assessed with primary astrocyte and OPCs, in isolation and in co-culture. The feasibility of increasing the cellular complexity of constructs further with populations of seeded microglial cells will be assessed. The ability to scale-up the number of constituent nanofibre layers

for the culture and alignment of glial cells in a 3-D construct will be tested with astrocyte mono-cultures.

Chapter 3: Development of a complex 3-D *in vitro* model of SCI

This chapter will follow the development and optimisation of methodologies to produce a 3-D, multicellular model of SCI *in vitro* based on organotypic cultures of neonatal mouse spinal cord tissue. A method will be developed to induce lesions of a range of sizes that completely transect the spinal cord and the reproducibility of the lesion size quantified. Analyses will be developed to quantify the pathological events within lesion sites and characterise the mimicry of the cardinal features of injury *in vivo* within the slice injury paradigm. Re-useable slice culture inserts that permit the culture and lesioning of slices will be developed and tested in comparison with the commercial, gold-standard slice culture insert and an existing alternative insert, towards lowering the cost of generating the injury model for screening applications.

Chapter 4: Evaluating the screening utility of an *in vitro* model of SCI for nanofibre-based repair strategies

This chapter will assess the potential of using the lesioned organotypic spinal cord slice culture model as a prototype screening system for nanofibre scaffolds ± coating with relevant biomolecules, intended to promote spinal cord regenerative processes post-injury. A method to incorporate frames of aligned nanofibres across lesion sites will be developed and tested. Finally, the potential of the implanted constructs to enhance regenerative processes will be evaluated.

A chapter dedicated to ‘Materials and Methods’ has been omitted from this thesis, as a significant proportion of the work pertains to the development of protocols, tools and methods of analysis. I believe that the current layout should improve the flow and make clear which protocols were developed/adapted, within each respective experimental chapter.

Chapter 2: Alignment of multiple glial cell populations in 3-D nanofibre scaffolds - toward the development of multicellular implantable scaffolds for repair of neural injury

2.1. Introduction

As discussed in section 1.4, combinatorial repair strategies utilising structural bridges have the potential to reverse the multifaceted pathology of SCI.[95,118,119] Briefly, the scaffold supports the regeneration of spared host tissue following implantation.[120,121] The addition of cells and biomolecules into the scaffold, as part of a combinatorial repair strategy, can promote repair mechanisms, reverse the growth-inhibitory environment of the lesion site and support the function of regenerating tissue.[51,54,59,122] Nanofibres fabricated by electrospinning have emerged as a favourable scaffold for tissue engineering because they have a large surface area to volume ratio for the attachment of cells[123] and can be collected as assemblies of varying designs and structures, including a highly aligned configuration.[46,124] Scaffolds fabricated with aligned topographical cues are considered more efficient at directing tissue regeneration, which is particularly relevant for the reconstruction of the intricate cytoarchitecture of spinal cord tissue.[54,125] Studies *in vitro* have highlighted the strong influence of aligned nanofibre scaffolds on the morphology of astrocytes and the distance of nerve fibre outgrowth from dorsal root ganglion (DRG) explants (as a model for PNS nerve fibre outgrowth), via contact-guidance.[60,68,111,117,126–128] Furthermore, preliminary studies assessing the feasibility of nanofibre bridge implantation within animal SCI models have corroborated the potential to enhance repair (**Table 1**). However, in general, these studies have been sparse and the constructs assembled were relatively simple, highlighting the technical challenges that have been associated with the scale-up of nanofibre-based scaffolds for therapeutic testing *in vivo*.

Table 1. Summary of constructs containing aligned nanofibres implanted into models of SCI *in vivo*			
Construct features	**Model of Rat SCI**	**Overall performance**	**Ref**
Multiple tubes (10-13 per spinal cord; diameter 360 µm) of aligned nanofibres (tube wall thickness 90 µm) filled with self assembling nanofibre peptides (SANPs) ± (BDNF + ciliary neurotrophic factor + vascular endothelial growth factor + ChABC).	Contusion via Multicenter Animal Spinal Cord Injury Study (MASCIS) impacter. Chronic injury model.	Significant anatomical, histological and neuronal regeneration and functional recovery seen in the channels with added biomolecules (greater than any other report using constructs that contained aligned nanofibres).	129
One half-cylinder per spinal cord (length 4 mm). Consisted of two layers: an inner mesh of aligned nanofibres (100 µm thick) and an outer mesh of random nanofibres (500 µm thick) ± rolipram.	Hemisection	Nerve fibre outgrowth mainly on the aligned nanofibre layer. Also a reduction in GFAP and CSPG staining intensity and significantly increased Basso, Beattie and Bresnahan (BBB) scores from animals implanted with constructs containing rolipram.	130
Aligned collagen nanofibres rolled into a spiral tubular structure (2.5 x 2 mm).	Hemisection	Significant cell penetration and infiltration into constructs. Absence of neuroglial scarring. Scaffolds supported nerve fibre sprouting.	126

A tubular scaffold (4 x 2 mm) containing a central nanofibre bundle (<100 µm diameter) embedded in a laminin-hyaluronic acid gel (± human nasal olfactory mucosa or embryonic spinal cord cells).	Complete transection	Partial recovery of function three months following lesion induction. Some evidence of axonal outgrowth and re-myelination.	[131]
Rolled nanofibres.	Hemisection	Integration of scaffolds with host tissue evidenced by the in-growth of connective tissue, blood vessels, Schwann cells and neural cell processes.	[132]

2.1.1. Controlling nanofibre density

Conventionally, aligned nanofibres are collected during electrospinning onto a 2-D substrate, such as glass coverslips or aluminium foil, attached to a rotating mandrel collector. The relatively short duration of each unit operation produces nanofibre meshes that typically contain supracellular pore sizes for the infiltration of cells seeded on the scaffold surface. Further manipulation of the nanofibre mesh is required after collection for the production of implantable scaffolds, so in this context, to-date the duration of each unit operation has been increased to fabricate a free-standing scaffold with superior stability.[133] With most collector designs an increase in the duration of each unit operation to increase the thickness of the fibre mesh collected usually decreases the local attraction of the spinning polymer for the collector, thus reducing the aligned configuration. Furthermore, collecting more nanofibres concurrently increases the packing density of the mesh (the fraction of the

mesh volume occupied by nanofibres), resulting in significantly smaller pore sizes that restrict cellular growth to the outermost layer of nanofibres: essentially a roughened 2-D surface.[111,116,133–135] This limitation is apparent from the designs of the scaffolds tested in live animal models of SCI (**Table 1**), which contain a sub-optimal contribution from the nanofibre component across the diameter. The nanofibre meshes were produced with a high packing density and typically rolled into tubes (**Figure 1A**), or a spiral structure (**Figure 1B**) containing less than ten layers across the diameter of the scaffold. By comparison, if the number of mesh layers was increased there would be a greater number of surfaces for the attachment of cells from spared host tissue (**Figure 1C**). However, without reducing the nanofibre mesh packing density, there would also be a greater impenetrable cross-sectional area. This suggests that the capability of aligned nanofibres as a strategy to direct outgrowth of spared host tissue has not been adequately assessed in the literature. In comparison, Gelain, *et al.* (2011) reduced the diameter of each scaffold and implanted between 10-13 into the lesion cavity of each spinal cord (**Figure 1D**), which is a simple method of enhancing the surface area of the aligned component of the repair strategy.[129] Furthermore, in this particular study, the central space within the tube of nanofibres was filled with SANPs, therefore substantially increasing the cross-sectional area of the aligned scaffold topography available for contact with spared host tissue. This may partly explain why extent of repair observed for this scaffold design was superior compared to all others reported. Furthermore, it shows the potential of a scaffold containing nanoscale topographical cues throughout the diameter to direct tissue regeneration and repair.

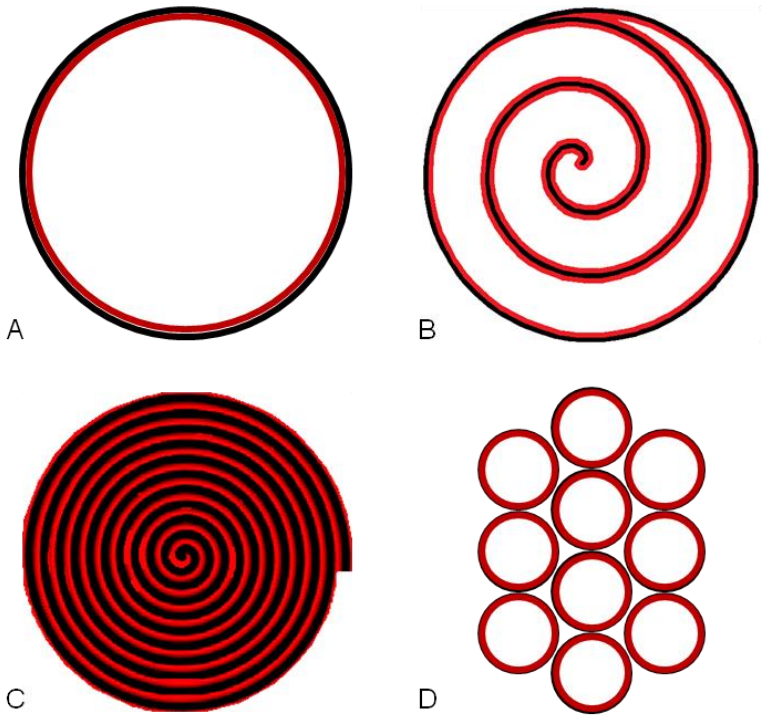

Figure 1. Schematic diagrams of cross-sections through the designs of current 3-D scaffolds containing aligned nanofibres with supracellular pore sizes, highlighting the current limitations in the area available for interaction with spared host tissue. *(A) A tubular structure represents the simplest scaffold design that requires the least manipulation following nanofibre (black) fabrication. At a nanofibre packing density with supracellular pore sizes there is also minimal surface area for contact-guidance of cells (red). (B) A spiral tubular structure is a more common used processing technique to increase the number of surfaces for cellular interaction across the scaffold diameter. (C) Rolling the nanofibre mesh further, enhances the number of surfaces for interaction. However, the impenetrable cross-sectional area will also accumulate unless the pore sizes are concurrently increased to permit cellular infiltration within each mesh layer. (D) Using multiple, smaller scaffolds within the same lesion volume is a simple method of increasing the number of surfaces available for cellular interaction without the use of more complex processing methodologies.*

2.1.2. Reconstructing the circuitry of supporting glial cells

A promising strategy to enhance regeneration is to reconstruct neuroglial cell circuitry in lesion sites via the implantation of constructs containing multiple populations of supporting neuroglia (viz. astrocytes, cells of the oligodendroglial lineage and microglia). These cells have important and diverse roles that maintain an optimal environment for neurological function (section 1.1.1). Furthermore, these cells play vital roles in regeneration following injury. Astrocytes are involved in synaptogenesis, which is necessary for the reconnection of regenerating nerve fibres with host neuronal circuitry.[136,137] Oligodendrocytes are responsible for the genesis of the insulating myelin sheath around regenerating nerve fibres, providing trophic support and conferring a faster rate of action potential conduction.[6] Microglia, the immune-competent cells of the CNS, infiltrate into lesion sites, where they are responsible for the breakdown and phagocytosis of cellular debris and toxic substances that are inhibitory to the outgrowth of nerve fibres.[21,22] Thus, the incorporation of organised glial circuits into lesion sites could provide a pro-regenerative niche for the outgrowth of nerve fibres with the ability to support the function of nerve fibres within the scaffold. Additionally, *in vitro* studies have demonstrated that a bed layer of pre-aligned astrocytes enhances the distance of nerve fibre outgrowth from co-cultured DRG explants.[60,138–140]

Despite the potential of this strategy to promote regeneration and support the function of nerve fibres within the scaffold, there are two principle explanations for the lack of reports testing their therapeutic potential in combination with aligned nanofibre scaffolds. Firstly, as mentioned above, the production of aligned nanofibre scaffolds has proved challenging without more sophisticated methods of processing nanofibres fabricated with a lower packing density: only one study has used cells

seeded onto scaffolds containing nanofibres, prior to implantation.[131] Second, the issues associated with the co-culture of multiple glial cell populations on scaffolds within a single compatible medium have limited the cell types used in the literature to predominantly NSCs. These cells are able to generate astrocytes, neurons and oligodendrocytes, making them a useful cell source for co-culture studies and also in the context of repair.[141] However, these cells tend to differentiate predominantly into astrocytes so they cannot be used to generate multiple defined ratios of the three cell types on demand. Furthermore, the use of NSCs for construction of the complete glial cell circuitry is limited as they are unable to produce microglial cells, which are generated in development from primitive myeloid progenitors.[142]

2.1.3. Technological gap: can the limitations of fabricating aligned nanofibre scaffolds with greater spatial and cellular complexity be addressed?

Techniques that separately address: (i) the difficulties of processing nanofibres with a low packing density for the production of 3-D implants; and (ii) the co-culture of all the glial cell sub-types have been reported. First, Ying, *et. al* (2011) describe a technique for the fabrication of a 3-D nanofibre-hydrogel composite, containing handleable nanofibre meshes with a relatively low packing density.[133] In brief, a knife-edged parallel electrode collector was used to capture a mesh of aligned nanofibres, which were unsupported between the electrodes. The use of this collector permitted the transfer of the nanofibre mesh onto portable acetate frames, which were then stacked and filled with collagen hydrogel to create a multiple layer nanofibre-hydrogel construct. The low line density (450 nanofibres/mm) and thickness (0.5-3.0 μm) of the nanofibre meshes used circumvented the problem of

cellular infiltration through each nanofibre mesh layer, when cells were applied within the hydrogel to the top mesh layer. The hydrogel supported the nanofibre configuration and further enhanced the 3-D environment of the scaffold. The constructs were used for mono-cultures of either corneal fibroblasts or nucleus pulposus cells, so the applicability for the culture of neural cells remains unknown. However, the other potential techniques reported, combining nanofibres with a hydrogel to assemble a 3-D composite, either produced a tubular structure[143] or contained random nanofibre configurations.[144,145] These are of much less benefit for the regeneration of neural tissue due to the uniaxial orientation of ascending and descending pathways in the spinal cord (section 1.1.1).

Second, mixed glial cultures represent a system whereby primary astrocytes, microglia and OPCs can be maintained together in one medium and pure populations of each consistently derived.[146] They have been used previously to generate co-cultures of astrocytes and oligodendroglia, although they were cultured on polystyrene nanofibres that were collected on a 2-D surface (glass coverslips) and used *in vitro* in the context of studying the processes of oligodendrocyte myelination.[147]

Hence, there is unexplored potential to enhance the spatial and cellular complexity of aligned nanofibre scaffolds by using 3-D, multiple layer nanofibre-hydrogel constructs to culture and align multiple glial cell sub-types in defined orientations.

2.1.4. Objectives

This chapter follows the development and optimisation of methodologies to assemble nanofibre-hydrogel constructs in order of increasing glial cell co-culture and nanofibre layer complexity:-

(i) **Astrocyte/OPC mono-cultures on single layer constructs,** to optimise the assembly process, establish cultures of viable cell populations in highly aligned conformations and quantify the extents of cellular elongation.

(ii) **Astrocyte and OPC co-cultures on single layer constructs**, to demonstrate the feasibility of increasing the glial cell complexity.

(iii) **Astrocyte mono-cultures on multiple layer constructs**, to optimise the assembly of constructs containing aligned glial cells over multiple stacked nanofibre layers.

The overall aim was to demonstrate the feasibility of enhancing the complexity of nanofibre-based constructs as part of a combinatorial strategy, towards the development of a multicellular, implantable scaffold for the repair of SCI.

2.2. Materials and methods

For all tissue extraction procedures, the care and use of animals was in accordance with the Animals (Scientific Procedures) Act of 1986 (UK) with approval by the local ethics committee.

2.2.1. Reagents and equipment

The syringe pump was obtained from KD Scientific (Holliston, MA, USA) and a high voltage power supply from Spellman HV (Pulborough, UK). Poly-L,D-lactic acid (PLA; 96% L: 4% D) was obtained from Purac BV (Gorinchem, Netherlands). Chloroform, dimethylformamide and rhodamine B were all from Sigma-Aldrich (Poole, UK). Collagen type I from rat tail was obtained from BD Biosciences (Oxford, UK). Tissue culture-grade plastics, media and media supplements were from Fisher Scientific (Loughborough, UK) and Sigma-Aldrich (Poole, UK). Recombinant human platelet-derived growth factor (PDGF-AA) and basic fibroblast growth factor were from Peprotech (London, UK). The following primary antibodies were used: rabbit anti-GFAP (DakoCytomation, Ely, UK), monoclonal anti-A2B5 (Sigma-Aldrich, Poole, UK) and monoclonal anti-myelin basic protein (MBP; Serotech, Kidlington, UK). Cy3- and Fluorescein isothiocyanate (FITC)-conjugated secondary antibodies were from Jackson ImmunoResearch Laboratoratories Inc. (West Grove, PA, USA). Vectashield mounting medium with and without 4', 6-diamidino-2-phenylindole (DAPI) was from Vector Laboratories (Peterborough, UK). DAPI powder was from Sigma-Aldrich (Poole, UK). Vybrant^{TM} carbocyanine dyes were obtained from Fisher Scientific (Loughborough, UK). The live/dead cell viability kit was from Invitrogen (Paisley, UK).

2.2.2. Fabrication and processing of electrospun aligned nanofibres

The experimental setup and operational parameters used in the production of all nanofibres were previously optimised to the laboratory environment (24^{o}C with 45 % humidity). A 2% (w/v) poly-L,D-lactic acid solution was prepared by dissolving the polymer in chloroform prior to the addition of dimethylformamide (7:3 solvent volume). The addition of rhodamine B into the solution (0.1 mg/mL) produced fluorescent nanofibres, to permit the visualisation of nanofibre interaction with multiple neural cell populations. The electrospinning setup (**Figure 2A**) consisted of a syringe filled with polymer solution and a mobile, knife-edged, parallel electrode collector (produced in-house) connected to a copper plate. A syringe pump forced the polymer solution at a rate of 0.025 mL/min from the needle of the syringe, towards the electrodes of the collector. A potential difference of ±6 kV was applied between the needle and the collector, which were separated by a working distance of 20 cm. Nanofibres were deposited between the parallel electrodes (separated by 4 cm) in an aligned configuration. The nanofibres used for all experiments were obtained across the central width (ca. 15 cm) of the collector where the nanofibre line density (number of nanofibres along a distance perpendicular to the axis of nanofibre orientation) remained homogeneous. Nanofibres were transferred onto cellulose acetate frames to be handleable and maintain nanofibre alignment.

Nanofibres fabricated for nanofibre-collagen hydrogel constructs (herein termed *'nanofibre-hydrogel constructs'*) with a single nanofibre layer were collected over a unit operation less than ten min in duration and acetate frames were affixed using a spray adhesive directly onto the parallel electrodes of the collector (**Figure 2B**). This produced portable '*nanofibre sheets'* with a low line density per acetate

frame. To fabricate '*nanofibre meshes*' with an increased line density for use in multiple layer nanofibre-hydrogel constructs, whilst maintaining the nanofibre alignment, an intermediate processing step was employed utilising a *'densification tool'* (**Figure 2C**). This compacted all of the nanofibres obtained after each unit operation, from the deposition area of the collector (60 cm^2) to the area of the tool (13.2 cm^2; **Figure 2D**). To further increase the line density, nanofibres from between one to two unit operations were combined onto the tool and transferred to a single acetate frame. The maximum length of each unit operation was restricted to 10 mins to prevent the build up residual charges and consequently the collection of misaligned nanofibres on the top layer of the nanofibre mesh.[104] All nanofibres were desiccated overnight and sterilized with ultra-violet light using a GS Gene Linker ™ UV chamber (Bio-Rad Laboratories, Hercules, CA) before use in experiments. Nanofibres were discarded if unused for periods longer than 2 months.

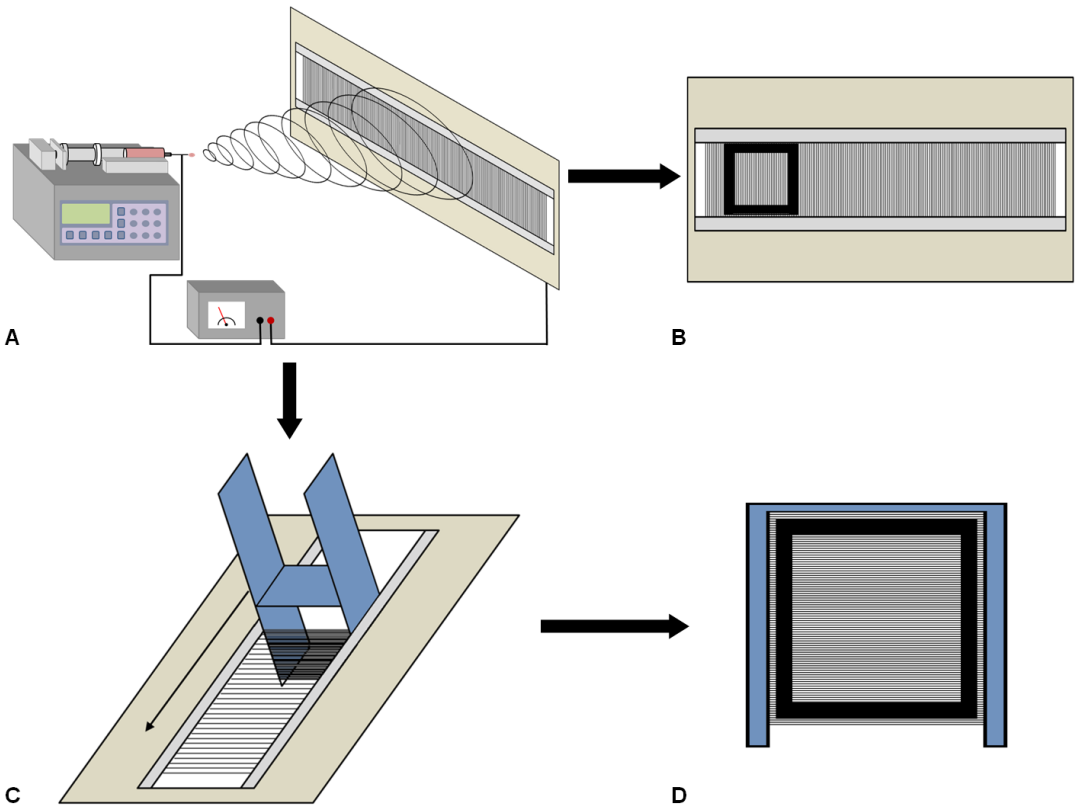

Figure 2. Schematic diagram showing the production of sheets of portable aligned nanofibres adhered to acetate frames. *(A) The electrospinning setup, consisting of a syringe loaded with polymer (pink), syringe pump (grey) and knife-edged parallel electrode collector (beige). (B) For single unit operations less than ten min, acetate frames (black) were sprayed with adhesive and applied directly onto the nanofibre collector. (C) The use of a 'densification tool' (blue) to increase the overall line density (number of nanofibres perpendicular to the axis of orientation) of nanofibres on each acetate frame. All nanofibres collected from the central area of the collector, from a single unit operation (≤10 min), were processed onto the tool. The line density could be increased further by adding nanofibres from more unit operations onto the tool. (D) The application of a single acetate frame onto the densification tool.*

2.2.3. Mixed glial cultures

Primary mixed glial cultures were prepared and each cell population (astrocytes, OPCs and microglia) subsequently purified using an established protocol.[146] Briefly, the cerebral cortices were dissected from whole rat brains of neonatal Sprague-Dawley rats (P1-3). Cells were dissociated and cultured at 37ºC in 5% CO_2/95% humidified air in flasks containing D-10 medium [Dulbecco's modified Eagle's medium (DMEM) supplemented with 2 mM glutaMAX-I, 1 mM sodium pyruvate, 50 U/mL penicillin, 50 µg/mL streptomycin, and 10% fetal bovine serum]. After 8-10 days, a confluent layer of astrocytes had attached to the bottom of the flasks, with a more loosely attached layer of OPCs and microglia proliferating above. The use of a rotary shaker at 200 rpm for 2 h preferentially removed microglia into the medium. To obtain OPCs, this medium was replaced with fresh, re-gassed medium and shaken for a further 16 h. Residual microglial contamination was removed from OPCs through the transfer of the resultant medium to non-tissue-culture grade Petri dishes for 30 min. Finally, by trypsinizing the remaining astrocyte bed layer and seeding astrocytes into a new culture flask, relatively pure populations of each glial cell sub-type could be obtained. Flasks containing mixed glial cultures or pure astrocyte cultures were maintained with medium changes every 2-3 days.

2.2.4. Nanofibre-hydrogel construct fabrication

The established protocol[133] for assembling 3-D constructs with multiple nanofibre layers was adapted for the culture of neural cells, on single layer constructs, as a basis for the optimisation and the scale-up of the number of constituent nanofibre layers. In this regard, many alterations and refinements were

made to the design and assembly of constructs, which are all detailed in section 2.3. However, the initial methodology used to fabricate both single and multiple layer nanofibre-hydrogel constructs is detailed below.

2.2.4.1. Single nanofibre layer mono-culture experiments (astrocytes or OPCs)

The first step in the assembly procedure (**Figure 3**) was the formation of a collagen hydrogel solution at a final concentration of 3 mg/mL, containing a stock solution of type I rat tail collagen, 10x DMEM solution, distilled water and 1N sodium hydroxide (all sterile). The volumes of each hydrogel component were calculated according to the stock collagen concentration, and the desired collagen solution concentration and volume. All the components were mixed thoroughly and the homogeneous collagen hydrogel solution left on ice (≤ 4 h) until required. Next, a pre-cut filter paper frame was placed on the centre of a hydrophobic polytetrafluoroethylene (PTFE) block in a Petri dish. Drops of collagen gel solution were slowly applied to the centre of the filter paper frame to produce a level base, which was cured for 30 min at 37^{o}C. During this time period, either astrocytes or OPCs were resuspended at a cell concentration of 2.5 x10^{5} cells/mL (from pure cultures or mixed glial cultures, respectively; section 2.2.3). A single frame of aligned nanofibres was placed on top of the base and the cells were seeded over the central seeding area. Cells were incubated for 30 min to permit their initial attachment to constructs and collagen hydrogel subsequently added around the outside perimeter of the seeding area to seal the nanofibres in place. After curing the hydrogel seal (15 min; 37^{o}C), the acetate frame was removed from the construct by cutting the nanofibres with a scalpel in between the frame and the seal. The PTFE

block was then removed and the construct transferred to a Petri dish, for culture purposes and to permit visualisation using light microscopy. Culture medium was added to all constructs (D10: astrocyte mono-cultures and glial cell co-cultures; OPC maintenance medium: OPC mono-cultures) and changed every two days thereafter.

Refinements to the seeding procedure, including the addition of numerous glial cell sub-types to produce *'mixed glial constructs,'* were made according to the design and quality of the constructs formed. Nanofibre-hydrogel constructs were used to evaluate the morphological effects of nanofibres on both astrocyte and OPC mono-cultures following culture. Cells seeded onto hydrogel constructs without nanofibres were used as a control for these experiments and constructs containing glial cell co-cultures. Furthermore, during the initial culture period, cells were simultaneously seeded onto tissue culture plastic ± nanofibre sheets (adhered to the surface), to monitor differences in the proportions of cells that: were phase-bright with light microscopy; had attached; and had aligned on nanofibres, compared with cells simultaneously seeded onto constructs. These parameters were considered important readouts of cell viability that significantly helped troubleshoot any procedural problems and optimise construct assembly.

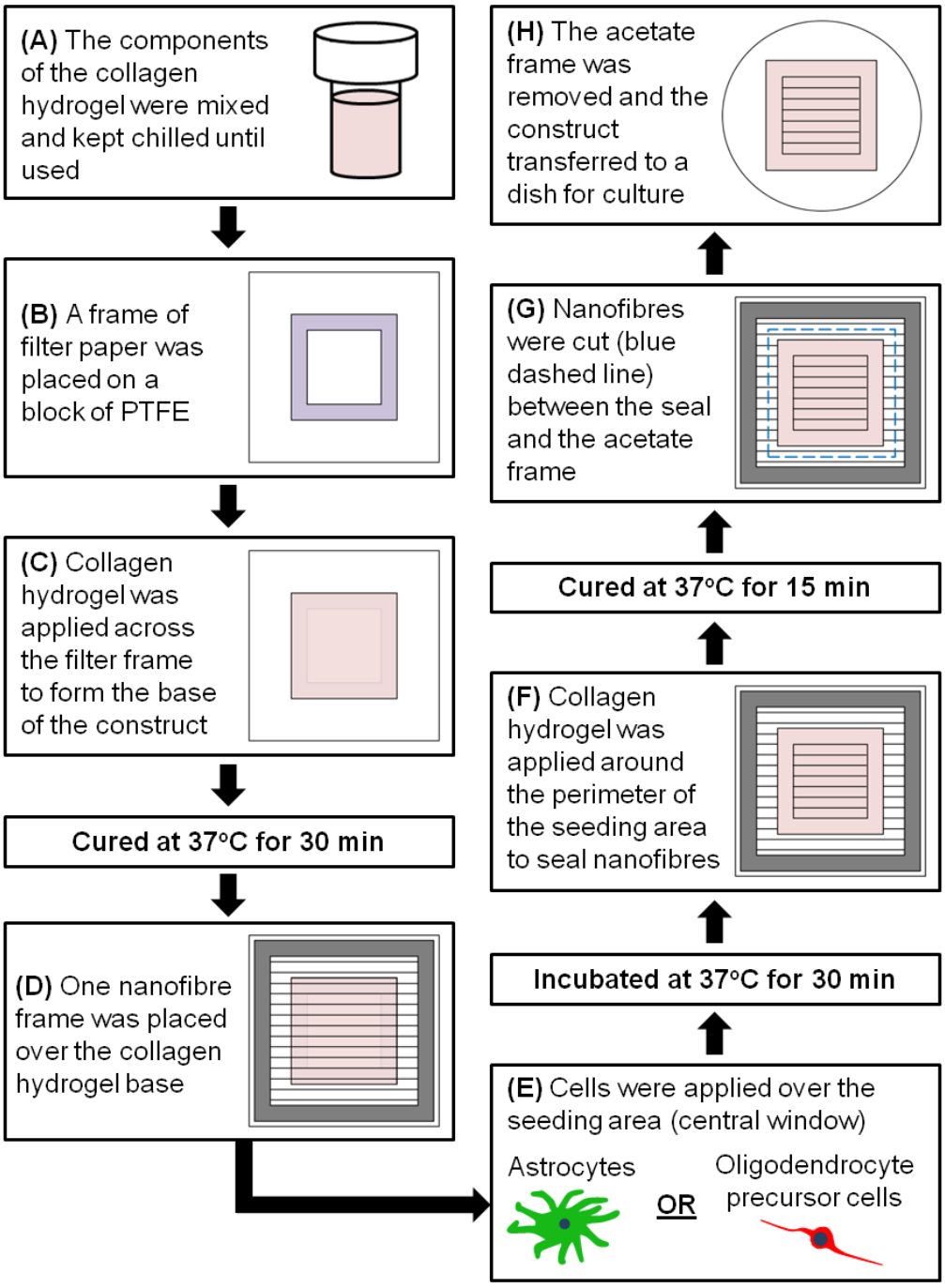

Figure 3. Schematic diagram depicting the process of single nanofibre layer-hydrogel construct production, adapted from an established methodology to produce 3-D constructs with multiple nanofibre layers.[133]

2.2.4.2. Multiple nanofibre layer mono-culture experiments (astrocytes)

The production of constructs with two nanofibre layers was used as an intermediate increase in complexity from single layer constructs and was used throughout the assembly of three-layer constructs as a control. Constructs containing multiple nanofibre mesh layers (**Figure 4**) had a few key differences in the design compared to the single layer constructs. The nanofibre meshes were produced with a significantly greater line density than the nanofibre sheets, in order to sequester the cells sequentially seeded onto each nanofibre layer. The density used previously by Ying, *et al.* (2011) was much lower to facilitate cellular infiltration, because their construct was pre-assembled prior to seeding cells simultaneously across all three nanofibre layers.[133] A square filter paper frame was placed on top of each nanofibre mesh layer to create distinct layers and to anchor the hydrogel after curing. The nanofibre meshes were stacked perpendicular to the adjacent layer to help visualise the influence of aligned nanofibres on the orientation of cells through the depth of the 3-D nanofibre construct formed.

Astrocytes were cultured as a basis for assessing the potential to further increase the complexity of the multi-cellular constructs produced. In initial experiments, 6×10^3 astrocytes were sequentially seeded onto each layer in equal intervals ranging between 40-120 min, to permit the initial attachment. Cells were plated onto tissue culture plastic immediately after each construct layer was seeded as a control to monitor cell viability at each stage of assembly. Excess medium was removed 60 min after seeding the final nanofibre layer with cells and collagen hydrogel was added to the centre of the construct to stabilize the nanofibres and complete the construct assembly. Following the removal of acetate frames (at 12 h),

culture medium was added and was changed every 2 – 3 days. Astrocytes were cultured for two weeks before imaging.

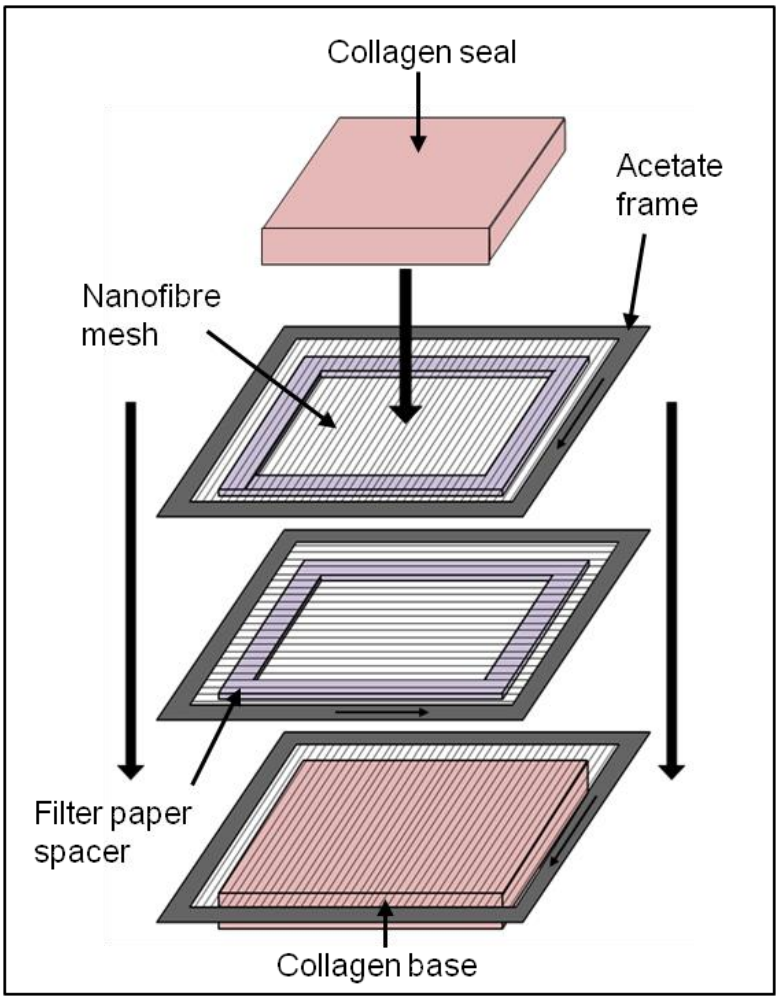

Figure 4. Schematic drawing illustrating the assembly of nanofibre-hydrogel constructs with three nanofibre layers. *One acetate frame (dark grey) with a nanofibre mesh adhered to the underside of the frame (black arrows indicating nanofibre direction) was placed on top of a collagen base (pink). Cells were seeded onto the nanofibre mesh and a spacer (light purple), nanofibre frame and cell seeding solution added two more times to produce a three layered construct. Collagen (pink) was added to the centre of the construct to finalise the fabrication process.*

2.2.5. Cell labelling

In every case, constructs were washed with phosphate buffered saline (PBS), fixed with 4% paraformaldehyde [PFA; room temperature (RT); 20 min] and washed again. Constructs were incubated in blocking solution [5% normal donkey serum (NDS) in PBS supplemented with 0.3% Triton X-100, RT; 30 min] and then incubated with primary antibodies [raised against A2B5 (marker of OPCs; 1:200 dilution), GFAP (marker of astrocytes; 1:500) and MBP (marker of mature oligodendrocytes; 1:200)] in blocking solution. Astrocytes and oligodendroglia were both visualised on constructs by double-staining with antibodies raised against GFAP, and A2B5 (two day co-cultures) or MBP (eight day co-cultures). Following washing, constructs were incubated with blocking solution and then with respective Cy3- and/or- FITC-conjugated secondary antibodies (1:200). The protocol for immunostaining constructs required optimisation from that used for staining dissociated cells on glass coverslips, as the intensity of fluorescence was too faint for the adequate microscopic detection of cells. Therefore the lengths of primary and secondary antibody incubations were increased to 24 h and 4 h, respectively. Performing these steps at room temperature (RT) enhanced the staining quality without concomitantly increasing the levels of background staining, so the protocol was considered optimal. Constructs were washed and mounted with Vectashield mounting medium containing DAPI nuclear stain (or without for constructs containing microglia stained with DAPI).

A live/dead cell viability kit was used to label astrocytes in multiple layer nanofibre-hydrogel constructs. Briefly, cell culture medium was removed from constructs and washed three times with PBS. Constructs were incubated in PBS

containing 10 µM calcein-AM and 1 µM propidium iodide (30 min; 37ºC), washed in PBS and immediately visualised.

A commercial cell tracking kit was used to visualise the co-existence of multiple glial cell sub-populations on single layer mixed glial constructs. Carbocyanine dye (5 µL/mL) was added to 1 x10^6 cells/mL suspended in culture medium and incubated at 37ºC. Cells were washed in culture medium to remove residual stain. The optimal incubation time for each neuroglial cell was investigated by removing cells incubated with dye every five min up to a total of 25 min and visualised with a fluorescence microscope. As the quality of staining was suboptimal (section 2.3.5), a different method was developed to stain live microglia with DAPI and then subsequently immunostain astrocytes and oligodendrocytes. To a suspension of microglia in 5 mL of D10 medium, stock DAPI was incubated at 20 µg/mL (15 min; 37ºC). Cells were subsequently centrifuged and resuspended in fresh medium twice before seeding onto constructs.

2.2.6. Imaging

2.2.6.1. Fluorescence microscopy

Constructs were imaged using an Axio Scope A1 fluorescence microscope (Carl Zeiss MicroImaging GmbH; Goettingen, Germany) fitted with an Axio Cam ICc1 digital camera. Filter sets 20 (to detect CY3 fluorescence), 49 (to detect DAPI fluorescence) and 38 (to detect FITC fluorescence) were from Carl Zeiss (MicroImaging GmbH; Goettingen, Germany), and the excitation and emission

wavelengths for these filter sets are 546/575-640 nm, 365/445-50 nm and 470/525-50 nm, respectively. Fluorescence images were captured with AxioVision software and merged in Adobe Photoshop CS5.1 (version 12.1).

2.2.6.2. Confocal microscopy

An inverted confocal laser scanning microscope (Olympus FV 300, Olympus, UK) was used to observe the segregation and orientation of live/dead stained astrocytes in nanofibre-hydrogel constructs over three layers. This employed in-line barrier filters for 510-530 nm (green) and 565-660 nm (red). All images were captured using a X10 lens objective. Visualisation of the constructs in 3-D was achieved by scanning sections at 10 µm intervals along the z-axis over a range of 250 µm. Three individual images over the full z-axis range were merged into a single representative image using ImageJ software (version 1.45s).

2.2.6.3. Scanning electron microscopy

Nanofibre frames at different packing densities and with and without fluorescence were mounted on aluminium stubs. Pre-cut O-rings of carbon pad were used to adhere nanofibres to the stubs and facilitate acetate frame removal without disrupting the nanofibre configuration. Nanofibres were sputter coated with gold for 2 min and nanofibers within the centre of the circular carbon pad visualised using a high resolution field emission scanning electron microscope (SEM; Hitachi S4500) operated at an accelerating voltage of 5 kV.

2.2.7. Analyses

2.2.7.1. Nanofibre characterisation

A Nikon Eclipse 80i fluorescence microscope was used with manual focus stepping at 0.5 µm to estimate the thickness of the collected fluorescent nanofibre mesh layer (TRITC emission wavelength of 605 nm). The distance between the top and bottom fibres was measured for six randomly chosen fields, across three nanofibre frames, produced in discrete electrospinning unit operations. For diameter analysis, nanofibres were fabricated ± rhodamine B and captured at X 5000 magnification by SEM. The nanofibres measured had a uniform shape across the length of the image and were visually separated from any clumps. At least 20 nanofibres were measured on each stub, across six stubs ± rhodamine B (n = 6 per group). For analysis of the nanofibre line density (number of nanofibres along a distance perpendicular to the axis of nanofibre orientation), images were captured at X 2000 magnification, which was the best compromise between the visualisation of an adequate number of nanofibres per field and sufficient resolution for the identification of individual nanofibres. The number of nanofibres across a 60 µm distance was counted for each image, three images per stub, across three stubs ± rhodamine B (n = 3 per group).

2.2.7.2. Assessment of cellular elongation

To assess the potential of nanofibre-hydrogel constructs to induce the elongation of astrocytes and OPCs, ImageJ software was used to measure the lengths

and widths of at least 90 individual cells per construct (three fields per construct; three constructs per group) from fluorescence images of constructs stained for GFAP or A2B5. The aspect ratio (length ÷ width) was calculated for individual cells as described previously.[60] Cells that showed evidence of attachment to nanofibres but remained rounded, without evidence of elongation, were excluded from the aspect ratio analysis. The aspect ratio for each cell was classified into three bins describing the extent of elongation: 'low' (2-4); 'medium' (4-8); 'high' (> 8).

2.2.8. Statistical analysis

Data were analysed using GraphPad Prism statistical analysis software (version 5.0). All data are expressed as mean ± standard error of the mean (S.E.M.). The number of experiments (*n*) refers to the number of mixed glial cultures from which astrocytes and OPCs were derived, with each primary culture established from a different rat litter. **Nanofibre diameter analysis:** A Student's t-test (two-tailed) was used to quantify differences in nanofibre diameter between nanofibres ± rhodamine B. **Nanofibre line density analysis:** Data were square-root transformed and a Student's t-test (two-tailed) was used to quantify differences in nanofibre line density between nanofibres ± rhodamine B.

2.3. Results

2.3.1. Electrospinning for the production of fluorescent aligned nanofibre frames

Portable sheets of non-fluorescent, aligned nanofibres were successfully produced over multiple unit operations using the existing setup and post-collection processing methodologies (**Figure 5**). Additional adjustments were made to the setup to reduce the incidences of misaligned fibres deposited between the parallel electrodes of the mobile collector. To ensure the overall conductivity of the collector remained constant, the soldering wire that linked the electrodes with the copper plate was replaced with copper wire. However, incidences of misalignment were mainly found when the nanofibres accumulated at specific regions along the knife-edged

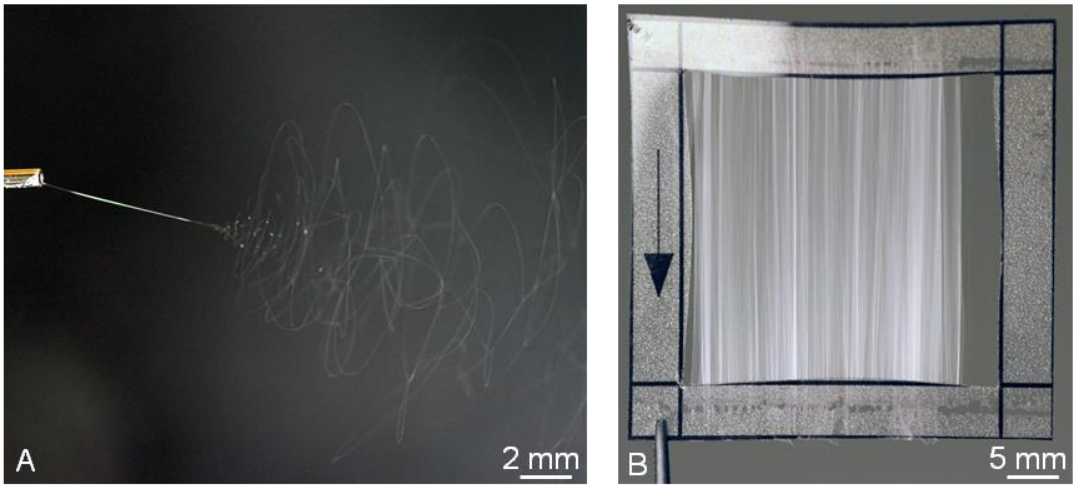

Figure 5. The production of portable frames of aligned nanofibres by electrospinning. *(A) Photograph showing the formation of the Taylor cone from the tip of the needle during a unit operation. (B) Photograph of an acetate frame*

containing a mesh of fluorescent, aligned nanofibres produced for multiple layer nanofibre-hydrogel construct experiments.

---

electrodes, due to the presence of residual adhesive after the application of acetate frames (during the processing of nanofibre sheets), or the build up of indentations along the surface of the sharp edges that formed over time. Therefore particular care was taken to remove any residual adhesive from the after each unit operation with an abrasive sponge soaked in 70% industrial methylated spirits (IMS) and the edges of the electrodes were regularly sharpened with a knife sharpener, respectively.

Fluorescent nanofibres were fabricated by the introduction of rhodamine B into the PLA polymer solution at 1 mg/mL. At this concentration no leaching of the bound dye was observed from the nanofibres into the surrounding hydrogel of the construct or the culture medium, and there was an absence of any noticeable uptake by cells cultured on the nanofibres as judged by fluorescence microscopy. Substantial leaching of dye was found at a higher concentration of 10 mg/mL, so the initial concentration used was considered suitable for all nanofibre-construct experiments.

Analysis of micrographs captured using SEM confirmed the production of electrospun fibres in the nano-scale size range, with representative micrographs of diameter for both fluorescent and non-fluorescent nanofibres shown in **Figure 6**. There was no significant difference between the diameters of fluorescent and non-fluorescent nanofibres produced (540 ± 16 nm *versus* 604 ± 33 nm, respectively).

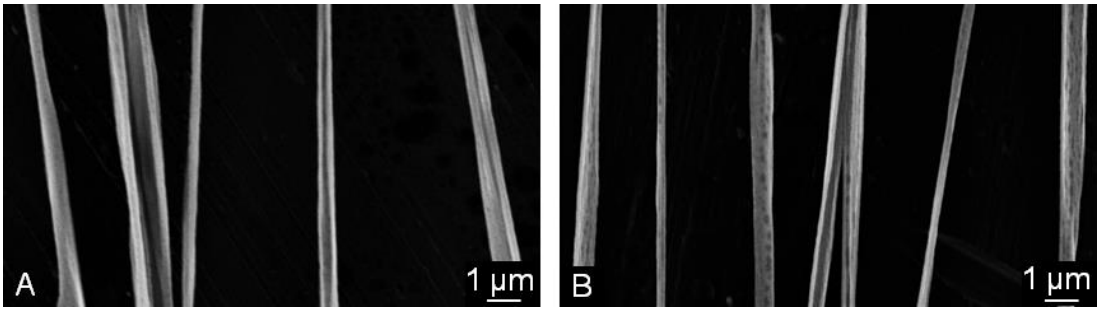

Figure 6. Representative SEM micrographs showing diameters of nanofibres collected. *(A) Non-fluorescent nanofibres. (B) Fluorescent nanofibres.*

2.3.2. Optimisation of nanofibre line density

The duration of each electrospinning unit operation was based on the optimal nanofibre line densities required for single and multiple layer nanofibre-hydrogel construct experiments. In order to investigate the potential of nanofibres to induce elongation of astrocytes and OPCs on single layer constructs, the optimal line density was considered one where the topographical cues from individual nanofibres acted on single cells. It was apparent that the nanofibre sheets fabricated from unit operations greater than four minutes contained too many incidences of overlapping nanofibres, which acted as a conflicting topographical cue and induced the elongation of astrocytes along multiple nanofibres. This increased the difficulty of visualising the processes of individual cells with respect to the nanofibres that they were attached to, which confounded the attempts made to standardise the analysis. Conversely, the nanofibre line density was considered too low from unit operations less than four min in duration, because there were not enough nanofibres over the cell seeding area. Therefore a unit operation of four min was chosen as the optimal duration for the production of nanofibre sheets (**Figure 7**). An analysis of SEM micrographs found no significant difference in line density between non-fluorescent

and fluorescent nanofibre sheets (136 ± 35 nanofibres/mm *versus* 108 ± 22 nanofibres/mm), suggesting the addition of rhodamine B into the polymer solution had negligible effects on the quantity of nanofibres deposited on the mobile collector.

The line density of the nanofibre meshes used in multiple layer nanofibre-hydrogel constructs needed to be high enough to prevent the astrocytes seeded on each distinct layer from mixing with layers below, thus distributing them evenly over each layer of the construct. There was an uneven distribution in cells found over the three nanofibre layers of constructs produced, when the densification tool was used to process all the collected nanofibres from a single ten min unit operation onto each acetate frame. The addition of nanofibres onto the tool from a further five min collection appeared to increase the number held on the top two nanofibre mesh layers, but after frames incorporating nanofibres from two separate ten min collections were used the cells were considered evenly distributed throughout each layer. The line density of the fluorescent nanofibre meshes (**Figure 7)** was 1563 ± 56 nanofibres/mm; approximately a 14 fold increase in line density compared to nanofibre sheets. The thickness of each mesh layer was 25 ± 1 µm.

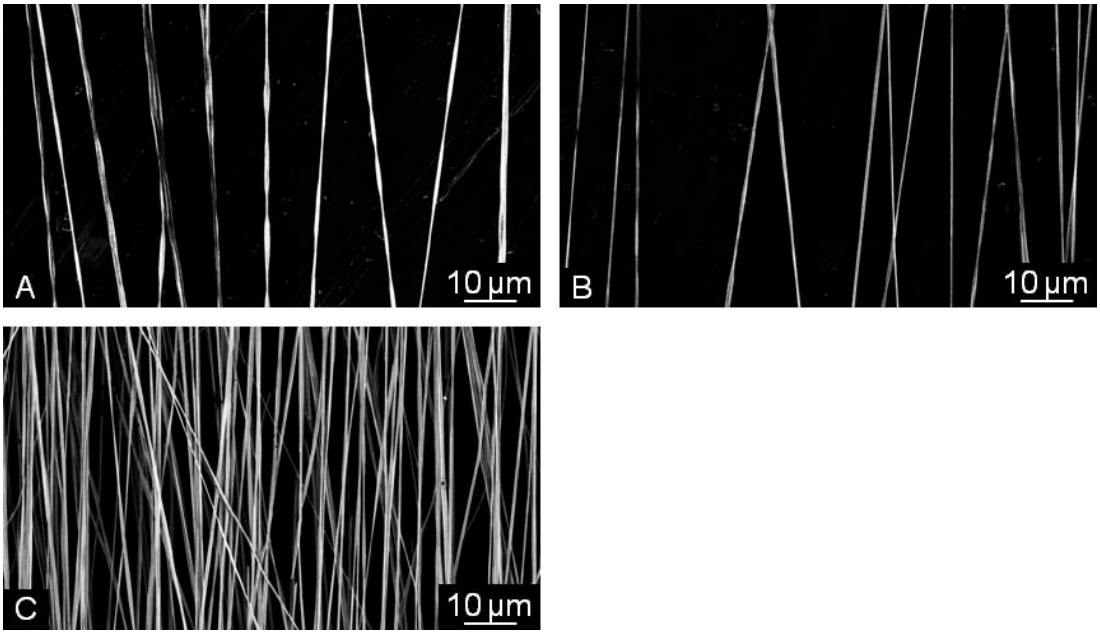

Figure 7. **Representative SEM micrographs showing the line densities of aligned nanofibres used in constructs**. *(A) Non-fluorescent nanofibres for single layer nanofibre -hydrogel constructs. (B) Fluorescent nanofibres for single layer nanofibre -hydrogel constructs. (C) Fluorescent nanofibres at a higher line density for multiple layer nanofibre -hydrogel constructs.*

2.3.3. Fabrication of single layer nanofibre-hydrogel constructs

A series of pilot experiments were performed to optimise the assembly process of single layer nanofibre-hydrogel constructs for the culture and elongation of astrocytes or OPCs, as a basis for increasing the complexity of constructs produced (viz the number of co-cultured neuroglial sub-classes and scale-up of the number of constituent nanofibre layers). The procedural modifications undertaken with respect to the initial production methodology (section 2.2.4.1) are summarised in **Table 2**.

Table 2. Summary of the main alterations made to the methodology of single layer nanofibre-hydrogel construct assembly	
Problem	**Solution**
The collagen hydrogel seal was ineffective at adhering the nanofibres to the construct	The timings of cell seeding and seal addition to the constructs were altered to prevent the hydrogel mixing with any remaining cell seeding solution and form an ineffective seal as a result.
Expense of experiments	The construct size was reduced to save on the cost of materials, medium components and the volumes of antibodies required.
Construct stability and mobility during transfer following assembly	The area of the filter frame base was extended to provide a surface to hold the assembled construct during transfer with forceps.
The hydrogel base broke apart during transfer	The hydrogel that formed the base was applied in sections to prevent it from getting under the frame before curing.
Issues containing the spread of fungal infection	Petri dishes small enough to contain an individual construct were used for glial cell culture in favour of 6-24 well plates.
Variability in production of the collagen hydrogel solution	A lower stock concentration of collagen solution was used to produce the neutralised solution, and refinements were made to the storage and handling of the solution.
Difficult to assess the elongation of individual cells when they are in contact with numerous other cells and nanofibres	The density of cells and nanofibres used was reduced, to visualise the processes of single cells on individual nanofibres.
The fluorescence intensity of immunostained cells was too faint for adequate detection	The protocol was altered to allow for longer primary and secondary antibody incubations, at room temperature.

2.3.3.1. Order of the assembly protocol

The main change made to the assembly protocol was re-ordering the timings of cell and nanofibre seal addition. The rationale for adding the cells before the completion of construct fabrication was to maximise the cellular attachment to the nanofibre sheet before any of the nanofibres had begun to descend into the hydrogel base. This was observed via light microscopy as discontinuous nanofibres across the base. However, this phenomenon was observed at least one hour after nanofibres were added, so there was ample time for the addition and attachment of cells. It was also hypothesised that the addition of the cells immediately following preparation from culture (trypsinisation and re-suspension) would ensure maximal viability of the seeded population. In practise, the viability of astrocytes remained optimal following three hours in suspension (and up to 30 min for OPCs), as confirmed by cells plated onto tissue culture-plastic controls.

The final issues were associated with the difficulty of producing an effective nanofibre seal. After the cell seeding solution was applied onto the construct base it was very difficult to restrict the positioning of applied hydrogel to the perimeter of the cell seeding area, even following removal of the majority of the seeding volume. This reduced the area available for the assessment of cell-nanofibre interaction and the effectiveness of the seal to anchor the nanofibres to the construct, resulting in the detachment of the nanofibres from the construct upon removal of the supporting acetate frame (**Figure 8A**). In light of these findings, the cells were removed from the culture flask and resuspended at the required density whilst the hydrogel seal was cured in the incubator. The acetate frames were detached from the construct immediately afterwards and the finished constructs transferred into suitable container for the addition of the cells (**Figure 8B**). This protocol alteration had the following

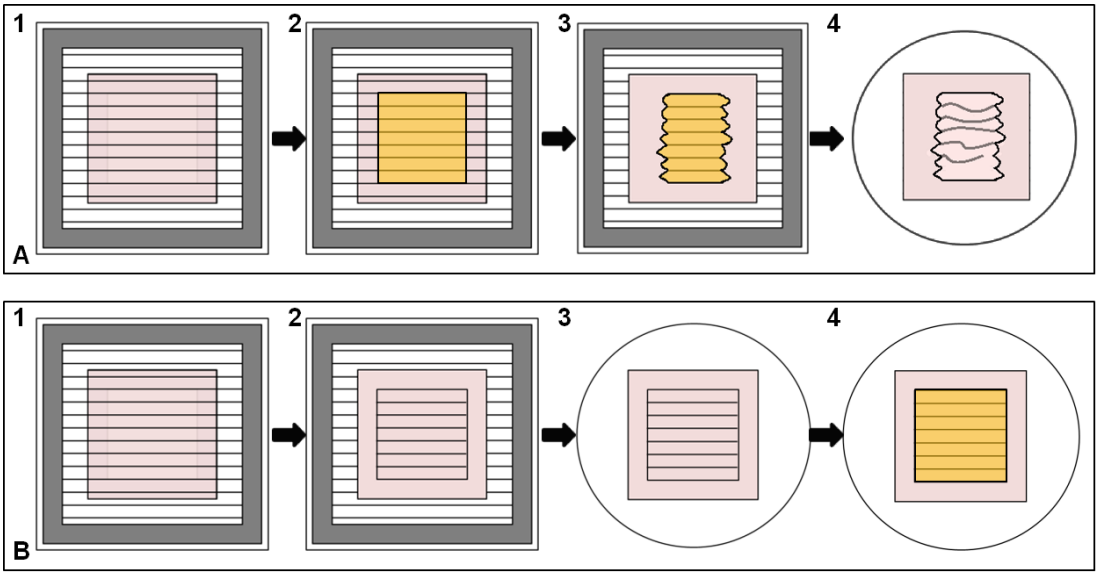

Figure 8. Schematic flow diagrams illustrating the changes made to the timings of cell and nanofibre seal addition. *(A) The existing methodology: (1) The construct base (pink) with a frame of aligned nanofibres (black) placed on top. (2) Cell seeding solution (gold) added over the construct seeding area. (3) After removal of the majority of the seeding solution, hydrogel was added around the perimeter of the seeding area, which flowed into the seeding area and formed a weak seal. (4) Detachment of the nanofibres from the construct following removal of the supporting acetate frame and transfer to a culture dish (circle). (B) Altered methodology: (1) Construct base with nanofibres. (2) Addition of the hydrogel to seal nanofibres. (3) Removal of acetate frames maintaining the aligned nanofibre configuration and construct transfer to a culture dish. (4) Addition of cells over the full area designated for cell addition.*

additional advantages: (i) any disruption to the cells and the nanofibres in the immediate time after seeding was kept to a minimum as the construct assembly had finished; (ii) the seal acted as an additional barrier maintaining the seeding volume in

place on the construct; (iii) the cells could be observed immediately after seeding as the PTFE block had been removed, thus allowing the initial cellular viability, attachment and elongation to be monitored; and (iv) the total time for construct production was reduced.

2.3.3.2. Design of constructs

The major technical problems experienced with the assembly of the initial constructs (**Figure 9A**) were attributed to their design, which was centred on the filter frame restricting the spread of the applied hydrogel to form a base with defined area. This component was re-designed to incorporate additional features and improve the reproducibility and ease of construct assembly. As a starting point, the dimensions of the constructs were reduced to permit culture and post-experimental staining inside a 6 well plate (**Figure 9B**) and to permit transfer to glass microscope slides for mounting and storage. With this design there was a combined decrease in the area of the cell seeding window and the area designated for binding the hydrogel base to the filter frame. However, sufficient room remained for the observation of cellular interactions with nanofibres. Another key design change was the increase to the length of the filter frame adjacent to the area designated for the hydrogel base. This increased the ratio of the total filter frame area to seeding window area with respect to the initial design tested (from 1.4 to 5.3), which gave the whole construct added stability following transfer to well plates for culture and post-culture staining. Elongated ‘tabs’ constituted a small section of the increased filter frame area and provided a surface to hold the assembled construct during transfer with forceps, which significantly reduced the disruption to the attached nanofibre-hydrogel

composite and enhanced the portability, overall quality and reproducibility of the constructs formed. The remaining area was used as a surface to cut the nanofibres prior to the detachment of the acetate frame from the constructs. It was found that the nanofibres remained adhered to the surface that they were cut onto; when this surface was the PTFE block surrounding the hydrogel base, removal of the block pulled on the nanofibres and detached them from the construct. Cutting the nanofibres on the filter frame itself ensured that they remained associated with the construct even if this occurred. Also, the area of the filter extensions was proportionally large compared to the size of the hydrogel base so that the nanofibres could be cut down on relatively far from the edge of the hydrogel base. This aimed to reduce the downward force acting on the fibres over the construct seeding area and prevent the nanofibres from sinking into the base due to this mechanism.

Further refinements were made to the size of the constructs to reduce the costs associated with their culture and post-culture staining. In this context, a single well within a 24 well plate was considered to be the smallest chamber that a construct could be reproducibly fabricated to fit within (**Figure 9C**). All of the features from the previous filter frame design were kept, although the position of the tabs was rotated 90^{o} in order to reduce the overall length. Also, the number of cells and the volume of the hydrogel base were reduced to reflect the size change. While the design of this construct was considered optimal, the tabs and the area for applying the nanofibre seal and cutting the nanofibres were all produced disproportionately small compared to the cell seeding window. This increased the difficulty of construct assembly and the incidences of error, which significantly affected the reproducibility of the constructs fabricated. Additionally, the development of a fungal infection during the culture period raised serious containment concerns about the culture of up

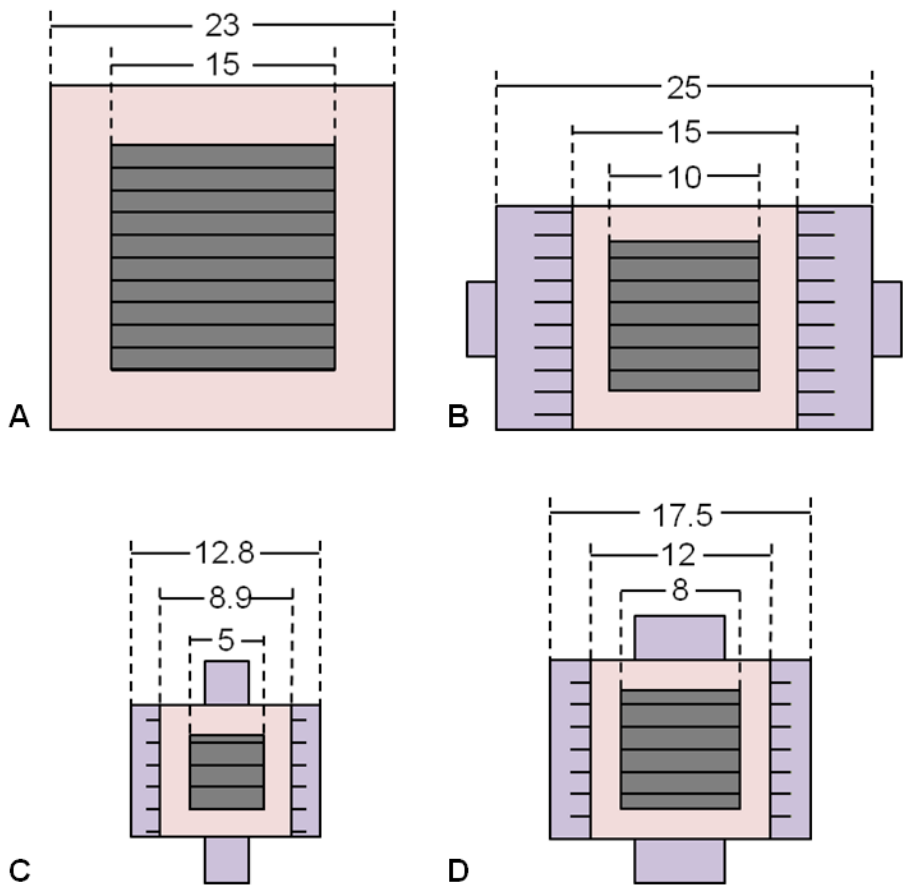

Figure 9. Schematic diagrams of the constructs produced at each stage of development, highlighting new features incorporated into the design of the filter paper frame. *(A) The initial design of the construct, illustrating the seeding area (grey) with horizontally aligned nanofibres (black) and the surrounding area containing the collagen seal (pink). (B) The first prototype construct designed for 6-well plates, featuring an elongated filter frame (purple) at the sides of the hydrogel base for cutting nanofibres onto and tabs at either end for construct transfer following fabrication. (C) The second prototype construct that was modified to fit 24-well plates, with re-positioned tabs to minimise the total size. (D) The final construct design used for all construct experiments, modified to fit 12-well plates. (Sizes of all diagrams are relative; units in mm).*

to 24 constructs in a single well plate, because potentially it could have spread across an entire batch of experiments.

Additionally, in an attempt to further reduce the costs of chemicals and procedures used for these smaller constructs, the size of the nanofibre sheets was decreased in combination with the width of the frame border (from 5 to 1.5 mm). However, these alterations were found to have detrimental consequences on the fabrication procedure. The thinner acetate frame was significantly more flexible, which increased the difficulty of attaching and removing the frames to the mobile electrospinning collector to produce level nanofibre frames. Also the removal of the acetate frame from constructs was more demanding due to the reduction in the area surrounding the construct for cutting the nanofibres. Thus the original frame size was unaltered for all remaining construct designs and experiments. However, these nanofibre frames could be adhered onto much smaller Petri dishes than used previously, which significantly reduced the volume of culture medium required for the production of the controls without hydrogel.

The constructs were re-sized a final time (**Figure 9D**) to permit their staining in 12 well plates and their culture within an individual, small Petri dish. In this context, the volumes of culture medium and immunostaining solutions required were considered reasonable. Furthermore, the use of individual dishes for each construct dramatically reduced the potential for the spread of infection between constructs in culture, maximising the number available from each batch for analysis in the event of any further infections arising. Also, this format reduced the duration that individual constructs were outside of the optimal culture conditions within the incubator reducing any deleterious effects caused by manipulation (e.g. medium changing, observation by light microscopy and post-culture fixation).

2.3.3.3. Preparation and use of collagen hydrogel

The neutralised collagen hydrogel was identified as a critical factor to the quality and reproducibility of the constructs assembled. The successful production of the hydrogel solution was dependent on the addition of four distinct components together in accurate volumes ranging between millilitres to microlitres. Incorrectly measured components resulted in hydrogels that were too structurally weak to produce constructs after curing and displayed a blotchy appearance under both phase and fluorescence microscopy. This made the observation of cells and nanofibres during culture sub-optimal and increased the levels of background fluorescence in post-culture immunostaining. In this context, stock collagen concentrations at 3.5 mg/mL were used, which had a relatively low viscosity compared to higher concentration solutions at 10.2 mg/mL and were easier to accurately measure volumes and mix with the other hydrogel components. Additionally, the added handling difficulties inherent with the higher stock concentration resulted in the introduction of bubbles into the final collagen solution, which were transferred into the produced constructs and further impacted on the visualisation of cells. Thus the lower stock concentration was used to produce the solution. Additionally, the final concentration of collagen hydrogel was varied to 2 mg/mL to validate the use of the 3 mg/mL concentration in constructs for neural cell culture.[133] However, construct production was less reproducible, the hydrogel was more difficult to manipulate and dispense into defined areas, and the structural integrity (important for building layered structures) was not maintained throughout the assembly and culture process. Additional protocol refinements with respect to the storage and handling of the neutralised hydrogel solution were implemented to maintain the homogeneity of the solution with time. The physical integrity of the solution appeared to deteriorate after

storage on ice (> 2h). Furthermore, a rise in solution temperature increased the time constraints during production because the solution began to cure. This was especially evident when the ambient temperature in the laboratory reached up to 34^{o}C. Using compacted ice to chill both the hydrogel components and the neutralised hydrogel prevented the accumulation of air pockets within as it melted over time and maintained the solution at a constant temperature. The effects of high ambient laboratory temperature were overcome by restricting the length of time the solution was out of ice to a maximum of five min and the effects of body heat mitigated by using a rack to place the final hydrogel (and the components during production) in the culture hood.

Following the production of a robust collagen hydrogel solution, refinements were made to the methods of applying the hydrogel to reproducibly form the construct base. Two critical features were the filter paper frame and the hydrophobic PTFE block. The latter was a hydrophobic, non-stick preparation surface that permitted the transfer of the construct after curing. It was found that the filter frame needed to be flush with the PTFE block otherwise a proportion of the hydrogel cured beneath the filter frame and contributed to the disintegration of the base during transfer off the PTFE block. This was achieved through the application of the hydrogel volume in numerous sections, firstly to the outer edges of the filter frame to hold it down onto the block and define the outer base boundary, followed by the remainder of the volume evenly across the middle. A reduction in the total volume of hydrogel used assisted the production of a level base, which helped disperse cells homogeneously over the seeding area.

2.3.3.4. Cell seeding

The final optimisations made to the assembly of constructs were the density of cells seeded and the volume of solution applied onto constructs. To visualise the attachment of individual cells to nanofibres, the concentration of the cell seeding solution was reduced from the 2.5 $x10^5$ cells/mL applied initially to 1.0 $x10^5$ cells/mL. The maximum volume of solution used for seeding onto constructs sized to fit within 12 well plates was 100 µL, but it was nonetheless difficult to maintain in position on the construct without it spilling over the edges before the cells had attached, which reduced the cell density. Conversely, cells were poorly distributed within volumes under 20 µL as the solution did not cover the entire seeding area. Thus, 60 µL was chosen as the optimal volume. Further, the solution was dispensed multiple times to control the distribution of the solution evenly over the seeding area, taking care to avoid contact with the nanofibres and the base hydrogel. Cells were seeded onto a similar sized area on tissue culture plastic to confirm cell density before application onto constructs. Cells were left to attach (2 h) before a larger volume of medium for culture was added. Cells were cultured on the initial constructs produced for approximately seven days, during which regular observations were made of the approximate percentage of cells aligned with nanofibres. It was found that four days of culture was a sufficient duration for greater than 95% of the astrocytes associated with nanofibres to have commenced elongation (*ca* 5% were associated with nanofibres without evidence of elongation). Thus mono-culture construct experiments were fixed at this time point for subsequent staining.

An overview of the final optimised protocol for the assembly of single layer nanofibre-hydrogel constructs is shown in **Figure 10**.

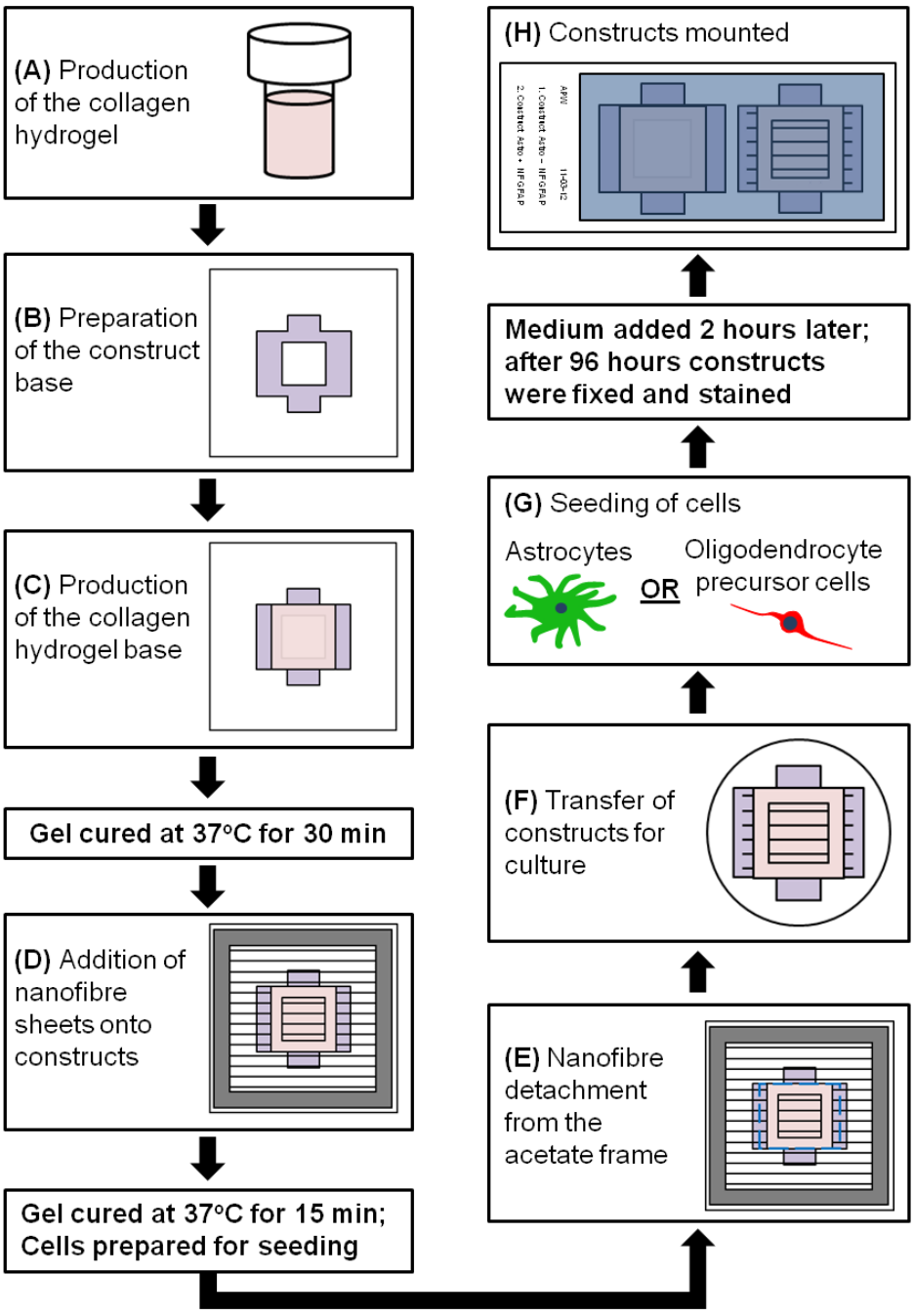

Figure 10. Schematic diagram depicting the final, optimised protocol used for the production of single layer nanofibre-hydrogel constructs. *(A) A 3 mg/mL collagen hydrogel was produced and kept chilled. (B) A frame of filter paper was placed on a block of PTFE. (C) Collagen hydrogel (125 µL) was applied across the filter frame to form the base of the construct. (D) One nanofibre frame was placed*

over the base and collagen hydrogel (20 µL) was applied around the perimeter of the seeding area. (E) Nanofibres were cut around the base (blue dashed line) on the filter frame. (F) The acetate frame was removed and the construct transferred to a small-sized Petri dish for culture. (G) Cells (at 1 x10^5 cells/mL) were applied over the seeding area in a 60 µL volume. (H) Constructs ± nanofibres were incubated in antibodies at RT (primary: 24 h; secondary: 4 h) and transferred onto glass microscope slides with mounting medium (blue).

2.3.4. Characterisation of single nanofibre layer mono-culture experiments (astrocytes or OPCs)

Astrocytes seeded onto control hydrogel constructs without nanofibres generally maintained rounded morphologies over the observation period (**Figure 11A**). In approximately 6% of astrocytes some evidence of process elongation was detected and one third of these cells assumed a bipolar morphology, which is possibly attributable to cellular attachment and elongation along straight sections of collagen fibrils. However, such cells had far shorter lengths and longer widths (*ca* fivefold lower aspect ratios) compared to those observed on nanofibre constructs.

The alignment and fluorescence of nanofibres remained within the nanofibre-hydrogel constructs after post-culture processing (**Figure 11B**). Furthermore, the fluorescence was still visible following storage at 4^{o}C for at least two years. Following the addition of astrocytes onto nanofibre-hydrogel constructs, cells initially displayed rounded morphologies characteristic of detached cells, but associated and attached to nanofibres by 15 min. Approximately 25% of the seeded population displayed evidence of elongation within two hours and both glial

fibrillary acidic protein-positive ($GFAP^+$) type I and II astrocytes could be observed in the cultures. Type II astrocytes are derived from OPCs and characteristically contain a smaller cell body and thinner processes, with considerably more processes than type I astrocytes. Significant cellular alignment with evidence of cell proliferation on nanofibres was observed over the following four days (**Figure 11C** & inset). The aspect ratios of individual astrocytes cultured on nanofibre-hydrogel constructs exhibited higher median values with a considerably wider distribution compared to control constructs (**Figure 11D**). On average, the length of aligned astrocytes was approximately 15 times greater than their width and six times the length of astrocytes on control hydrogel constructs.

Strikingly, OPC mono-cultures lacked evidence of elongation at all time points in both control and nanofibre-hydrogel constructs. Extensive attachment of cells to nanofibres was observed by four days (> 80%). However, the majority of cells appeared rounded and phase dark, with extensive cell clumping and debris, suggestive of cell death (**Figure 12**). This was found irrespective of whether OPCs were cultured in maintenance medium, which is a chemically-defined medium that maintains OPCs in culture, or D10 medium, used to culture astrocytes, microglia and parent mixed glial cultures, and typically results in the differentiation of OPCs into mature oligodendrocytes.

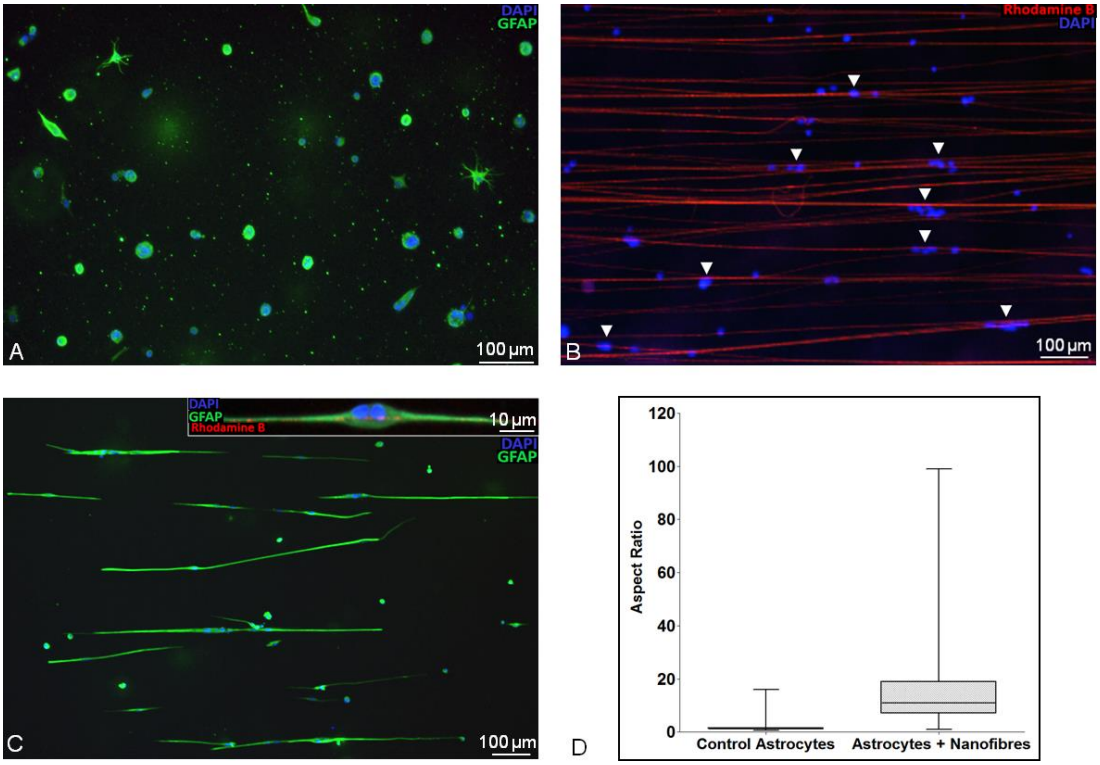

Figure 11. Aligned nanofibre-hydrogel constructs support astrocyte proliferation, alignment and elongation. *(A) Fluorescence micrograph of GFAP$^+$ astrocytes following culture on control hydrogel constructs for four days. (B) Fluorescence micrograph illustrating the alignment and retention of fluorescence by nanofibres within the collagen-hydrogel constructs during the post-culture period (white arrowheads demarcate nuclei of some astrocytes associated with nanofibres). (C) Fluorescence micrographs of the proliferation (inset) and elongation of astrocytes over the four day culture period. (D) Aspect ratios of individual astrocytes cultured on control constructs versus nanofibre-hydrogel constructs.*

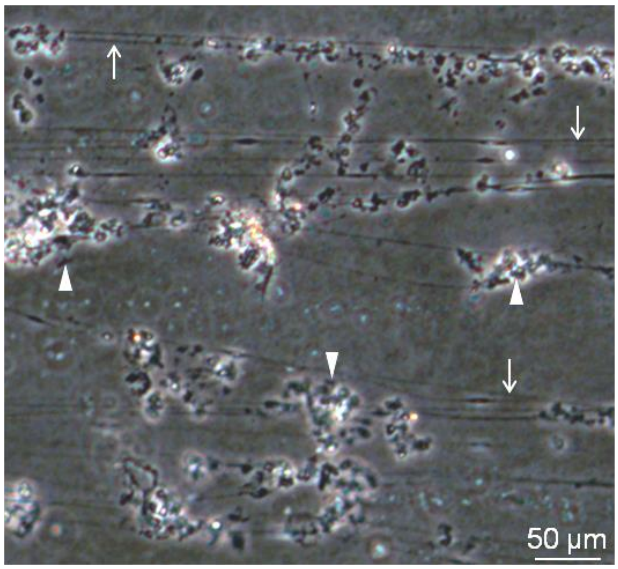

Figure 12. OPC viability was poor on constructs ± nanofibres. *A typical phase-contrast micrograph showing the majority of OPCs cultured on constructs with aligned nanofibres (white arrows) as rounded and phase dark, with extensive cell clumping and debris (white arrowheads).*

2.3.5. Development of seeding and staining protocols for multicellular construct assembly

Strategically, OPCs were sequentially seeded onto constructs with a bed layer of pre-aligned astrocytes following two days of culture and co-cultured for a further two days to permit the attachment and alignment of OPCs to the nanofibres for analysis of cellular aspect ratios. In pilot experiments, OPCs and astrocytes simultaneously seeded onto constructs displayed poor viability in the initial 48 hours, although they recovered after six days of co-culture. However, sequentially seeding the cells produced viable cultures from the start and eliminated the presence of cellular debris from the seeding area, which improved the quality of immunostaining for the imaging of constructs. The density of OPCs seeded was the

same for the astrocyte and OPC mono-cultures, as there was judged to be sufficient space surrounding the astrocytes in order to visualise the attachment and elongation of single cells along individual nanofibres. However, it was found that a 60 µL seeding volume was too difficult to maintain in position on the seeding window as the constructs were wet following the culture of astrocytes. Therefore the seeding volume was reduced to 30 µL and the density of cells doubled to 2 $x10^5$ cells/mL, which was used as the standard protocol for the addition of cells to constructs used previously for cell culture. The immunostaining of co-cultures found cross-specificity of A2B5 antibodies for OPCs and astrocytes (a problem faced with many of the markers for neuroglia at various developmental stages). However, the strength of the fluorescence signal was considerably lower for $GFAP^+$ astrocytes than for OPCs, and thus it was easy to distinguish respective neuroglial sub-populations after merging micrographs of the red and green channels together. Additionally, it was important that fluorescent nanofibres were used for the analysis of OPC aspect ratios in order to identify cells unattached to nanofibres, since OPCs typically display a bipolar morphology on tissue culture plastic, which could have confounded the measurements of OPCs elongated on nanofibres alone. Although both nanofibres and OPCs were captured using the same fluorescence channel (red), it was still possible to accurately distinguish cellular processes from nanofibres, the latter being significantly narrower under high magnification.

The length of some co-cultures (in nanofibre-hydrogel constructs only) was extended for an additional six days (total duration of co-culture eight days), to confirm if the constructs could support the development of multiple cell types [importantly the differentiation of OPCs into mature myelin basic protein-positive (MBP^+) oligodendrocytes] and to visualise the interaction of more established co-

cultures with the topographical cues provided by the nanofibres. For identification, $GFAP^+$ astrocytes and mature MBP^+ oligodendrocytes produced two separate immunostaining profiles with greater morphological differences between them than astrocytes and OPCs.

As a final level of complexity, microglia were cultured with astrocyte-OPC co-cultures to produce proof-of-concept *'mixed glial constructs'* containing all of the supporting neuroglial sub-classes together. However, the production of these constructs further increased the difficulty of simultaneously imaging all the cell types present, as only three fluorescence channels were available. In the first instance a commercial cell staining kit was tested, with the rationale that each cell could be labelled with a separate dye before seeding onto the constructs. The kit consisted of three carbocyanine dye solutions (DiI, DiD and DiO), each with a different fluorescent colour. Each dye is lipophilic, so they were separately incubated with cells in suspension. Optimal incubation lengths were determined with astrocytes and DiD, as a basis for the remaining neuroglial cell sub-types and dyes, with performance readouts of extent of membranous labelling and the intensity of fluorescence signal observed. At 20 min of incubation the cellular staining was punctate, which was also verified with OPCs stained with the DiO dye. Also fluorescence bleed-through from the red/green channel was observed, which was increased at 25 min. Although, evidence of elongated stained cells was observed by 24 hours, the aforementioned problems, in addition to the inherent reduction in signal strength with continued culture and cellular proliferation, suggests the use of these dyes are ineffective and unsuitable for identifying multiple cell populations after short-term culture on constructs. A relatively simple solution to the overall imaging problem was the labelling of the nuclei of microglia with DAPI (a robust

and widely-used stain) before seeding onto mature, eight day co-cultures, containing multiple neuroglial subtypes that had been successfully imaged previously. To a suspension of microglia in culture medium, DAPI was initially added at 20 µg/mL, incubated for 15 min and re-suspended twice in fresh medium. However, the DAPI leached into the surrounding cells during the culture period (4 h), so the concentration was reduced to 10 µg/mL, the incubation time increased to 20 min and a further re-suspension in fresh medium performed to remove any remaining dye. No leaching was subsequently found and microglia had attached with some evidence of elongation four hours post-seeding. Constructs were fixed, stained and placed on glass slides in mounting medium without DAPI.

2.3.6. Characterisation of single nanofibre layer co-culture experiments (astrocytes and OPCs ± microglia)

The majority of OPCs seeded on control hydrogel constructs containing astrocytes pre-seeded for two days displayed rounded morphologies and lacked bipolarity (**Figure 13A**). By contrast, the addition of OPCs to nanofibre-hydrogel constructs containing pre-aligned astrocytes dramatically promoted OPC survival, attachment and elongation over the subsequent two days of co-culture. Cells with the distinctive bipolar morphology of OPCs with evidence of cell proliferation on nanofibres could be clearly observed from 24 h (**Figure 13B** & inset). An analysis of the aspect ratios of individual OPCs co-cultured with astrocytes shows morphological profiles similar to aligned astrocytes (**Figure 13C**). Classification of the distributions of astrocyte and OPC aspect ratios (**Figure 13D**) reveals a greater proportion of astrocytes displaying ‘high’ aspect ratios. The bipolar profiles of OPCs

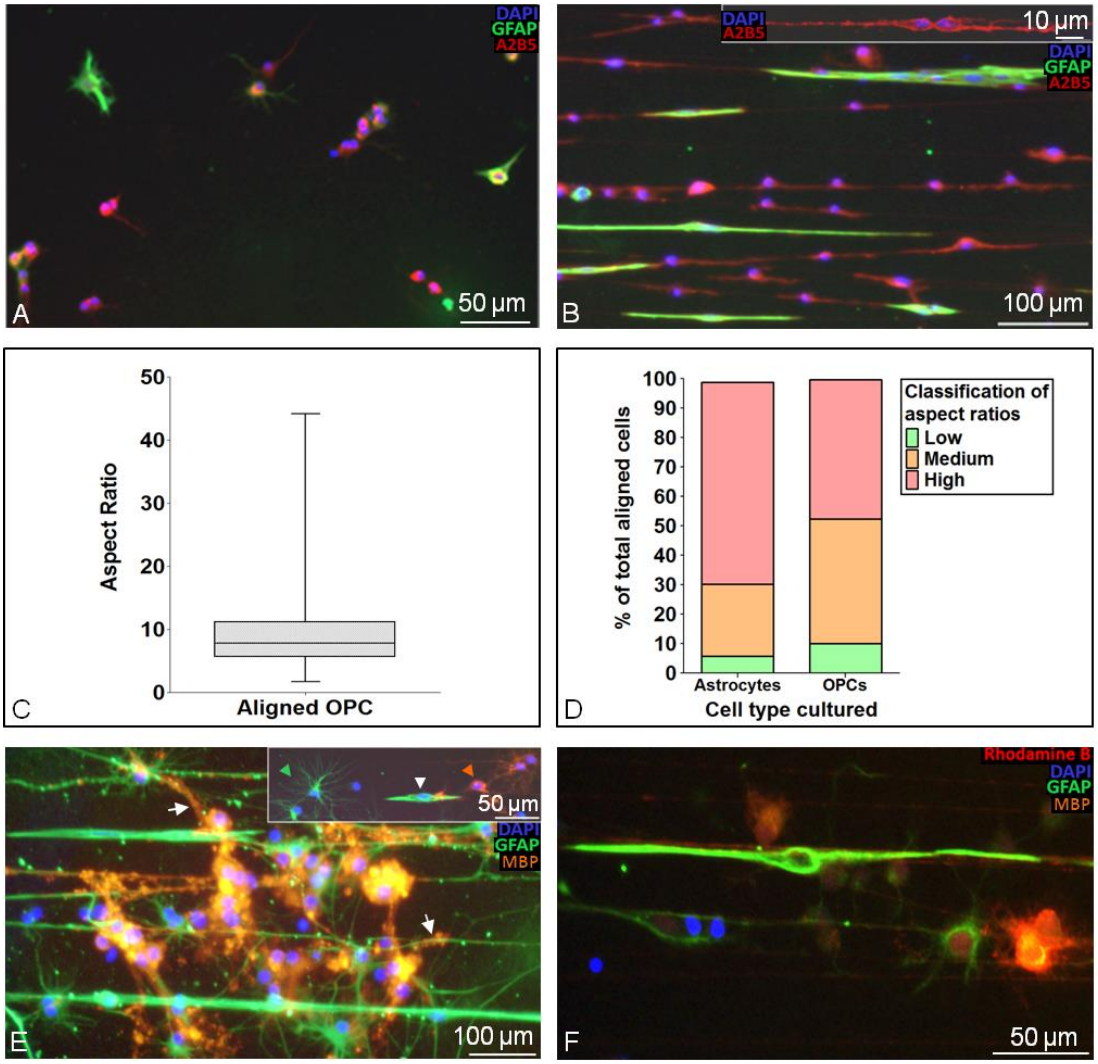

Figure 13. Increasing the cellular complexity of nanofibre-hydrogel constructs.

(A) Fluorescence micrograph of control hydrogel constructs pre-seeded with GFAP$^+$ astrocytes for two days, followed by two days of co-culture with A2B5$^+$ OPCs. (B) Fluorescence micrographs of OPCs and pre-seeded astrocytes on nanofibre-hydrogel constructs cultured for the same time as controls (inset showing OPC proliferation). Note the bipolar phenotype of the precursor cells. (C). Aspect ratios of individual OPCs cultured on nanofibre-hydrogel constructs containing pre-aligned astrocytes. (D) Classification of the aspect ratios of astrocytes and OPCs cultured on nanofibre-hydrogel constructs. (E) Fluorescence micrographs after eight days of co-culture, showing the co-existence of astrocytes and oligodendrocytes on

*nanofibre-hydrogel constructs with presence of complex, highly processed, membrane-elaborating phenotypes, characteristic of mature oligodendrocytes (for comparison, see precursor forms in **Figure 13B**). White arrows indicate potential contacts between aligned oligodendrocytes and astrocytes. (Inset) Clear morphological distinction between type II astrocytes (green arrowhead; left), type I astrocytes (white arrow; centre), and oligodendrocytes (red diamond arrow; right) within the same microscopic field. (F) Fluorescence micrograph demonstrating the assembly of mixed glial constructs, containing both GFAP$^+$ type I and type II astrocytes, MBP$^+$ oligodendrocytes and DAPI-stained microglia.*

---

with 'low' aspect ratios were more distinguished than the counterpart profiles of type I astrocytes, typically containing much finer processes that accentuated the circular shape of the cell body. When the period of astrocyte-OPC co-culture was extended to eight days, OPCs displayed the potential to differentiate into complex process-bearing MBP$^+$ oligodendrocytes elaborating large sheets of membrane. Such cells appeared to contact both nanofibres and pre-aligned astrocytes (**Figure 13E**). Astrocytes with distinct type I and II morphologies could also be found (**Figure 13E** inset). Additionally, it was feasible to further enhance the cellular complexity of the constructs with seeded primary microglial cells that showed significant attachment and survival following co-culture with the above glial populations over a four hour culture period (**Figure 13F**).

2.3.7. Scale-up and optimisation of 3-D constructs containing multiple layers of nanofibres

2.3.7.1. Optimisation of construct assembly

The filter frame and the hydrogel base of the multiple layer constructs were kept identical to that optimised for single layer constructs (12-well plate design size). A template was made for the reproducible production of the spacers, as inaccuracies in their shape increased the difficulty of placing them in the correct position around the cell seeding window of the filter frame. With regards to the nanofibre meshes fabricated, the nanofibres remained on a level plane following storage but the acetate frames *per se* were found to contort parallel to the direction of nanofibre alignment (**Figure 14A**). When placed over the base, the elasticity of the acetate frames made them spatially unstable which prevented the reproducible layering of the meshes and the accurate application of defined volumes of seeding solution. A second acetate frame was adhered to the underside of the nanofibre frame to decrease the flexibility and to keep the whole nanofibre frame level (**Figure 14B**). An added benefit of the second frame was that it shielded the forceps from the adhesive, which adhered to the forceps as a repercussion of using more adhesive to hold the high density meshes in place (compared to nanofibre sheets) and increased the difficulty of placement over the construct. Thus these modified nanofibre frames were significantly easier to use during the assembly protocol and improved the reproducibility of the constructs formed.

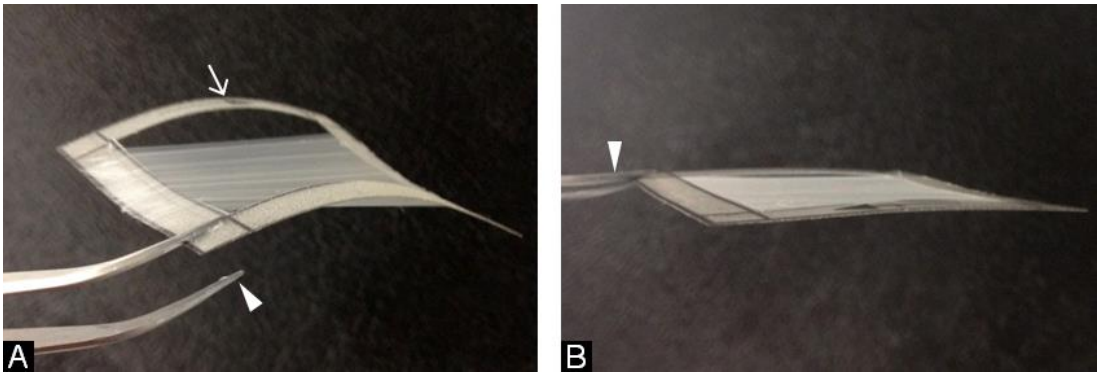

Figure 14. Improving acetate frame stability to fabricate multiple layer nanofibre-hydrogel constructs. *(A) Nanofibre meshes were adhered to a single acetate frame and found to contort parallel to the direction of nanofibre alignment (white arrow). The extra adhesive applied (in comparison with frames containing nanofibre sheets) adhered the frame to the forceps (white arrowhead). (B) Joining another acetate frame to the nanofibre meshes stabilised the frames during storage and shielded the adhesive from the forceps (white arrowhead), so that the frames could be placed over constructs easily.*

2.3.7.2. Development of a sequential cell seeding protocol

Astrocytes were seeded immediately following the placement of each nanofibre mesh layer onto constructs. It was found that doubling the number of cells applied per layer to 1.2 $x10^4$, from 6 $x10^3$ in single layer construct experiments, aided the visualisation of cellular alignment across multiple nanofibre layers. The increase in nanofibre line density compared to single layer constructs produced a more hydrophobic surface, which helped sequester the seeding solution of 60 µL over the seeding area. However, this concurrently increased the technical difficulty of spreading the solution, so approximately half was applied first to wet the area. The

technical difficulty associated with performing this step increased for the nanofibre mesh layers applied thereafter, as they were loosely suspended over the base. Additionally, there was a tendency for the solution to penetrate through to the mesh layer/s underneath, which occasionally occurred before the volume had been spread over the whole seeding area. An increase in seeding volume to 120 µL (at half the cell concentration) for the second and third layers ensured there was enough volume to apply over the seeding area when this occurred, but not too much in total that it overflowed from the construct. The seeding solutions required removal with an aspirator tip applied to the edge of the base filter frame after incubation, prior to the addition of the next nanofibre layer, to prevent the flow of solution off the construct. Cells were seeded onto each layer at intervals ranging between 40 to 120 min, although the former duration was considered long enough to permit the attachment of cells without unnecessarily increasing the total duration that the cells were kept in suspension, for seeding onto the final layer.

Three hours after seeding cells, 200 µL of collagen hydrogel was added over the top nanofibre layer to stabilise the multiple layered structure. This was two hours later than initially anticipated to facilitate the attachment of cells to the nanofibres in each layer. The use of the aspirator to remove the final seeding solution critically prevented the dilution of the hydrogel, facilitating the formation of a solid construct. It was advantageous to leave the hydrogel for two hours before the acetate frames were detached from the constructs, to ensure the hydrogel had fully cured and to reduce the duration before culture medium was applied, maximising cell viability and the hydration of the construct for culture.

2.3.7.3. Development of a nanofibre frame cutting tool

A scalpel was used to detach the nanofibre mesh layers from the acetate frames with the same technique applied for constructs containing a single nanofibre sheet layer. However, this was a challenging step due to the large increase in the number of nanofibres compared with nanofibre sheets, as a result of the increased line density and the number of layers. This influenced the reproducibility of nanofibre detachment from the acetate frames, which resulted in disruption to the nanofibre configuration within the construct following frame removal. The extra stability provided by the relatively large volume of hydrogel used to seal the nanofibres, compared to single layer constructs, failed to prevent this disruption from occurring. Thus, a tool was designed to surround the entire construct and cut down on all of the nanofibres at once. Furthermore, with the tool pressed down it could protect the nanofibres attached to the construct, allowing a scalpel to be used in conjunction to ensure the complete the detachment of all nanofibres around the perimeter of the tool before frame removal. Additionally, to maintain the sterility of cultures the tool needed to be autoclavable and to maintain physical integrity following repeated cycles. The simplest design conceived was four single-edged razor blades fixed in a perpendicular arrangement (**Figure 15A**). The blades were orientated with the sharp edges on the bottom to press the tool down from above and the blades were positioned relative to the size of the construct, the PTFE block and the acetate frame (**Figure 15B**). The detachment of the nanofibres on the PTFE block, compared with the specially designed sections of elongated filter frame (introduced during the optimisation of single layer nanofibre-hydrogel constructs) did not result in nanofibre detachment and a disruption to the aligned configuration. This is likely to be due to the significantly increased line density of the meshes and the increased

support provided by the hydrogel over the construct area. The tool was autoclaved several times and there was no evidence that the integrity was compromised (e.g. blades altering position). Overall the tool and the modified procedure prevented any incidences of nanofibres remaining attached to the acetate frames in this step of the construct assembly.

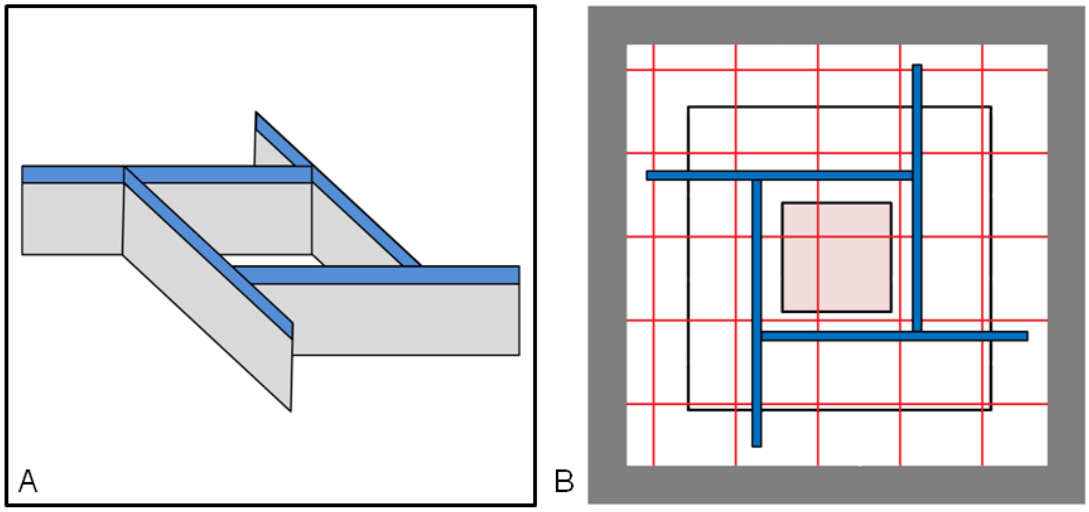

Figure 15. The design of an in-house produced tool to reproducibly cut multiple layers of stacked nanofibre meshes from their acetate frames following collagen construct assembly. *(A) Schematic of the tool consisting of four, single-edged razor blades (grey) that were joined together in a perpendicular arrangement. The metal spine (blue) on the top of the blades allowed the tool to be pressed downwards. (B) Schematic from the position above a partly assembled construct: the tool (blue) placed on a PTFE block (white) around the outside perimeter of a multiple layer nanofibre-hydrogel construct (pink) to detach the perpendicularly stacked nanofibre meshes (red) from the surrounding acetate frames (grey).*

2.3.7.4. Staining and imaging constructs

A three layer nanofibre-hydrogel construct was fixed, immunostained and mounted in a pilot experiment, using the same protocol as that optimised for single layer constructs. The main differences found were the use of considerably greater volumes of mounting medium and coverslip sealant, as a result of the greater thickness of the construct. Despite the satisfactory quality of the immunostaining and visualisation of cells on each layer (**Figure 16**), the use of a live/dead cell viability kit was the preferred option because it: (i) was a more inexpensive staining technique compared to immunocytochemical staining; (ii) was technically easier and quicker to perform; and (iii) gave an added readout of cellular viability after the two week culture period.

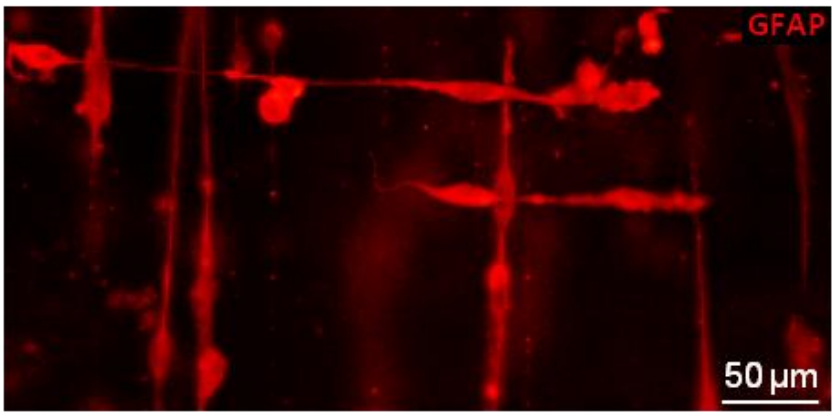

Figure 16. Constructs containing astrocytes seeded over three distinct (stacked) nanofibre layers (orientated in a perpendicular configuration) were successfully immunostained and mounted on a glass coverslip.

2.3.8. Characterisation of multilayer scaffold experiments

A photograph of the final three layer construct produced is shown in **Figure 17A**. Astrocytes were successfully seeded sequentially onto multiple, stacked nanofibre layers (**Figure 17B**). Clear spatial separation of the individual nanofibre layers in perpendicular arrangements and associated astrocyte alignment could be detected in all three layers (**Figure 17C**). Nanofibre detachment was rarely observed and astrocytes were viable in all three layers (> *ca* 70% cell viability).

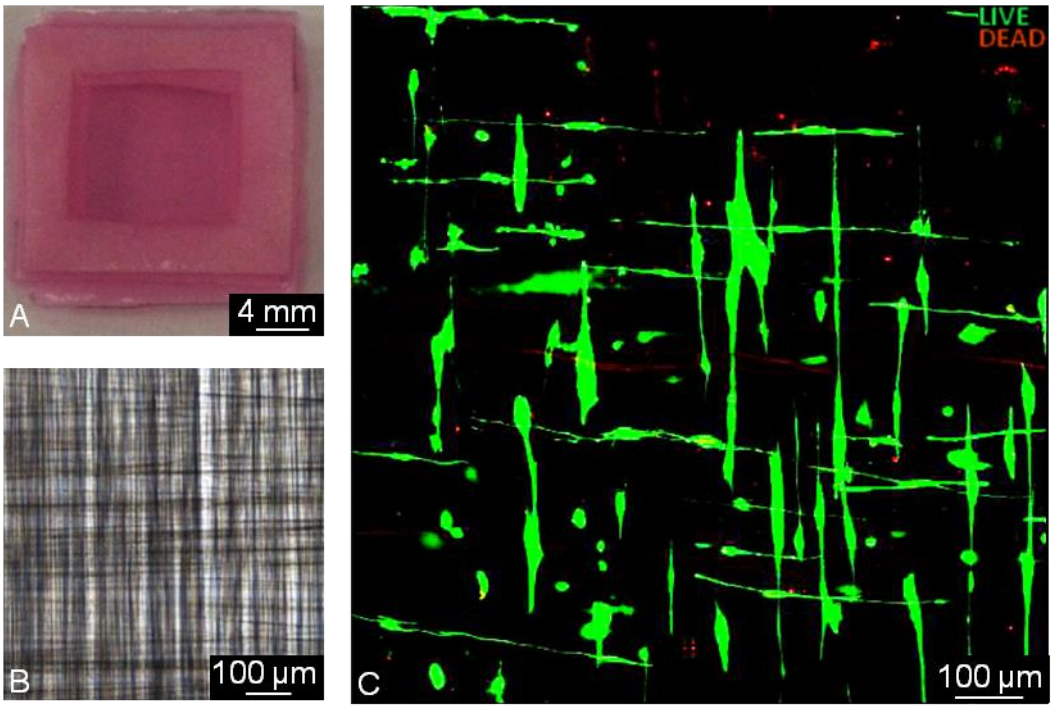

Figure 17. The alignment of astrocytes over multiple nanofibre mesh layers demonstrates the potential to increase the complexity of the produced constructs. *(A) Photograph of the assembled three nanofibre layer construct. (B) Phase micrograph of the nanofibre meshes, stacked perpendicularly in constructs. (C) Superimposed fluorescence micrographs of the three nanofibre mesh layers taken at depths of 30, 120 and 250 µm, showing live/dead stained astrocytes after*

two weeks of culture. Cellular alignment with three distinct (stacked) nanofibre layers orientated perpendicular to each other is observed.

2.4. Discussion

This is the first report of a nanofabricated 3-D scaffold for neural applications with the nanofibres arranged through the depth of the structure as the principal topographical cue. It represents an enhanced order of spatial complexity compared to other nanofibre scaffolds reported to-date.[54] Additionally, for the first time, primary astrocytes and cells of the oligodendroglial lineage were co-cultured together on nanofibre scaffolds by exploiting the ability to co-culture neuroglial cells, generated from mixed glial cultures, within a single medium. Both the astrocytes and OPCs survived, proliferated and aligned with the nanofibres in co-culture, attaining lengths far greater in magnitude than previous reports.[60,139] This illustrates the strong potential of nanofibres as a strategy to promote the directional growth of a range of glial cell types. The significant attachment and survival of seeded primary microglial cells to the constructs containing co-cultured astrocytes and oligodendroglia demonstrates the potential to further enhance the cellular complexity, producing a complete system of CNS supporting glia. The potential to scale up the co-cultures with the alignment of astrocytes over multiple stacked nanofibre layers further demonstrates the utility of the technique for neuro-regenerative applications.

2.4.1. Optimisation of nanofibre-hydrogel construct assembly for neuroglial cell culture

It was clear from the pilot studies that the existing assembly methodology and design of nanofibre-hydrogel constructs required optimisation. The identification of factors that were critical to the viability of cells and their interaction with nanofibres prompted a change in the sequence of steps to orchestrate a reproducible and efficient assembly procedure. The design features added to the filter frame reduced incidences of experimental error inherent in the more challenging methodological steps, whilst the reduction in filter size facilitated the culture of constructs in smaller chambers, thereby reducing the costs of production, culture and staining. Refinements made to the basic storage and handling of the collagen hydrogel enhanced the quality and robustness of assembled constructs, and reduced the influence of the ambient temperature on reproducibility. The in-house produced nanofibre mesh cutting device was an effective solution to simplify the task of detaching the multiple layers of nanofibre meshes from their acetate frames, whilst preserving the aligned arrangement of nanofibres within the construct. Further, it highlights the opportunity to design novel, bespoke tools and solutions to improve the reproducibility of more difficult procedures. The final innovation was the production of fluorescent nanofibres to facilitate the visualisation of cellular attachment and alignment with the topographical cue, which was invaluable for the optimisation of construct design and performance and the robust analysis of cell aspect ratio. Additionally, it facilitated the identification of cells that were unattached to the nanofibres but had elongated parallel to the orientation of nanofibre alignment from the analysis, thus eliminating incidences of type I statistical error.

2.4.2. The contrasting viability of OPC and astrocyte mono-cultures

The survival/elongation of OPCs seeded as a single population on both nanofibre-hydrogel constructs and control hydrogels was limited and the reasons for this are unclear. OPCs have previously been cultured on nanofibres as mono-cultures, with survival and differentiation into mature MBP^+ oligodendrocytes (albeit on 2-D coverslips).[147,148] Furthermore, the observation that the majority of astrocyte and OPC co-cultures on control hydrogel constructs remained rounded with a failure to extend processes suggests that the collagen hydrogel *per se* could have been an unfavourable environment for growth. This may be related, at least in part, to the compliance of the hydrogel substrate. Previous reports have shown that astrocytes show normal assembly and organisation of the actin cytoskeleton, with a larger area of spread, on less compliant culture substrates (greater than c.a. 2 kPa), compared to softer substrates below 1 kPa where the cells appear rounded and viability is significantly reduced.[149] This is also in accordance with the rapid attachment to coated tissue culture plastic that has a high stiffness[150] and the formation of the astrocyte bed layer in mixed glial cultures.[146] It is reasonable to assume that the nanofibres provided a stiffer substrate for support of the astrocytes and therefore the improved viability was observed on nanofibre-hydrogel constructs compared to controls without nanofibres, as judged by evidence of proliferation and extensive elongation of processes on nanofibres *versus* the controls that showed morphologies typical of astrocytes cultured on compliant surfaces. The Young's elastic modulus of the 3 mg/mL collagen hydrogel ± nanofibres requires testing in order to further corroborate this hypothesis and characterise the interactions with the cultured cell populations. Interestingly the optimal substrate compliance for the survival and proliferation of OPCs *in vitro* is $\leq$1 kPa,[151] which falls within the range where

astrocytes exhibited poor survival. Furthermore, the outgrowth of DRG neurites grown on 3-D gels is optimal at very low compliances comparable to that of CNS tissue,[149] so it demonstrates the need to co-culture mixed populations of neuroglia with neurons to determine the optimal substrate compliance for all the cells to co-exist in culture together. Nonetheless, the significant survival and alignment shown by OPCs following co-culture with astrocytes is an observation that is consistent with the major supporting roles played by astrocytes *in vivo*[152] and in mixed glial cultures as the supporting bed layer,[146] suggesting that aligned astrocytes may provide survival cues for OPCs. Indeed, platelet-derived growth factor and leukemia inhibitory factor present within astrocyte conditioned medium have been shown to promote the survival of OPCs *in vitro*[153] and insulin-like growth factor-1,[154] ciliary neurotrophic factor[155] and neurotrophin-3[156] of astrocyte origin have all separately been shown to support OPC survival.

2.4.3. Increasing the complexity: towards the development of a 3-D multicellular implantable scaffold for repair of SCI

Repair strategies consisting of scaffolds with aligned topographical features, in combination with therapeutic cell populations have the potential to direct and enhance the otherwise randomly orientated, limited growth of spared nerve fibres from the margins of spinal cord lesions. In the initial development and testing of various aligned scaffolds, populations of cultured astrocytes are commonly used: as a promising cell type for transplant therapies; as a predictor of material compatibility for the culture of neural cells; and for assessing the potential of the material to align neural cells. However, there has been little focus on aligning the other supporting

glial cell populations, such as the cells of the oligodendrocyte lineage, which is surprising given the neuroprotective effects exerted by oligodendrocytes and their potential to enhance functional recovery through myelination of regenerating nerve fibres. Furthermore, aligned Schwann cells have been shown to enhance peripheral neuronal cell migration and myelination.[157]

In this study, astrocytes aligned with nanofibres showed a far wider distribution of aspect ratios and higher median values than previous reports and the OPCs showed a similarly high potential for alignment and elongation. This corroborates previous results that have demonstrated aligned nanofibre scaffolds are particularly capable of enhancing the directional growth of supporting neural cells.[60,68,127] Increasing the spread of the glial cell populations over the length of the construct should maximise their availability for interaction with host regenerating nerve fibres across lesion sites. The populations of astrocytes and mature oligodendroglia present following the extended culture period suggest that the constructs have significant capacity to support the growth and development of a range of neural cell types. Further investigation is required to determine whether a sub-population of OPCs remained on the constructs and the proportions that differentiated towards mature oligodendrocytes or type II astrocytes.

The attachment of microglia to the constructs further enhanced the glial complexity achieved, producing a complete and potentially repair-mediating neuroglial cell supporting system. However, to test the potential in relevant models of SCI, further work is required to replicate the glial cell co-cultures over multiple nanofibre layers, towards the production of an implantable device. Proof that the number of constituent, stacked nanofibre layers could be scaled up was demonstrated with the alignment of astrocytes over three nanofibre mesh layers. However, to

increase the spatial complexity of constructs intended for SCI models *in vivo*, the nanofibre packing density would need to be much lower to permit the infiltration of host tissue within each layer. Further, these multiple layer constructs would require pre-assembly in order to increase the cellular complexity, using the sequential seeding protocol for the production of mixed glial constructs. In this context, other seeding protocols could be investigated as alternatives to obtain maximal glial cell viability, such as the simultaneous seeding of all the cell populations within the hydrogel seal itself.[133] Following the optimisation of these steps, further work is required to process the constructs into an implantable form. This includes plastic compression of the constructs, which essentially expels a large quantity of excess fluid within the collagen hydrogels, drastically increasing the density of cells and collagen within the construct whilst reducing the overall thickness.[158] Further viability testing would be required following this step, although previous findings have shown that the impact of this technique was minimal on astrocyte populations within hydrogels.[60] Removal of the filter frame and the rolling of the constructs into a tight tube would constitute the final stage in preparation before insertion into a relevant injury model.

2.4.4. Conclusions

It is feasible to enhance the complexity of nanofibre-based constructs to include multiple elongated, glial cell populations and scale-up the number of constituent nanofibre layers. The next chapter builds on the theme of enhancing spatial and cellular complexity, by developing a 3-D, multicellular *in vitro* model of SCI that replicates cardinal features of injury *in vivo* for screening the regeneration-

promoting capacity of combinatorial repair strategies, such as the construct developed here.[a]

[a] A considerable amount of data in this chapter has been accepted for publication by *Nanomedicine (NBM)*. The article is included here as Appendix 1. Also an image from the study was used as Biomedical Picture of the Day, included as Appendix 2.

Chapter 3: Development of a complex 3-D *in vitro* model of SCI

3.1. Introduction

The absence of significant functional recovery following SCI is due to the inhibitory environment that is non-permissive to axonal outgrowth and the limited intrinsic repair capacity of the spinal cord. As discussed in section 1.1.2, a mechanical insult to the vertebral column in the form of a blunt force or penetrating object causes the primary injury to the spinal cord. Possible mechanisms of injury include: shear or compressive forces; dislocation; fracture; and laceration. The extent of the structural damage induced is dependent on the particular mechanism, but generally includes a combination of the severing of axons; disruption to the vascular system, leading to more wide-spread swelling and ischemia; and the necrosis of neurons and glia. The disruption initiates a range of pathophysiological changes that progress in both rostral and caudal directions from the lesion epicentre over the following days to months, termed the secondary injury.[18] With respect to the stereotypical cellular responses following the primary injury, microglia, the immune-competent cells of the CNS, become activated in response to the damage. They display 'activated' morphologies (characteristically rounded phenotypes, in contrast to 'resting' microglia with multiple ramified processes), release pro-inflammatory cytokines and infiltrate lesion sites, where they are responsible for the phagocytosis of cellular debris and toxic substances.[21,22] Astrocytes, which perform many homeostatic roles crucial for the optimal function of the nervous system, become hypertrophic, proliferate and upregulate expression of GFAP within and adjacent to lesions, to form a scar which constitutes a critical physical barrier to axonal regeneration.[26] Neurons undergo necrosis and Wallerian degeneration due to the primary insult, the unfavourable extracellular environment (excitotoxicity, ionic dysregulation, free radicals and factors secreted by cells)[14,19] and a lack of trophic

support resulting from the demyelination of nerve fibres.[159] Limited, spontaneous sprouting of nerve fibres may occur from lesion margins, although the extent and duration is dependent on the particular neuronal tract and the age of the animal.[160]

Over 100 years have passed since the first experiments were performed in animals to re-create SCI in the controlled setting of a laboratory.[161] Complex experimental models of SCI in live animals mimic the biological sequelae of human SCI, and have therefore been essential to our understanding of the intricate pathological mechanisms that cause chronic injury. Furthermore, modern pre-clinical injury models have shown the potential of synthetic constructs within the field of regenerative medicine to enhance repair following delivery into sites of injury.[99,162] These preliminary readouts of safety, mechanism(s) of action, and functional and behavioural improvements are necessary for further development and optimisation of constructs prior to first-in-man studies. The injuries that current models can mimic are: compression and/or contusion; complete or partial transection; and ischemia. Compressive/contusive injuries are seen most commonly in patients and therefore have the widest clinical relevance.[11] However, each different model has its own specific advantages. Transecting injuries provide the most effective testbed for assessing anatomical regeneration of axons and readily permit the implantation of synthetic devices of a defined size, while ischemic insults produce a unique type of injury, often leading to paraplegia, spasticity and rigidity.[163]

It should be noted that there are several ethical and practical drawbacks relating to animal experimentation in the context of neurological injury. The production of such injury models can be a highly invasive and time consuming process, usually requiring high technical expertise. Depending on the model, the procedures can result in serious adverse effects such as infections, paralysis or

movement disorders, bladder dysfunction and so on.[164] Even in the hands of a skilled operator, surgical procedures can inherently generate significant inter-animal variability, requiring large animal group sizes for statistical validity.[164] Following lesion induction, introduction of synthetic constructs into injury areas usually requires re-anesthetization, with the second procedure involving similar risks to the induction of the original injury. *In vivo* models necessitate the use of analgesia and rigorous post-operative monitoring of animals, which must be housed individually.[119] The requirements for specialist staff and infrastructure in particular, place major financial constraints on such work.[165,166] All of these considerations have prompted the global drive for the Reduction, Replacement and Refinement of animal experimentation (the 3R's principle).[167] In particular, there is a major current need to develop facile, high-throughput *in vitro* models that mimic pathological features of injury sites *in vivo* (and therefore have biological validity), in order to reduce animal usage and suffering, as well as costs and technical difficulty, thereby facilitating the screening of pro-regenerative materials.

Despite the need for such biologically-relevant testing systems, 'reductionist models' described to-date typically lack the ability to mimic multi-faceted components of SCI pathology and the complexities of cytoarchitecture *in vivo*.[11] The CNS is a particularly challenging tissue system in this regard, due to the complex cellular dynamics and intricate (cardinal) pathophysiological events displayed after neurological injury, as detailed above. Nonetheless, 2-D reductionist tools in current widespread use, e.g. microfluidic devices, have provided useful insights for tissue engineering, as these permit the study of fundamental, isolated aspects of neuronal regeneration and response to materials/biomolecules post-injury,[41,42] without the potentially confounding reactions of other cell types. Additionally, reports

demonstrating the ability to increase the complexity of the culture systems, e.g. spatial complexity,[168,169] show the integrity of such injury paradigms and the value of their predictions, despite the differences in complexity compared to live animal SCI models.

Multicellular, 3-D organotypic slice cultures (slices of immature tissue that develop comparably to the donor organ in an *ex vivo* environment) could offer a solution to the above challenges. For example, such tissue arrays are increasingly being used for long term, high throughput assays in experimental neurology.[170] They provide a versatile bridge between isolated cell culture and *in vivo* experiments (**Figure 1**) wherein the cytoarchitecture of the tissue and structural relationships of cells are maintained, allowing for parameters of neural regeneration, e.g. neuronal survival,[171] nerve fibre regeneration,[172,173] and collateral axon sprouting to be evaluated.[174] These models offer several advantages including the ease of manipulation/observation of *in vitro* preparations.[170] Various ages, neuroanatomical areas and species, including human foetuses[175] and transgenic models,[176,177] can be used as tissue donor sources, offering high flexibility to study neural pathologies and disease mechanisms.

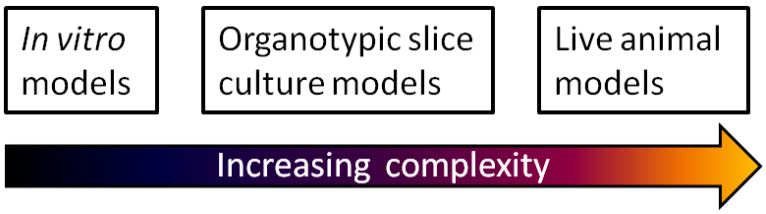

Figure 1. The complexity of published SCI models. *Schematic illustrating the relative complexities of SCI models.*

Slice cultures are amenable to electrophysiological techniques,[178] molecular biology methods,[179] time lapse video microscopy[180] and dynamic confocal imaging,[166,181,182] which has greatly expanded the utility of this approach. Indeed, lesioned organotypic spinal cord slice cultures have been generated as a higher-throughput tool to study specific mechanisms of injury and predict *in vivo* responses to pharmacological agents.[44,166] A summary of the advantages and disadvantages of experimental SCI models is given in **Table 1**.

Table 1. Qualitative comparison of experimental SCI models		
Model	**Advantages**	**Disadvantages**
In vitro	Can establish initial cellular responses to various factors/conditions for proof-of-principle and further development	Lack of complexity limits the predictive value
	Most inexpensive models	
	Examine mechanisms underlying injury and regeneration in isolation	
	Technically simple and rapid to generate	
	Limited ethical issues	
	Can be monitored in real time	
	No regulatory permissions required	
Organotypic slice cultures	3-D slices possess a relevant *in vivo* neurocytoarchitecture and ECM structure	Contain limited vascular components (i.e. blood brain barrier)
	Contain multiple cell populations	Lack of a blood supply (no circulating component of the immune system in response to injury)
	Facile culture and maintenance of multiple slices for weeks/months	
	Can model adult human tissues in development, injury and repair	
	Provides a way of reducing animal usage, according to the 3R's principle of animal use in experimentation	

Model	Advantages	Disadvantages
	Limited ethical issues	
	Can be monitored in real time	
Animal models	Evaluate regenerative processes following device/synthetic construct implantation	High animal usage: - Ethical issues - Technically complex procedures to learn
	Predict the actions and detailed/complex side effects of treatments prior to testing in humans, including optimal doses and the window of application	Procedural problems: - Infection - Technically demanding
	Assess behavioural and neurophysiological responses to treatment i.e. recovery of function	Costly and time-consuming to generate and maintain
	Can replicate the variety of injury mechanisms	Low-throughput screening model for evaluation of repair strategies.
		Variability between animals: - Genetic - Anatomical
		Require regulatory permissions i.e. UK home office licence
		Difficult to monitor in real time

3.1.1. Technological gap: can the complexity of *in vitro* models of SCI be increased for screening material-based repair strategies?

Despite the critical advantages of slice models detailed above, few laboratories have utilised this approach to simulate neurological injury (and subsequent regenerative events). In terms of SCI, three separate models have been reported to-date. Two models of neurotrauma were established by weight drop onto slices, prepared either in the transverse[166] or the longitudinal plane.[183] Whilst these models mimicked some of the responses to injury *in vivo*, overall the characterisation of pathology was basic (e.g. cell death), the type of injury model is only suitable for assessing the effects of pharmacological agents or cells (not biomaterials) and transverse slices are not suitable for the assessment of regeneration in an anatomically relevant orientation (i.e. longitudinally). An additional, basic model of transecting injury in mouse spinal cord slices was described by Bonnici & Kapfhammer (2008).[44] The parasagittal organotypic spinal cord slice cultures were found to maintain ventrodorsal patterning, contain neuronal synaptic connections and undergo myelination *in vitro*. They were able to induce complete transecting lesions in these slices and showed that younger slices with shorter pre-lesion culture times displayed greater endogenous regeneration than older slices and longer pre-lesion culture times. Whilst this pioneering study represents a significant milestone in SCI modelling, the size of lesions induced (100 μm, longitudinally) was sub-optimal for the visualisation and accurate assessment of regenerative events across lesion sites. Further, the model lacked versatility in terms of the induction of a range of lesion sizes and was limited in the ability to model different severities of injury. As detailed above, neurological injury *in vivo* results in stereotypical and cardinal neuropathological responses such as reactive astrogliosis and infiltration of immune

cells, including the resident CNS microglia. These glial responses were not characterised in the above study. Characterisation of the cardinal pathological features following injury was conducted only in neurons and the analysis of the extent of outgrowth was semi-quantitative (subject to interpretation).

3.1.2. Objectives

The aims of this chapter are:-

(i) Primarily, to enhance the versatility of the basic slice model of SCI described above by facilitating the induction of different lesion sizes, in order to cater for a range of model severities. In order to do this, the production and handling of slice cultures was optimised for lesion induction and an in-house tool designed to reproducibly induce complete transecting lesions in slices.

(ii) To characterise and quantify pathological events such as reactive gliosis and immune cell infiltration following lesion induction. The protocols developed were used to conduct quantitative assessments in order to characterise the multicellular response to injury.

(iii) To reduce the cost of producing this SCI model, which may be prohibitively expensive for screening applications. The utility of the model developed here for evaluating the regeneration-promoting effects of synthetic polymer scaffolds is described in Chapter 4.

3.2. Methods

3.2.1. Reagents and equipment

Millicell culture inserts (PICM0RG50), Omnipore^{TM} (JHWP04700) and Isopore^{TM} (HTTP01300) membranes were from Millipore (Watford, UK). Needles (21 gauge) were obtained from BD Biosciences (Oxford, UK). Disposable scalpels and size 15 surgical blades were obtained from Swann-Morton (Sheffield, UK). Rabbit and mouse anti-neuronal class III β-tubulin antibodies (clone TUJ-1) were from Covance (Princeton, NJ), biotin-conjugated lectin (microglial marker; from *Lycopersicon esculentum*, tomato) and monoclonal anti-biotin FITC-conjugated secondary antibodies were from Sigma-Aldrich (Poole, UK).

3.2.2. Organotypic spinal cord slice cultures

Mouse pups aged 0-5 postnatal days (P0-P5) were anaesthetized by cryoanaesthesia and rapidly decapitated, followed by removal of the forelimbs and transection across the lower abdomen with removal of the abdominal organs. The skin surface was sprayed with 95% ethanol, a dorsal midline incision made using a scalpel, and the skin flaps retracted to expose the spinal column along with retraction of the thick dorsal neck muscles to increase the ease of tissue extraction. Next, a midline incision was made along the length of the spine using fine microdissecting Vannas spring scissors (Stoelting UK). A 1.5 cm length of spinal cord was rapidly dissected out from the thoracolumbar region (using the point of attachment of the last true rib to define the upper margin for dissection) and placed in ice-cold slicing

medium [Earle's balanced salt solution (EBSS), supplemented with 100 U/mL penicillin, 100 µg/mL streptomycin and 250 ng/mL amphotericin B, and buffered with 25mM HEPES].[44,184,185] The cord was transferred onto the chopping plate of a pre-set McIlwain tissue chopper and sliced lengthways in the parasagittal plane (350 µm thickness). Slices from the extreme lateral margins of the cord were discarded as these showed a tendency to fragment. Using our procedures, five to seven slices could be derived from each spinal cord. Slices to be used in experiments were selected under a dissection microscope to check for intactness and transferred to pre-cut Omnipore membrane 'confetti', resting on the Millicell culture insert membrane (two/three slices per insert). A wide-bore pipette (plastic Pasteur pipette with the narrow end cut off) was used to facilitate ease of slice transfer. The sectioning procedure from dissection to preparation of slices was rapid (10-15 min), with the entire procedure taking no more than one hour. Slices were cultured at the air-medium interface (**Figure 2**) within 6-well plates, with culture medium [50% minimum essential medium, 25% heat-inactivated horse serum and 25% EBSS supplemented with 36 mM D-glucose, 100 U/mL penicillin, 100 µg/mL streptomycin and 250 ng/mL amphotericin B] for up to 16 days *in vitro* (DIV). Cultures were incubated in humidified 95% air/5% CO_2 at 37^{o}C with 80% medium changes every two days. In all cases the number of experiments, *n*, refers to slices obtained across different animals and litters. Cultures were lesioned at 1-8 DIV and were fixed within 7 days of lesioning. Both 'younger' (P0 mice: lesioned after 1 DIV; fixed 7 days later) and 'older' (P5 mice: lesioned after 8 DIV; fixed 7 days later) models of intrinsic nerve fibre outgrowth were established. A series of improvements were made to the culture and handling of slices (with respect to the procedures described above), which are detailed in section 3.3.1.

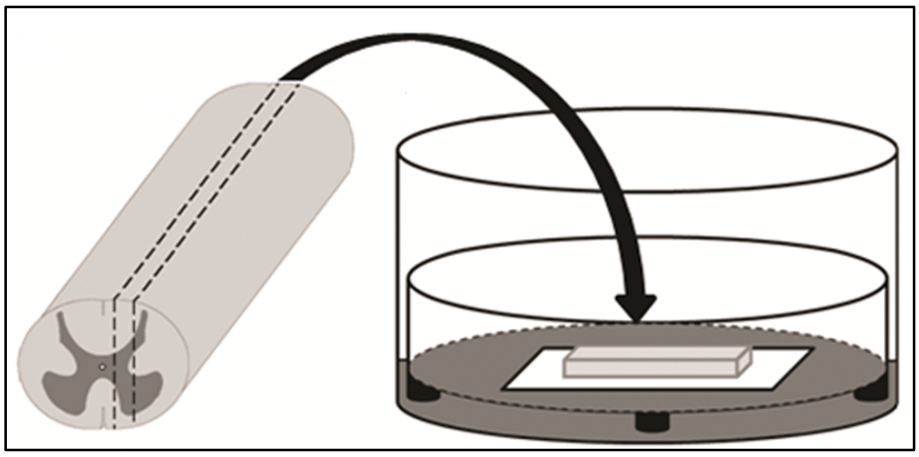

Figure 2. The production of organotypic spinal cord slice cultures. *Schematic diagram illustrating spinal cords cut lengthways in the parasagittal plane and transfered to culture inserts, where they were maintained at the air-medium interface.*

3.2.3. Lesioning spinal cord slice cultures

Tissue was lesioned in preliminary experiments using a basic setup. The aim was to produce a complete transecting lesion of a reproducible size, with regular, evenly spaced lesion margins, in a rapid procedure to prevent the slices from drying out. A dissection microscope (X 40 magnification) was sterilised with 70% IMS, then the sharp edge of a 21 gauge needle (**Figure 3**) was used to lesion slices. Two sequential transecting motions were performed and a ruler used as a guide to generate lesion sizes ≤ 1 mm. However, this was not reliably achieved using this procedure. First, the membrane of the culture insert and the confetti were deformable when pressure was applied and they were regularly inadvertently cut. The resultant gap acted as a barrier to regrowth in the slice, which confounded attempts to

Figure 3. Example of the needle used as the preliminary lesioning tool for slice cultures. *The bevelled edge of the needle tip (21 gauge; 4 cm total length) was used as the cutting edge during lesioning, illustrating the simplicity of the preliminary tool's design.*

measure, for example, the infiltration of microglia into the lesion site. Second, both the confetti and the insert were not fixed in position within the Petri dish and would frequently move during lesioning. Third, multiple transecting motions were often required to completely sever the spinal cord slices, which exhibited variability in the ease of cutting (possibly related to the age of the tissue and the presence of the lining of the spinal canal). These factors delayed the completion of the procedure and most of the preliminary lesioned slices dried out, with adverse effects on viability confirmed by live/dead staining and a more opaque/white appearance evident when viewed with a dissection microscope. However, it was necessary for lesioning to be performed within the culture chamber, as the manipulation involved in transferring culture inserts and/or confetti into a separate dish/holder was found to reduce slice viability and further increase the chances of infection, inherent to these complex procedures. The development and optimisation of the focal lesioning method is discussed in greater detail section 3.3.2.

Additionally, Isopore membranes (Millipore) were evaluated as a replacement to the Omnipore membranes used to produce the confetti, for both the culture and lesioning of slices. They were comparable to the Omnipore membranes because they were hydrophilic, contained a similar pore size (c.a. 0.05 µm smaller) and could be autoclaved.

3.2.4. O-ring slice culture inserts

An alternative method of culturing slices on re-useable 'O-rings' has been published, which is based on the use of a PTFE membrane filter with very similar properties to the commercial insert membrane (also PTFE; pore size 50 nm smaller) and a re-useable O-shaped plastic plate with feet. To prepare O-ring inserts for use, the membranes were placed onto the O-rings and wetted with medium, causing the membrane to loosely adhere to the O-ring. Then confetti was added to the membrane over the central hole (culture area). The suitability of re-useable O-ring slice culture inserts for generating the slice lesion model, including the development of an in-house produced alternative is discussed in section 3.3.4.

3.2.5. Staining and imaging procedures

Both live/dead and immunocytochemical staining of slices were performed following the protocol described in section 2.2.5. However, the duration and temperature of antibody incubations are detailed in section 3.3.1. The blocking solution for lectin consisted of 10% NDS in PBS and for TUJ-1 staining was 5% NDS with 0.3% Triton X-100. Samples were incubated with lectin (1:200) and anti-

β-III tubulin antibody (TUJ-1; 1:1000) in blocking solution, followed by respective Cy3- and/or- FITC-conjugated secondary antibodies (1:160 anti-biotin, otherwise 1:200). Slices were imaged and processed using the protocol as described in section 2.2.6.1.

3.2.6. Analyses

3.2.6.1. Slice viability

An assay was developed to determine the proportions of live and dead cells within the intact slices, using the readouts from live/dead staining and adapting an existing method of quantifying image fluorescence.[186] Slices (P0-P5; *n* = 3) were cultured for 6-16 DIV prior to staining. Corresponding green (live) and red (dead) fluorescence micrographs of a central field within the length of each slice were captured at X 50 magnification and with consistent exposure settings. All micrographs were converted into greyscale and the integrated density (mean grey value per unit area) from both live- and dead-stained micrographs were calculated using ImageJ software (version 1.45s; NIH). The mean control integrated density values from four acellular areas adjacent to the slice was calculated for each micrograph and subtracted from that obtained for the whole micrograph, producing a corrected density value. Thus, the viability for each slice was calculated by expressing the corrected integrated density of the live-stained micrograph as a percentage of the sum total from both stained groups.

3.2.6.2. Lesioning tool blade spacing

To assess the reproducibility of lesioning tool construction, the diameter of lesions induced in slices was investigated across five litters; 3-14 slices in each litter. Fluorescence micrographs of slices stained with DAPI were used to calculate the mean distance between lesion margins from each culture, representing different experiments with independent assembly of the lesioning tool.

3.2.6.3. Astrocyte reactivity analysis

An assay was devised to quantify the relative expression of GFAP (as a function of immunofluorescence intensity) at slice lesion margins versus areas in the body of the slice. P0-P2 slice cultures were established and lesioned after 1 DIV. Slices were left for a further 6 days before fixing and immunocytochemical staining with antibodies raised against GFAP. Each half of a lesioned slice was separately imaged at X100 magnification, with consistent exposure settings across all captured images. Micrographs were converted to greyscale and a grid was merged and adjusted with each image to identify three equidistant and clearly stained points along the length of the lesion margins. The grid points marked the beginning of optical density (OD) profiles that were generated using ImageJ software, and extended 400 µm perpendicularly into the slice body. The three profiles generated from each slice half were adjusted, so that the first OD values began at the lesion margin, and averaged with the corresponding slice half to form a single profile for each slice. A separate region was defined in the body of each slice half, at *ca* 1 mm from the lesion site, which was representative of baseline intensity values, where the $GFAP^+$ astrocytes displayed characteristically un-reactive morphologies and low

GFAP expression levels. A corrected fluorescence intensity profile from the lesion margin of each slice (n = 6) was produced by subtracting the baseline intensity from each value in the averaged trace. Each corrected profile was averaged with traces from the other slices and the average OD in the zones 0-100 µm, 100-200 µm and > 200 µm from the lesion boundary were compared to quantify differences in intensity.

3.2.6.4. Microglial infiltration analysis

An assay was developed to determine whether an acute microglial infiltration occurred into the lesion sites. Spinal cords were extracted from P0-P2 mice, lesioned after 2 DIV and fixed 0, 5 and 10 days post-lesioning (n = 3 per time point). The numbers of lectin-positive (lectin^{+}) microglia were counted within the lesion site of each slice, using a grid overlaid onto each image. The total number of microglia per unit area per slice was averaged at each time point.

3.2.6.5. Statistical analysis

Data were analysed using GraphPad Prism statistical analysis software (version 5.0). All data are expressed as mean ± S.E.M. The number of experiments (n) refers to the number of slices obtained across different animals, often from different litters. **Lesioning tool blade distance analysis**: A one-way analysis of variance with Bonferroni's post-hoc tests was used to assess differences between the blade distances from each instance of tool construction. **Astrocyte reactivity analysis**: the average OD in the zones 0-100 µm, 100-200 µm and >200 µm from the lesion boundary were square-root transformed and compared by a one-way ANOVA

with Bonferroni's post-hoc tests. **Microglial infiltration analysis**: a log-transformation of the average total number of microglia per unit area per slice at each post-lesioning time point (n = 3) was conducted. A one-way ANOVA with Bonferroni's post-hoc tests was used to compare differences.

3.3. Results

3.3.1. Optimisation of organotypic spinal cord slice culture and immunostaining protocols

A series of pilot studies highlighted the need for improvements to the existing methodology of slice preparation, to address: the prevention and containment of infection; the sub-optimal viability of slices; and the post-culture immunostaining of slices. Fungal contamination was a recurring problem during these initial studies, as each insert (up to six per 6-well plate) was repeatedly exposed to air (and contamination) during culture, medium changes, lesion induction and application of treatments, with greater risk of fungal spores from contaminated wells spreading to neighbouring wells. The placement of culture inserts into individual Petri dishes improved their isolation and the use of a large Petri dish to hold up to five individual dishes acted as a further barrier for added protection against the spread of any infection present in the culture. Further, Fungizone (amphotericin B) was introduced into the slice culture medium as a preventative measure, without any negative effects observed on the viability of slices cultured thereafter. Additional steps to improve

containment during the induction of slice lesions are detailed in the following section.

The established live/dead staining protocol provided a good indication of slice viability and guided the optimisation of slice production. As expected, dead cells generated by the slicing procedure accumulated around the edges of the slices during the initial culture (recovery) period.[185] However, the live/dead staining of slices revealed sub-optimal viability, as judged by the presence of considerable numbers of dead cells within the body of the slice (**Figure 4A-C**). The incubation of the slices on ice immediately following the trauma of sectioning from the spinal cord is a crucial step for tissue recovery because it reduces cell death. Increasing the duration of this step from 30 min to 1 h produced slices with reduced numbers of dead cells present in the main body (**Figure 4D-F**). The viability of the slices quantified using the method developed was 96% (± 2%), suggesting that the slices were generated with high viability.

The initial immunostaining protocol produced relatively low fluorescence intensity necessitating optimisation. The incubation lengths of lectin and anti-GFAP antibodies were increased from 16 h to 36 h (at 4^{o}C) to facilitate antibody penetration through the tissue. The NDS component of the blocking solution for lectin was increased to 10% to reduce non-specific background staining during the longer incubation periods. Samples stained with TUJ-1 antibodies were incubated for 24 h at RT to further facilitate the penetration, with no change in the intensity of background staining detected at the increased temperature. Secondary antibody incubations were increased from 2 h at 4^{o}C, to 3 h at 4^{o}C (anti-biotin and GFAP) and 4 h at RT (TUJ-1).

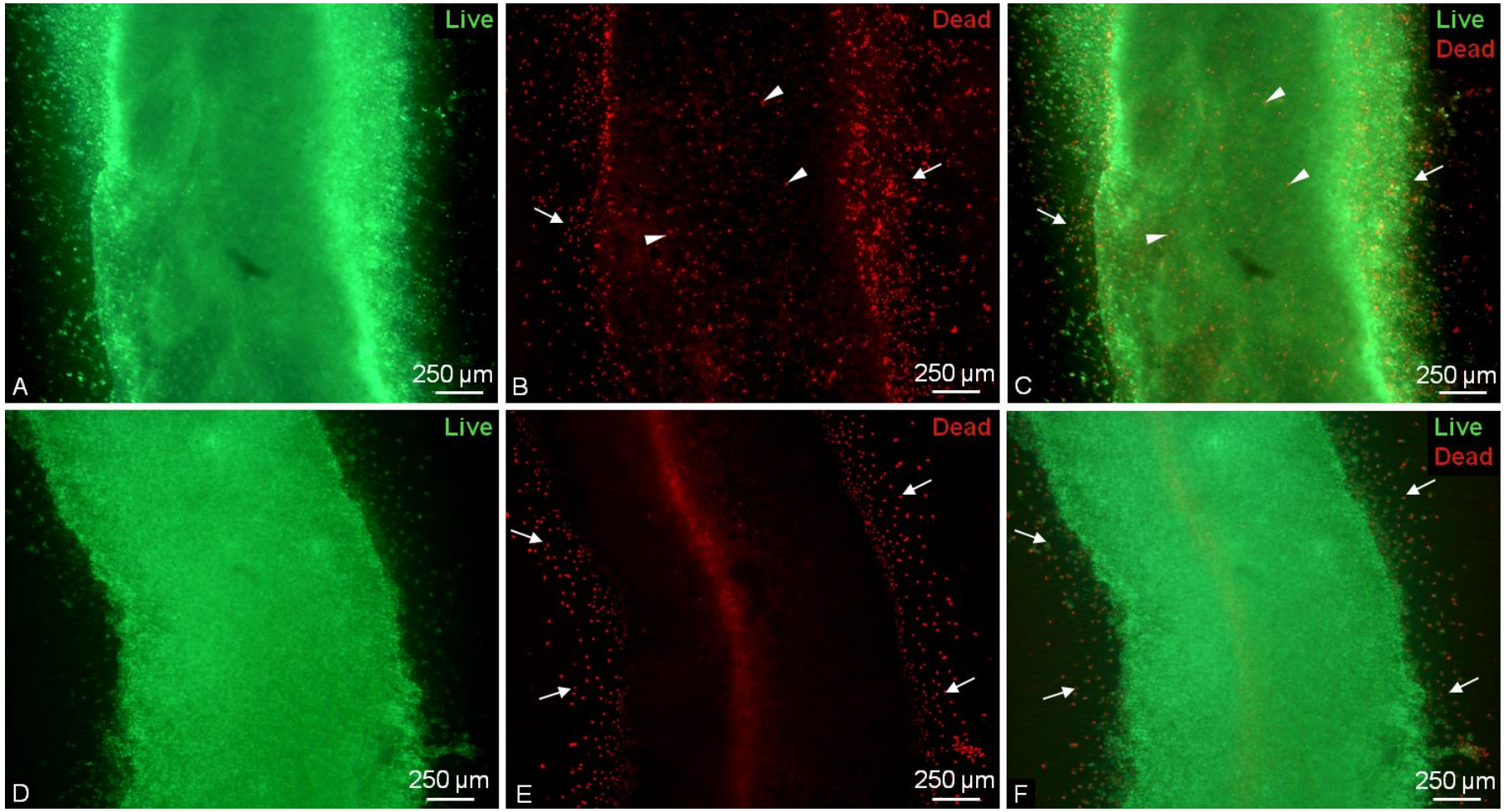
Live
A
250 µm
Dead
B
250 µm
Live
Dead
C
250 µm
Live
D
250 µm
Dead
E
250 µm
Live
Dead
F
250 µm

Figure 4. The contrasting viability of slices following different incubations on ice prior to culture. *(A) Representative fluorescence micrographs of a slice (P5; fixed at 6 DIV; n = 6) incubated on ice for 30 min, stained with calcein for live cells. (B) The same field as (A) with ethidium bromide straining for dead cells. (C) Corresponding merged micrograph of (A) and (B). A considerable number of dead cells were found around the slice edges (white arrows) and in the main body of the slice (white arrow heads), the latter indicative of a slice with poor viability. (D-F) Micrographs of a slice (P5; fixed at 6 DIV; n = 6) incubated on ice for 60 min, with the same stains as (A-C). Predominantly live cells can be found in the main body of the slice with fewer dead cells found in the main body and around the slice edges (white arrows), typical of a slice with good viability.*

3.3.2. SCI model development and optimisation

3.3.2.1. Lesioning protocol optimisation

The first procedural alteration was the use of a dissection microscope with greater magnification (X 12.5), providing superior operator imaging for placement of the tool over the slice, in turn reducing the induction of tears in the confetti. A surgical mask with hair protection was worn during the procedure when the microscope was used, to improve overall sterility. To improve lesioning reproducibility, the shape of the confetti supporting slices (**Figure 5**) was redesigned

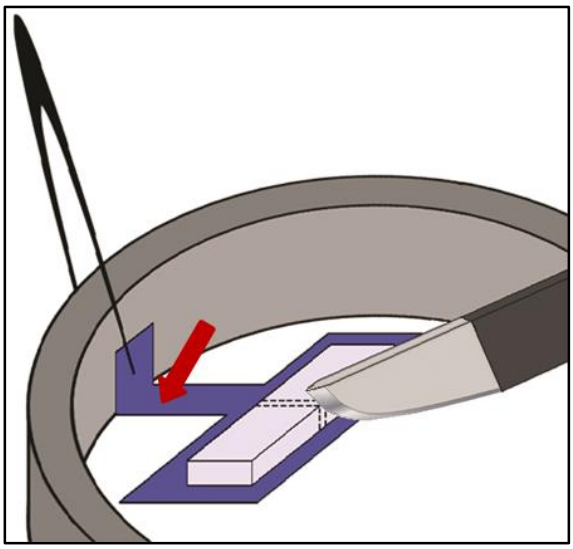

Figure 5. Inducing defined lesions in slice cultures. *Following a defined culture period, slices were lesioned by holding an elongated section (red arrow) of confetti (purple) together with the wall of the insert (grey) using forceps, thus keeping the slice stationary.*

---

to feature elongated tabs on the sides, which facilitated the use of forceps to grip the culture insert wall and confetti together, thus stabilizing the slice during lesioning. An aspirator fitted with a 200 µL pipette tip was found to effectively remove the debris, from the lesion site itself and adjacent to the slice, where most of the debris gathered post-lesioning. Direct aspiration of the lesion site without prior withdrawal of the material to one side often resulted in aspiration of slice parts beyond the transecting cuts and more poorly defined lesion boundaries.

A significant proportion of nerve fibre outgrowth from the lesion margins of a small number of the younger slices appeared to follow the aligned membrane (PTFE) fibres that formed the confetti (**Figure 6**). Ideally the orientation of nerve fibre growth should not be influenced by the culture substrate, to mimic the random

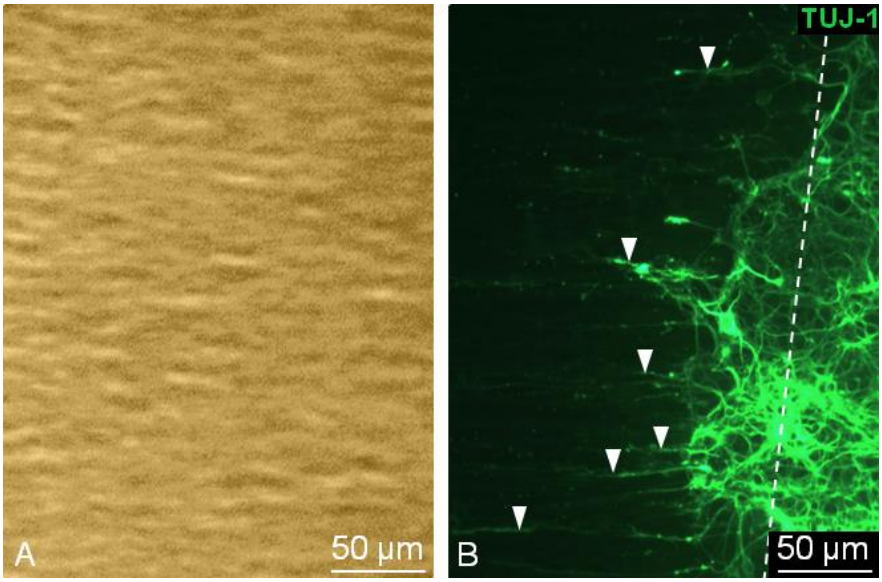

Figure 6. Evidence of nerve fibre outgrowth following the aligned fibres of the confetti membranes. *(A) Bright-field image showing the confetti fibres (aligned left-to-right). (B) Counterpart fluorescence micrograph showing the outgrowth of nerve fibres from a lesion margin (white dashed line) in a P0 slice lesioned at 1 DIV and fixed at 5 DIV. Nerve fibres that appear to follow the direction of the confetti fibrils are marked with white arrowheads.*

---

orientation of outgrowth found *in vivo* and to robustly evaluate the effects of scaffolds with aligned topographies on inducing unidirectional nerve fibre outgrowth (Chapter 4). Isopore membranes were the only alternative available for purchase from the supplier Millipore without a fibrous construction. However, they were more compliant than the Omnipore membranes, which made cutting the confetti to the correct size during setup and their transfer (± slices attached) with forceps extremely difficult. Additionally, they were optically opaque so the informed placement of slices after sectioning was not feasible and further observation during culture and lesioning was not possible until post-culture staining. Therefore a permanent

alternative to the Omnipore membrane was not found. However, it was discovered that wetting the Omnipore membranes with 70% ethanol revealed the orientation of the membrane fibres before they were cut to make confetti. In this way they could be orientated parallel with the lesion margins and the unidirectional growth of any spared nerve fibres due to the confetti fibrils would be instantly recognisable.

3.3.2.2. Development of a lesioning tool

3.3.2.2.1. Preliminary tools

The fine needle (**Figure 3**) adopted as the lesioning tool in preliminary experiments was the least effective of the tools tested, because it was difficult to accurately and reproducibly apply a force to the slice without disturbing the confetti and insert membrane beneath it, which often generated unclear lesion margins. In comparison, the extra sharpness and length of a conventional scalpel blade made it easier to cut across slices. However, all single-bladed cutting instruments required two sequential, parallel transecting motions to produce the injury, increasing the procedural difficulty and lesion size variability, whilst restricting the minimum possible lesion size to approximately 750 µm. In this context, once the first transecting cut was made, inducing the lateral transecting motions close to the first tended to loosen the slice from the confetti. Due to this added difficulty, slices were exposed to the air in the flow hood for long periods and a noticeable reduction in the slice viability was observed by live/dead staining.

3.3.2.2.2. Double-bladed prototypes

A new lesioning tool was conceived based on two thin wires (ca. 50 µm). It was envisaged that they could be adhered to the bottom surface of a holder, with a central space left in the middle to facilitate pressing the tool through the slice. As no such tool was commercially available, one was produced in-house using a tooth pick to fashion a plastic holder and wire from a metal scourer, which was glued to the holder (**Figure 7A**). Two equally spaced parallel grooves were created at either end of the operational side of the tool, in order to hold the metal wires in place (**Figure 7B**), with the distance between them measured using a micrometer. Four prototypes ranging from 250-1000 µm were produced in order to show that they could be maintained less than 1 mm apart. The tool was drawn through each slice with small lateral movements made to ensure the complete severing of nerve fibre tracts. However, the tool did not reproducible generate lesions with straight edges. This was mainly due to the wires used, which: tended to twist, reducing the effectiveness of the cutting surface; did not remain parallel along their length; were prone to moving apart, with greater inaccuracies between them observed at the smaller distances; and were not strong enough to use repeatedly over a number of cultures. Nonetheless, the length of time to lesion the slices was significantly shortened as the procedure was much easier to perform, setting a precedent for future prototypes.

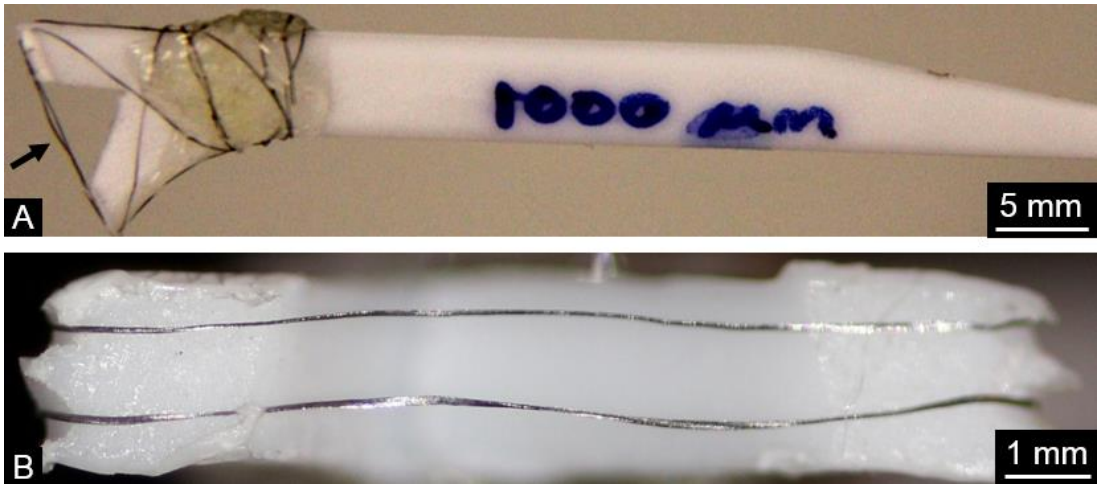

Figure 7. **The first custom-designed lesioning tool prototype with two cutting surfaces.** *(A) Photograph showing a horizontal view of the plastic holder with wires attached to one end with glue. The wires are applied at the intended lesion site with the handle oriented perpendicular to the slice [black arrow indicates the perspective in (B)]. (B) View from below showing the parallel wires with an approximate separation of 1 mm.*

A further double-bladed prototype tool was constructed, consisting of two single-edged blades attached together. This much simpler design, in combination with a reliable cutting surface, was intended to address the problems encountered with the wire tool. However, the blades were far too long to comfortably manoeuvre into position over the slice given the limited space available within the confines of the culture insert while using a microscope to visualise the procedure. Attempts to manually reduce the length of the unused sections of the blades, without sophisticated machinery/methods, proved too difficult due to the strength of the material. Furthermore, a shortened tool would only be re-useable in the short-term until the sharpness of the blades would noticeably deteriorate, requiring a replacement to be produced.

3.3.2.2.3. Final tool design and optimisation

Upon evaluation of the prototypes assembled and their performance during testing, scalpel blades were considered the most effective for the intended purpose, as they are designed to cut through tissue, are inexpensive, come in a variety of sizes and fit a holder that is comfortable to operate by hand. Given these clear advantages a double-bladed prototype was designed to improve upon the advantages of using a single-bladed scalpel. Two surgical scalpel blades (size 15) were taped together to ensure they were fixed in position relative to each other (**Figure 8A**) and glued into an empty scalpel holder. The application of tape in-between the blades was shown to act as a spacer to increase the lesion size induced. This more facile design improved maneuverability, and the sharp cutting edge significantly improved the speed and accuracy with which lesions could be induced. The efficient cutting of the tissue facilitated the complete removal of slice debris in between regular, evenly spaced, distinct lesion margins (**Figure 8B**), which enabled the visualization of regenerative events across lesion sites.

The only improvements made to this prototype were extra steps taken to aseptically assemble the tool with fresh, sterile blades prior to lesioning each slice culture. The sample holder was sterilized in 70% ethanol for 10 minutes and allowed to dry. New pre-sterilized scalpel blades were fixed with tape, placed in an empty scalpel holder and secured inside. Initially it was thought that a spring loaded catch could be used to hold blades in place, facilitating their addition and removal from the holder. However, it was hypothesized that the spring would have to apply considerable pressure on the blades in order to sufficiently fix them in place, so an easier way of achieving the same goal was to fasten them in place with tape and plastic paraffin film (Parafilm).

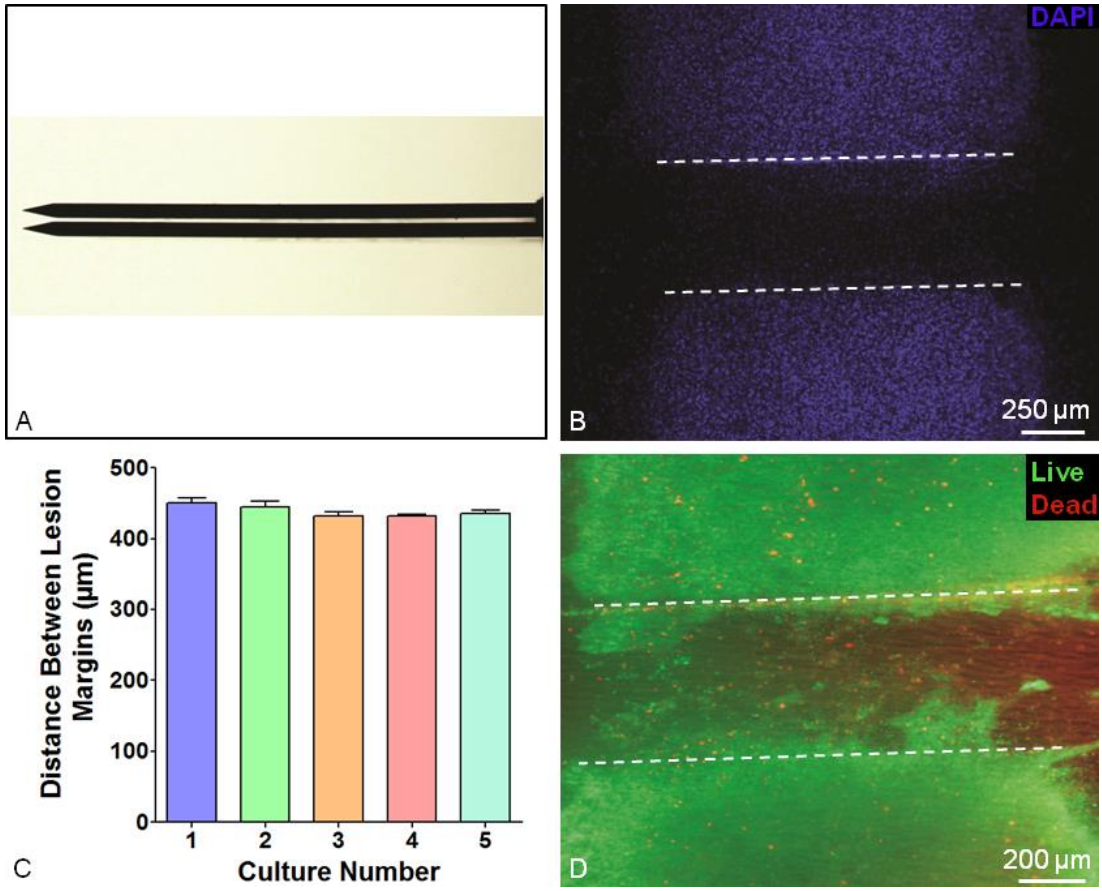

Figure 8. Inducing lesions in spinal cord slices with a double-bladed scalpel. *(A) Photograph of the assembled scalpel blades, demonstrating equal spacing along the length of the blades. (B) A tissue slice stained with DAPI at 2 days post-lesioning, showing clear demarcation of lesion margins (white broken lines). (C) Bar chart of the distances between lesion margins, showing the reproducibility of the lesioning procedure across different experiments (each culture was derived from a separate litter, and five slices were lesioned for each culture;* n *= 5; for each culture, a lesioning tool was freshly assembled). (D) Representative live/dead-stained fluorescence micrograph of a slice 5 days post-lesioning reveals some dead cells within the lesion (white broken lines) with high viability in the main body of the slice.*

Using this tool, the measurements of induced lesions revealed a mean distance of 439 µm (± 4 µm; coefficient of variation = 2 %) between lesion margins, which was highly reproducible across five separate cultures, each representing separate occasions of tool assembly (**Figure 8C**). Live/dead staining of lesioned slices 7 days post-injury (**Figure 8D**) demonstrated that the procedures did not significantly impact overall slice viability for further experimentation, as evidenced by a central band of live cells within the slice body with few dead cells interspersed around the area of injury.

3.3.3. Characterisation of the cardinal pathological responses of cells within lesioned slices

3.3.3.1. Astrogliosis at lesion margins

Clear and even GFAP staining was observed throughout slices; notably, $GFAP^+$ cells at lesion margins were intensively reactive and hypertrophic (**Figure 9A**). These cells differ markedly from $GFAP^+$ astrocytes away from the lesion site, which exhibited normal, polygonal morphologies and fluoresced with lesser intensity (**Figure 9B**). The average GFAP fluorescence intensity profile from the lesion margins across multiple slices is shown in **Figure 10A**. Quantification of the fluorescent intensity profiles shows significantly greater intensity in the first 100 µm adjacent to lesion margins, indicating an increase in astrocyte reactivity (**Figure 10B**).

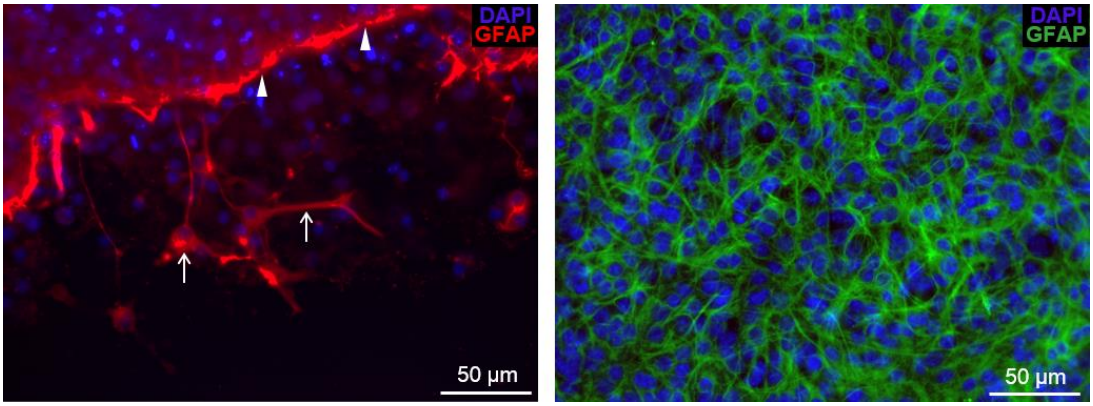

Figure 9. Astrocytes show reactive properties at lesion margins suggestive of astrocytosis. *(A) Representative fluorescence micrograph of a lesion margin 12 days post-lesioning shows intensely reactive astrocytes with increased GFAP (astrocyte marker; arrowheads) expression and hypertrophic morphologies (arrows). (B) Representative fluorescence micrograph of a field within a slice body shows astrocytes with polygonal morphologies and with reduced GFAP expression compared to those at the lesion margins of (A).*

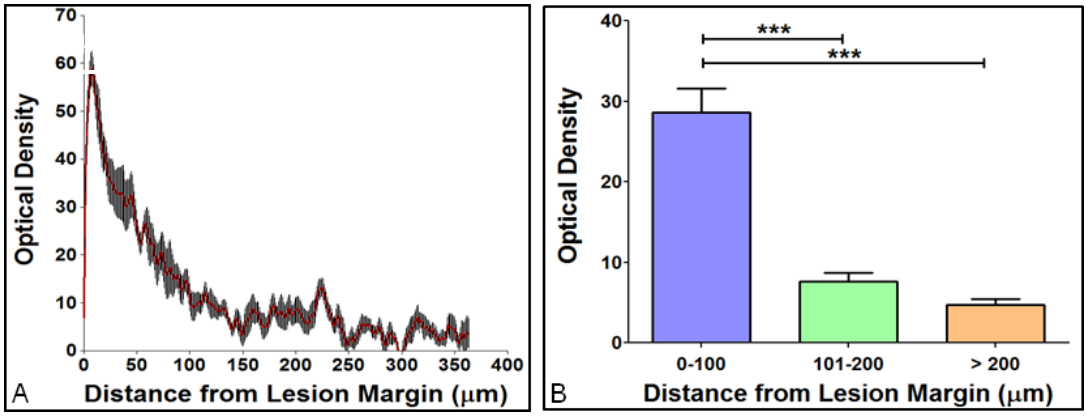

Figure 10. Quantification of fluorescence intensity corresponding to GFAP expression in astrocytes. *(A) Line graph of the mean optical density profiles (red) for GFAP$^+$ astrocytes in six lesioned slices 7 days post-lesioning showing a peak in expression at lesion margins. (B) Bar graph showing a significant difference*

*between the average optical densities for GFAP$^+$ slices between the first 100 µm from the lesion margins and two adjacent regions further into the slice body (one-way ANOVA with Bonferroni's post-tests; ***p < 0.001; n = 6).*

3.3.3.2. Microglial infiltration into lesion sites

Lectin$^+$ microglia were identified in immunostained slices and displayed rounded 'activated' morphologies within the lesion site (**Figure 11A**). In contrast, 'resting' microglia located in the main body of slices exhibited numerous ramified processes. A significant increase in the number of microglia within the lesion site was found at 5 days post-lesioning (**Figure 11B**) with a decrease in number after 10 days.

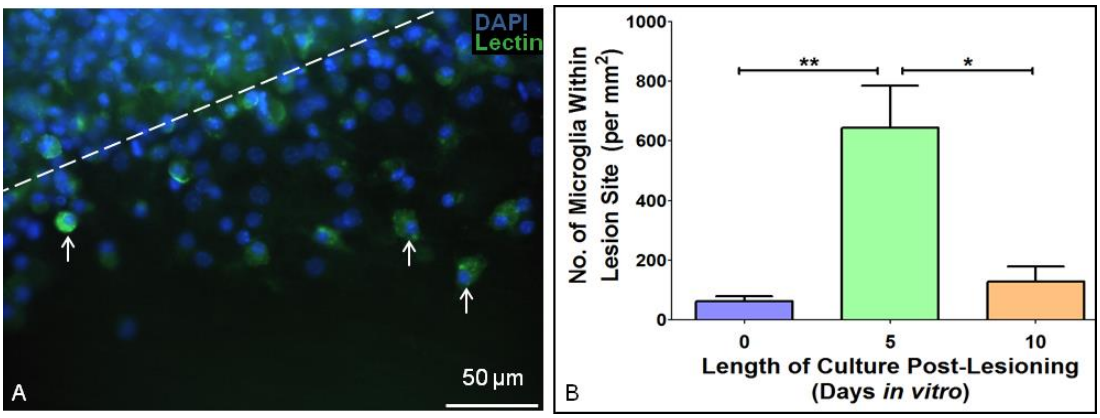

Figure 11. Infiltration of microglia into lesion sites. (A) *Representative fluorescence micrograph of a lesion margin 12 days post-lesioning shows the infiltration of rounded, lectin$^+$, activated microglia into the lesion site (white dotted line: lesion margin). (B) Bar graph quantifying numbers of lectin$^+$ microglia in*

*lesion sites at 0, 5 and 10 days post-lesioning, demonstrating a peak in infiltration at 5 days (*p < 0.05, **p < 0.01;* n = *3 per time point).*

3.3.3.3. Intrinsic nerve fibre outgrowth from lesion margins

After seven days of culture, nerve fibre outgrowth into the lesion within young slices was extensive, randomly orientated and comparable from both margins of the lesion (**Figure 12A**). In each slice approximately half of the area enclosed between lesion margins contained outgrowing nerve fibres, which in some areas joined both slice halves together. By contrast the outgrowth in older slices was relatively limited, but also with random orientations (**Figure 12B**). Nerve fibres were never observed to extend more than one quarter of the distance between the lesion margins (ca. 110 µm) in the central half of lesion sites and the incidences of spontaneous nerve fibre sprouting along the width of the lesion margins was significantly less than in the younger slices. Additionally, a sub-population of TUJ-1^{+} cells displayed the morphological phenotypes of spinal cord interneurons (**Figure 12C**), which were particularly evident along the lesion margins of the older slices due to the lower density of nerve fibre outgrowth present in this region.

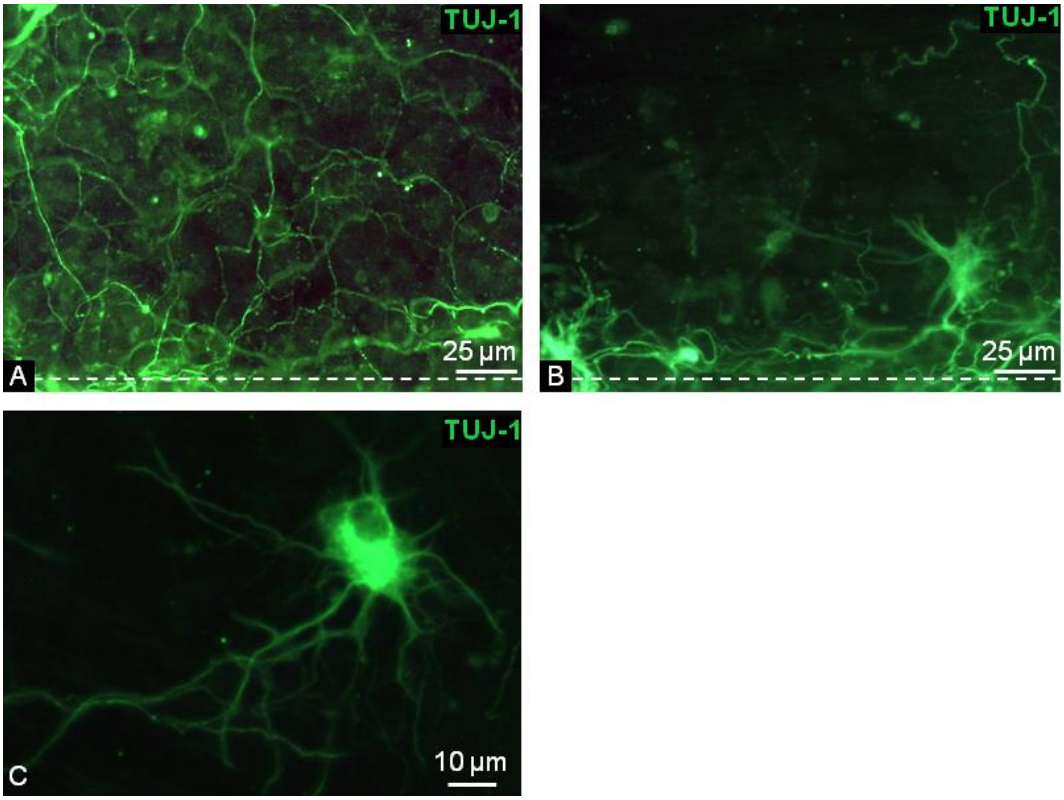

Figure 12. The spontaneous and randomly orientated outgrowth of nerve fibres from lesion margins is dependent on the age of the slice at derivation and the duration of pre-lesion culture. *(A) Representative fluorescence micrograph of extensive, random outgrowth of TUJ-1^{+} (pan-neuronal marker) nerve fibres in lesions in young slices (P0; lesioned at 1 DIV; stained 7 days later:* n = *6). (B) Representative fluorescence micrograph of relatively limited, random outgrowth of TUJ-1^{+} nerve fibres in older slices (P5; lesioned at 8 DIV; stained 7 days later:* n = *6). (C) Representative fluorescent micrograph of a likely TUJ-1^{+} interneuron at the lesion margins of older slices.*

3.3.4. Reducing the expense of the lesioned slice culture model for screening applications

3.3.4.1. Commercial culture inserts and the existing alternative

The slice injury model developed here was considered cost-prohibitive with regards to its use as a screening tool. The main expenses incurred (**Table 2**) were associated with obtaining the animal tissue, the commercial slice culture inserts and the antibodies used for immunostaining. Antibodies represented the greatest expense, but the volumes of antibodies could not be reduced as the staining procedure could only be reliably performed within suitably sized containers (12-well plates). This estimate is likely to vary depending on the particular antibodies used and the number of slices that require staining. The price for the animal tissue represented less than 10% of the total cost. The commercial inserts (**Figure 13A**) represented 28% of the total cost and are required for each culture because they cannot be re-used, as the materials do not withstand autoclaving and there is no way of replacing the membrane. An alternative method of culturing slices on re-useable 'O-rings' has been published (**Figure 13B**). The membrane is relatively expensive but the use of this technique to culture slices can reduce the overall cost by 16%.

Table 2: The main costs incurred to produce and characterise each lesioned slice culture			
Item	**Units required per culture**	**Cost per unit (£)**	**Cost per culture (£)**
Animal tissue (Mouse litter)	1.00	20.00	20.00
Dissection medium	1.50	1.40	2.10
Commercial inserts	16.00	4.90	78.40
OR			
O-ring inserts	16.00	2.10	33.60
Confetti membranes	6.00	2.10	12.60
Culture medium	2.00	1.30	2.60
Antibodies			170.00
		Total using Commercial inserts:	**284.70**
		Total using O-rings:	**239.70**

[Estimates are based on: 7 spinal cords extracted per animal; 48 slices generated per culture; 3 slices cultured per insert; 75 mL dissection medium and 100 mL culture medium required; 42 slices used for immunostaining (14 slices used for each of the three primary antibodies)].

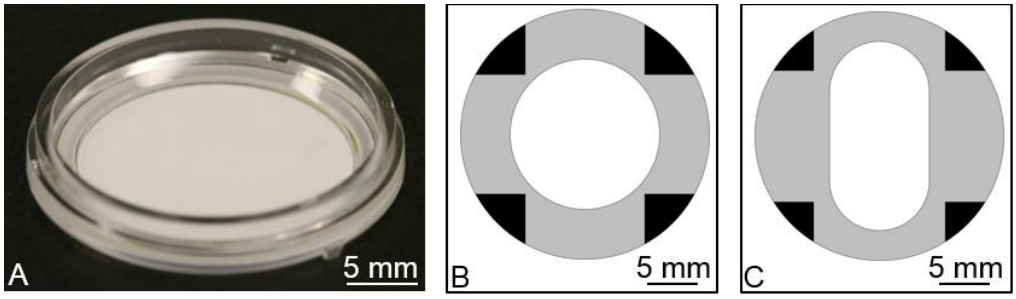

Figure 13. Existing commercial and re-useable slice culture inserts. *(A) Photograph of a commercial organotypic slice culture insert available from Millipore. (B) Schematic showing a view from underneath existing O-rings (feet in black). (C) Schematic of a prototype O-ring developed in-house (same view as B).*

The O-ring inserts were re-designed to address the problems for culturing and lesioning spinal cord slices. The O-ring inserts have a smaller area available for culture than the commercial inserts and were developed for substantially smaller sized hippocampal brain slices and it was not possible to fit more than two spinal cord slices over the culture area. Additionally when the tool was pressed into slices, the membrane (not adherent to the O-rings) would yield and not offer sufficient resistance for successful lesioning. A further issue during culture was the presence of bubbles that formed beneath the culture area. This could occur due to agitation of the insert during slice/confetti transfer or when the medium was changed, as discarding spent media lowered the medium level below the membrane, such that air could become trapped here even as fresh medium was added. It is not clear whether these bubbles would be detrimental to slice health, but the issue was resolved by gently lifting and replacing the membranes over a full complement of medium

The first prototype produced was a minor alteration to explore the limitations of the existing design. The insert assembly process was kept unchanged, but the dimensions of the O-ring culture area were altered (**Figure 13C**) to accommodate the rectangular shape of slices. Additionally, it was reasoned that the wider O-ring sections parallel to the length of the slice could be used to keep the slice stationary when the lesioning tool was pressed downwards, by providing a surface onto which the culture membrane and the confetti tabs could be pinned down with forceps for stability. However, in practise the membrane could not be sufficiently secured to induce lesions effectively and the design still permitted the culture of only two slices, so a new design was required with significant alterations.

3.3.4.2. Production of in-house designed slice culture inserts

A factor critical to the replication of lesioning procedures achieved with the commercial inserts was finding a way to secure the membrane to the O-ring. The incorporation of an expanded culture area would also increase the number of spinal cord slices that could be simultaneously cultured and increase their overall separation relative to each other. However, it was considered desirable to continue using the O-rings within 35 mm Petri dishes, and it was recognised that there were limits to the extent that the insert diameter and ring width could be altered, as, respectively, space was still required surrounding the outer perimeter of the insert to perform medium changes and the membrane needed sufficient space to be adhered to the sides of the insert to be kept effectively taut.

The design features of commercial inserts (**Figure 14A**) were analysed in order to conceive a novel re-useable insert design that addressed the problems found with the existing O-ring inserts for slice culture, whilst retaining the fundamental aspects that make the technique work. To maintain the culture membrane at the air-medium interface the feet needed to be retained to raise the culture membrane off the bottom of the Petri dish, up to the surface of the medium. The commercial inserts have a lip surrounding the perimeter, reducing the chances of medium splashing over slices during transport and these could be exploited for increased slice stability during lesioning by pinning the elongated confetti tabs to this lip with forceps (**Figure 5**). However, part of the insert wall immediately surrounding the membrane was sloped, which actually increased the difficultly of gripping the insert with forceps and this was identified and a feature that could be improved. It was envisaged that an insert composed of three identical, ring-shaped units (PTFE), four screws and four nuts (cellulose acetate) could address the above considerations (**Figure 14B-D**). The

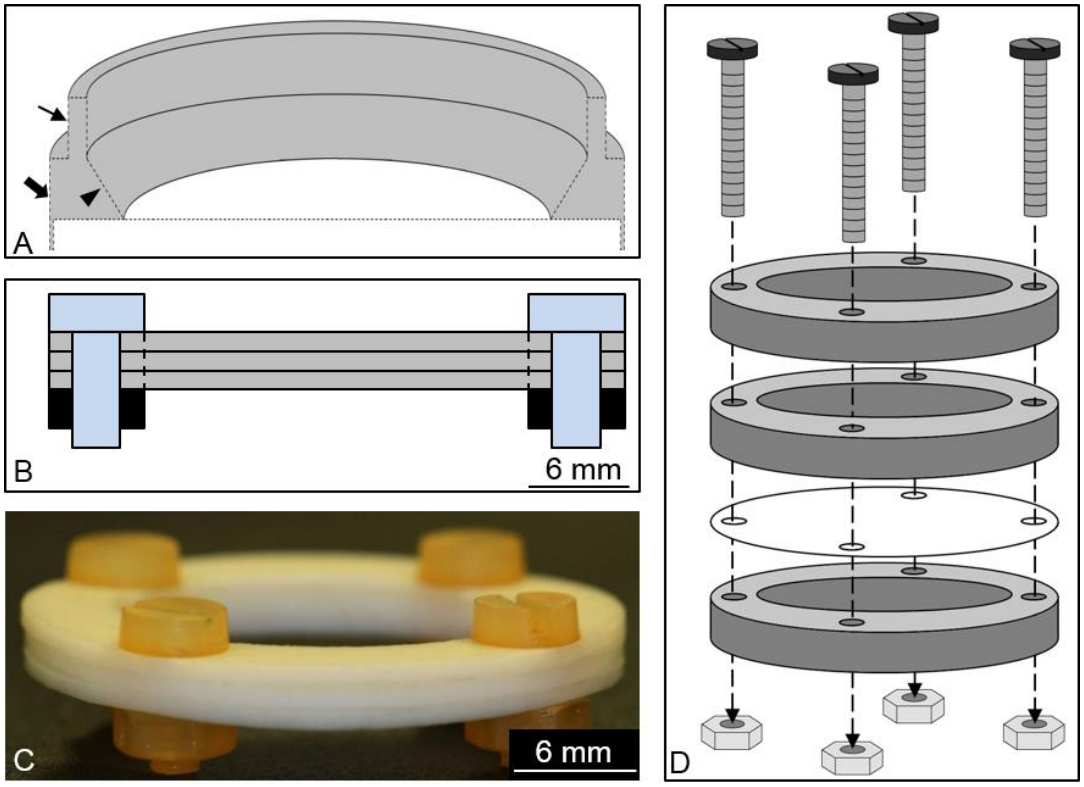

Figure 14. Design of an alternative re-useable slice culture insert. *(A) Schematic illustrating a cross-sectional view of commercial organotypic slice culture inserts purchased from Millipore, with the main features highlighted (arrow: insert lip; arrowhead: sloping wall; block arrow: feet). Note: not to scale. (B) Schematic illustrating a cross-sectional view of in-house designed O-ring inserts (O-rings: grey; screws: blue; nut: black). (C) Photograph of assembled in-house produced O-ring inserts. (D) Schematic illustrating the assembly of O-ring inserts with a separate Omnipore™ membrane placed between the stacked O-rings to form the slice culture membrane. Note: not to scale.*

---

simple design and use of relatively inexpensive materials aimed to reduce the manufacturing costs, with only the rings requiring bespoke tooling. The overall diameter of each ring and the culture area were enlarged (and the ring width slightly

decreased), compared to the O-ring inserts, permitting the culture of up to three slices per insert while also providing access around the insert to change the medium. The stacking of each ring and the placement of the culture membrane between the bottom two rings introduced a lip that was uniform in thickness from top to bottom, making it easier to grip the wall and confetti with forceps and therefore further improve slice stability during lesioning. The incorporation of four identically placed holes around the ring perimeter facilitated the use of four screws (with nuts) to adhere the rings in place and secure the membrane in a level configuration. The screws that protruded from underneath the bottom ring were produced with sufficient length to raise the level of the insert off the bottom of the container. It was considered advantageous to assemble the inserts prior to autoclaving to ensure reproducible production and sterility.

3.3.4.3. Testing the robustness and performance of assembled inserts

The inserts were subjected to a number of assessments to validate their suitability as a re-useable replacement for commercial inserts and the existing O-ring inserts in the long-term (**Table 3**). To establish whether the inserts were affected by commonly used laboratory chemicals and fixatives that would be used in conjunction with slice staining procedures, inserts were submersed in 4% PFA, 2.5% glutaraldehyde and 70% ethanol for 1 hour each, with washing between incubations. No discolouration of the materials or leaching was observed and there was no effect noted on the structural integrity of the inserts following manual testing, with regards to deformation and breakability, flatness as judged with a spirit level and the ease of

assembly afterwards. Also there was no noticeable effect with respect to the insert integrity following autoclaving.

Table 3. Validating the reusability of in-house produced O-ring inserts

	Outcome measure			
Test	Discolouration	Deformation	Breakability	Level surface
4% PFA	✗	✗	✗	✓
2.5% glutaraldehyde	✗	✗	✗	✓
70% ethanol	✗	✗	✗	✓
Autoclave (ca. 30 cycles)	✗	✗	✗	✓

To assemble the inserts correctly, the membrane between the O-rings needed to be taut so that it could be fixed in a level position once the screws were tightened. Whilst the membrane was found to deform to a greater extent than did commercial inserts, it did not impact on the lesioning procedure. The membrane could be secured with greater tension but with increased risk of tearing, so the method of assembly required alteration to produce greater membrane tautness, e.g. use of a restraint. When the inserts were used for slice culture the volume of medium used per well was increased two-fold to take into account the overall increase in height of the membrane compared to existing inserts. This did not result in increased use of medium, as the medium was changed every four days, compared to every two days with the commercial inserts and existing O-rings. The design of the inserts still occasionally resulted in air bubbles becoming trapped underneath the membrane. One solution to this problem would be the removal of the bottom O-ring underneath the culture membrane, to mimic the design of commercial inserts. However, this was readily resolved by tilting the inserts, which was far more effective than performing the same procedure with the existing O-rings, as the whole structure (including fixed

membrane) was more stable. The viability of cultured slices was 95% (± 3%), which was comparable to slices cultured on commercial inserts. These inserts were successfully adopted for the culture and lesioning of slices over 30 subsequent cultures, with no further issues found and generating a saving of approximately £1350.

3.4. Discussion

This is the first report of a 3-D model of SCI *in vitro* that displays multiple cardinal features of injury *in vivo*: an enhanced order of complexity compared to existing models. From the organotypic spinal cord slice cultures, 5-7 spinal cord slices can be routinely obtained from a single animal (depending on age), permitting the assessment of several treatment conditions (with control) within the same batch of slices, thereby reducing experimental variability and successfully addressing the 3R's principle of reducing animal usage. The procedures used to generate, culture and visualise slices were meticulously optimised to determine the most effective protocol for generating the injury model and, given the added complexity of the tissue, may be considered relatively facile compared to many other *in vitro* models.[169] Furthermore, the optimisation of the lesioning procedure when using the in-house produced culture insert and lesioning tool significantly improved the robustness and reproducibility of the lesions induced. The developed culture also reduced the overall cost of performing the experiments, which is a significant factor for increasing the utility and practicability for screening applications. Overall the model illustrates the potential for organotypic slice cultures to mimic a biologically

relevant, 3-D injury environment and further expands the potential utility of organotypic slice cultures for screening potential treatments for injury.

3.4.1. Development and optimisation of procedures to generate a reproducible model of SCI

The poor viability of slices produced during the pilot studies and the inadequate prevention of fungal infections emphasised the requirement to refine and optimise slice production and culture. The modifications made were mainly associated with slice handling as opposed to major procedural changes, as the protocols were adapted from established cerebellar[187] and spinal cord[44] slice culture protocols. The use of the live/dead staining kit gave a simple and rapid readout of slice viability to guide the optimisation process throughout. The results from the optimised procedure demonstrated that slices could be produced with high viability from a range of animal ages and maintained for three weeks. The immunostaining protocol routinely used for 2-D culture was adapted to effectively stain slices, and compares favourably to the alterations made for the constructs in chapter 2. In this regard, antibody incubations were increased in duration to enhance their penetration through the depth of the sample, 12-well plates being the smallest containers that could accommodate slices for staining, given the sample size and the aim of keeping the volumes of expensive antibodies to a minimum.

A superior and successful slice lesioning protocol was developed by making a series of improvements to the initial procedures. The preliminary aim was to limit the trauma inflicted on the slices to the induced lesion, in order to maintain the overall viability of slices for subsequent culture and analysis of cellular pathology. In

this regard, increasing the ease with which the procedure was performed was key to decreasing the total time taken to lesion each slice and thus the susceptibility of the slices to dehydration. This was achieved by maintaining individual inserts within separate culture chambers, incorporating elongated tabs into the design of the confetti membrane and designing an efficacious, double-bladed lesioning tool. Additionally, following the relocation of the lesioning procedure to within a sterile flow hood (with the necessary precautions taken to limit the risk of operator-caused contamination within this environment) and the use of isolated culture chambers, the incidences and spread of fungal contamination was markedly reduced within cultures. These procedural changes reduced the number of failed experiments, successfully addressing the 3R's principle of reduced animal usage. Increasing the reproducibility of the lesioning procedure was required to produce a standardised screening model of injury, capable of providing directly comparable, biologically relevant predictions of the response of spinal cord tissue to materials and treatments with reduced methodological and resultant physiological variability. First, the use of a microscope with a more powerful (X12.5) objective improved the accuracy with which lesions could be induced and permitted more accurate quality control through the identification of incorrectly lesioned slices. Second, the confetti tabs facilitated the stabilisation of the slice, reducing procedural difficulty. Third, the facile assembly of the tool allowed for reproducible blade spacing and a defined lesion size.

3.4.2. Lesioning tool development and future tool design for further process refinement

Of the various tool designs conceived the most robust, efficient and reproducible was also the simplest. The lesioning tool was developed to produce lesions with a diameter greater than 100 μm (the smallest lesion width attainable using a single cut with a conventional scalpel)[44] and less than 1 mm, which was considered ample space for clear visualisation of the cellular/tissue responses to injury. Although the lesion tool produces a particular (minimum) distance between lesion margins when assembled as described here, the use of a spacer of defined thickness can increase this variable to meet the demands of the application. In this regard, the trauma of removing a substantial proportion of the slice (≥ 1 mm) was found to be detrimental to slice viability, so modelling such a large lesion may require additional methods to increase the distance without reducing the length of tissue, e.g. placing the slice on top of pre-folded confetti that can be pulled apart following lesion induction, separating the two pieces of tissue.

The lesioning protocol and established lesioning tool induced high quality lesions with defined, straight margins and the removal of debris, within which cardinal features of pathology were subsequently observed. Nonetheless, the whole procedure was technically difficult to perform and there will be a degree of variability inherent in the lesions produced between experimenters, due to the necessary skill and experience required to perform the technique reproducibly. A further refinement to the design of the tool would be its attachment to a stand for support, simplifying and steadying the movements required (**Figure 15**). The stand would require optimisation to ensure: it could be sterilised before use; the scalpel could be easily mounted; and it would allow enough range of movement to position

the scalpel over the slice and be easily controlled by the experimenter. The movement required could be simplified further by mounting a spring between the scalpel and the stand so that a downward push would depress the tool and cut the tissue. There are still opportunities to improve the tool design further for simplification of operation, although these refinements may become increasingly complex and cost-prohibitive. In this context, the model could be adapted using

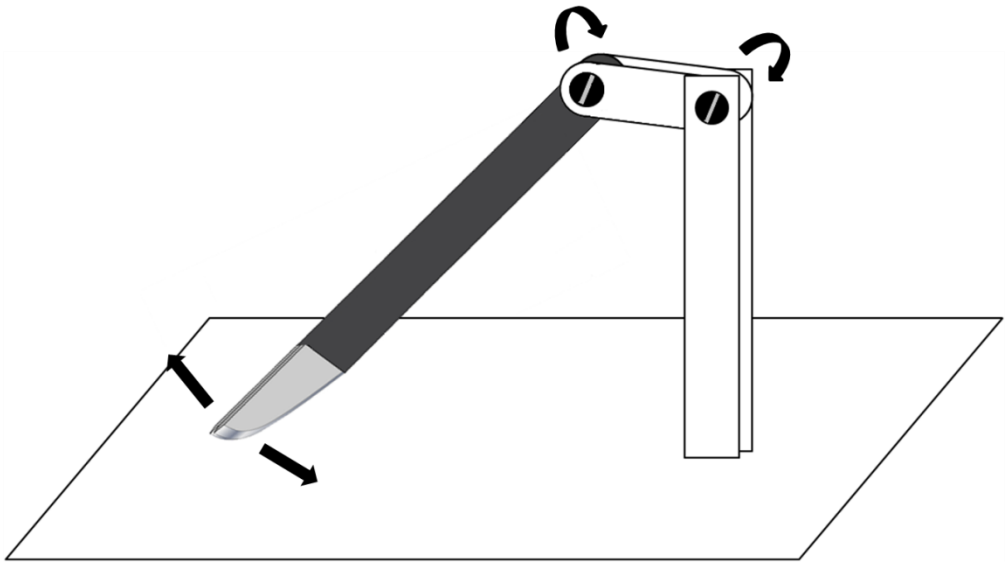

Figure 15. Schematic illustrating a potential improvement to the design of the lesioning tool. *Fixing the scalpel holder of the tool to a stand would remove lateral movement, allowing more precise placement of the tool. A linker segment between the tool and stand could increase the range of movement for positioning over the slice.*

---

automation to scale-up processes for even higher-throughput pre-clinical screening (multiple cultures at once), exploiting the increase in accuracy and reproducibility that technology can provide. For example, in theory with the co-ordinates of a slice a robotic arm could be programmed to replicate the series of pre-defined movements

typically required to lesion slices (completely or semi-autonomously), making the labour-intensive procedure more manageable on a larger scale and further reducing variability. However, currently this application may be an unrealistic option, given: (i) the inherent difficulties associated with the precision cutting of soft nervous tissue on a delicate membrane; (ii) the possibility that a typical protocol (number of movements) for lesioning slices may be impossible to generate without the need to e.g. improvise or repeat movements; (iii) the risk of increasing the number of wasted slices due to methodological errors and optimisation problems; (iv) in practise, unanticipated difficulties requiring experimenter input to resolve e.g. partial/incomplete cutting; and (v) it may be prohibitively expensive and/or time-consuming to setup and optimise.

Depending on the scale that screening would be conducted on, opportunities exist to further automate the entire culture and lesioning process, from the generation to the fixation of slices post-culture, using a robotic cell culture system such as the CompacT SelecT (TAP Biosystems). The sealed environment within such systems reduces contact between the experimenter and the sample, which maintains the optimum conditions for culture and has the potential to further reduce incidences of infection. Additionally, equipment may be integrated for the production of a customised process, such as the hypothesised robotic lesioning setup (discussed above) and e.g. equipment (in parallel) designed to deliver biomolecules or culture and transplant cell populations into lesion sites for screening purposes.

3.4.3. Pathology of lesioned slices

This study demonstrates that three cardinal pathological features of SCI *in vivo* can be mimicked in slice lesions, viz. post-traumatic astrogliosis,[188] infiltration of lesions by activated microglia[185,189] and limited random outgrowth of nerve fibres[160] from the lesion margins of slices derived from older animals. Reactive and hypertrophic astrocytes as seen within the lesion model here are hallmark features of the glial scar *in vivo*.[28] Microglial infiltration dynamics in the lesion model are broadly comparable with their acute infiltration characteristics *in vivo*.[22,189] This indicates that acute inflammatory responses can be mimicked within the lesion sites *in vitro*. The mechanisms underpinning their transient infiltration of lesion sites is not fully clear. Further, *in vivo* reports suggest that a second, more sustained wave of microglial infiltration can occur later in the injury process (ca. 60 days post-lesioning).[190] It will be of interest to determine if this phenomenon is mimicked in this model. The above findings highlight the utility of the model in mimicking *in vivo* neurological injury and subsequent neuropathological sequelae. The analyses developed here can be used to quantify pathological responses following lesion induction. These methods can be further repeated to monitor changes in the response following various interventions/treatments, for example pharmacological agents, transplant populations etc.

Responses of cells of the myelinogenic lineage (OPCs and oligodendrocytes) and the extent of myelin damage were not assessed here. It should be noted that the onset of myelination in mouse spinal cord *in vivo* occurs by the day of birth (P0) with extensive myelination reported by P10.[191,192] Therefore, it can be expected that inhibitory molecules associated with myelin and its breakdown products will be expressed in the slice lesions. Some pilot experiments were conducted, which

demonstrated the presence of myelin within injury sites using immunostaining. However, this approach was deemed inappropriate to accurately quantify myelin damage/loss in lesion sites. Detailed electron-microscopic analyses will be required to robustly address this issue, which was out of the scope of the current study and timeframes.

Whilst this model cannot provide functional readouts of regenerative events, such as locomotor activity, possible using *in vivo* models, the slices are entirely compatible with electrophysiological recording methods. Indeed, electrophysiological recordings from spinal cord slices have been reported by several groups.[193–197] Pilot studies conducted using the developed injury paradigm have shown that it is possible to introduce a platinum/iridium stimulating electrode and glass recording electrode on either sides of the lesion margins and deliver a 0.1 mA stimulus. It was possible to record small responses at 72 hours post-lesioning when a small lesion diameter was induced (data not shown). However, ion channel blocker studies would be required e.g. voltage-gated sodium channels with tetrodotoxin, in order to validate these observations.

The culture paradigm described here cannot currently serve as a complete replacement of *in vivo* SCI models because, for example, the influence of the systemic circulatory components on repair cannot be addressed. Further refinements to the model are possible, for example, there is the potential to add both circulating immune and blood brain-barrier components, to further enhance the sophistication and biological relevance of the system. The basic model may also be adapted to the study of compressing and contusing (as opposed to transecting) spinal cord injuries. Two models of injury (older and younger) have been described here by modulating the age of tissue for slice derivation as well as timings of lesion induction. The

spontaneous sprouting of nerve fibres observed from the margins of lesioned spinal cord slices in this paradigm, which declines with the age of donor tissue and is influenced by pre-lesioning culture time, has been reported previously.[44] The two models can be exploited for different biomedical applications for example drug therapies to stimulate axonal regeneration in older tissue. Both models are suitable for studying the responses of the non-neuronal, (supporting) glial cells in lesions.

3.4.4. Commercial applications of the in-house developed inserts

The issues that prevented reliable lesioning of spinal cord slices in existing, reusable O-ring slice culture inserts were successfully addressed to produce customised inserts in-house, by incorporating design features from the commercial inserts,[184] the gold standard insert for organotypic slice culture, along with application-specific requirements to aid lesioning. In general, the problems were associated with an overly simplified design with respect to the commercial inserts and with the size of the insert membrane, which was insufficient for the accommodation of multiple spinal cord slices. The in-house developed inserts are relatively simple in design for ease of assembly. Slice viability was comparable between the in-house and commercial inserts, thus validating the utility of the in-house design as an alternative insert for slice culture. Furthermore, the in-house inserts were preferred to the commercial inserts for generating the model, as the slices were more stable during the lesioning procedure and more infrequent medium changes were required during culture. Additionally, the overall cost of slice culture was successfully reduced, which is an important factor when considering the number of inserts required for the use of slice cultures as a screening system, on an ongoing

basis**.** The robust design compared to existing O-rings, with the enhanced performance and reduced cost compared to commercial inserts, suggests that the inserts could have potential as a commercial product (**Figure 16**).

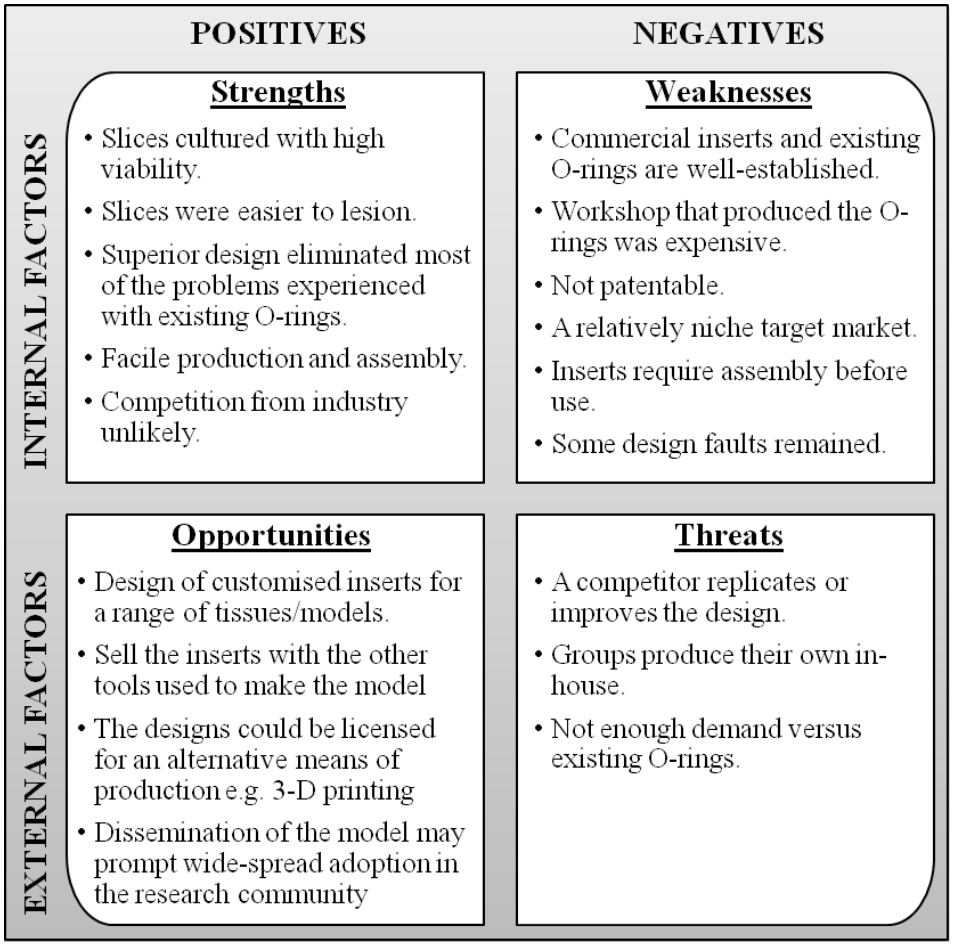

Figure 16. Strengths weaknesses opportunities threats (or SWOT) analysis. An evaluation of the commercial potential of the in-house produced O-ring inserts, with respect to the existing inserts available.

After further assessment, the main practical disadvantages of using the inserts as a reusable alternative compared to commercial inserts is the time required for

assembly, *ca* five minutes per insert (and additional time to sterilise in an autoclave), which could increase the slice culture preparation time by an average of 80 minutes (based on an average of 16 inserts used per culture). Cost-related issues include sourcing a less expensive workshop for the production of the rings that is capable of manufacture at a larger-scale. The cost per insert is reduced by half compared to commercial inserts, with purchase of the culture membrane representing the main material expense (also the case with the existing O-rings). From a commercial perspective the inserts are not patentable because there a number of potential ways to reproduce the same simple design as the established commercial and existing O-ring inserts. Additionally, the target market for using the developed inserts is small, given that the benefits of using the new inserts are currently only associated with generating the spinal cord slice injury model (although the increased membrane area may prove suitable for the culture of slices derived from older animals and larger species) and it is unclear how widespread the adoption of the lesioning model will be. Thus, there may be no need to purchase them compared to the existing O-rings. To compound the potentially low demand is the duration that the other inserts have been used for (commercial inserts: 13 years; existing O-rings: 7 years), which could be a barrier to significant market penetration. Furthermore, as the design of the inserts is very simple and the materials are widely available, they are easy to replicate or improve by a commercial competitor. An established brand synonymous with quality and greater marketing capability would threaten to limit the market penetration for the in-house developed inserts. However, a small market size and the one-off cost of purchasing the inserts are likely to deter commercial competitors from developing their own, at least in the short-term until a significant share of the insert market is gained.

Through consideration of all the above factors, the inserts are likely to have limited commercial potential if sold in their current form as individual reusable inserts. One approach to increase demand is to sell them as part of a kit with the other tools used to make the SCI model, i.e. the lesioning tool (and future derivatives), confetti templates etc. Indeed, the dissemination of the model could prompt wide-spread adoption in the research community for screening purposes and this kit would provide researchers with a convenient, more inexpensive means of generating the model. Additionally, the inserts could also be used to establish injury models in slice cultures generated from other CNS regions, or non-neural tissues. However, it is considered that the inserts could be customised further for various novel applications depending on the particular physical manipulation of the slices and the requirements of the procedures involved. In this context, the basic features of the inserts can remain the same but many design aspects could be altered, for example, the height of the culture membrane in the dish, the height and shape of the wall surrounding the culture membrane and the overall size and shape (rectangular, multi-chambered etc.). The dish could also be customised to include multiple chambers, partitions or holders to help with the particular procedure, deliver the treatment and/or monitor the slices e.g. microscopy or electrophysiology. Expanding the range of inserts for various novel applications in this way is likely to increase the overall demand. Furthermore modifications such as these would be patentable. In every case, however, the inserts would need to be rigorously tested to ensure production of typical slices and high viability.

With the emergence of 3-D printing and increasingly wider access to such technology in research institutions, scope exists to license the designs for consumer production in-house via online distribution channels e.g. Authentise

(http://www.authentise.com), which would eliminate production and delivery costs, and may discourage groups from producing their own inserts in-house. However, the use of such design distribution technology is generally restricted to non-scientific items, raising the possibility for producing a more scientific version to meet the needs of bespoke tools in the science community. Additionally, the PTFE that is currently used to form the in-house designed O-rings cannot be used for 3-D printing, so potentially suitable alternatives such as cellulose acetate could be tested.

3.4.5. Conclusions

The production and handling of slices has been optimised to produce a robust and reproducible model of SCI *in vitro* that replicates multiple cardinal features of neurological injury *in vivo*. This increase in complexity compared to other *in vitro* models described to-date demonstrates the potential of injured organotypic slice cultures for investigating injury pathology and could provide a model for the screening of novel treatment strategies for neurological repair, whilst reducing the high current reliance on live animal testing. The in-house production of customised O-ring inserts facilitated a reduction in the overall expense of the lesion model; a particularly important consideration for screening applications.[b]

[b] Most of the data in sections 3.3.1-3.3.3 have been published. The main article is included here as Appendix 3 and features in an article included as Appendix 4.

Chapter 4: Evaluating the screening utility of an *in vitro* model of SCI for nanofibre-based repair strategies

4.1. Introduction

'Combinatorial' neural tissue engineering strategies have been suggested to be essential in promoting various aspects of neural regeneration within the complex, multi-faceted pathology of SCI, such as nerve fibre regeneration, suppression of scar formation and immune responses and promotion of blood vessel growth.[198–202] The use of implantable synthetic bridges can aid regeneration by providing: aligned topographies and gradients of chemical guidance cues to direct regeneration; inhibitory molecule suppressors to promote growth; components of the ECM to promote the adhesion of neural cells to the scaffold; and transplant cell populations to replace lost/damaged cells.[51,54,59]

Evaluation and optimization of bridges is currently the subject of intensive research globally although no approaches have been successfully translated into the clinic to-date.[121] The results from rat SCI injury models have shown that the implantation of aligned nanofibre scaffolds in particular is an approach with high regenerative potential.[120] For example, Liu, *et al.*, (2012) produced a tubular scaffold (2.5 x 2.0 cm) of either aligned or randomly orientated collagen nanofibres folded into a spiral arrangement (4-5 layers).[126] Scaffolds comprised of aligned nanofibres were still visible one month following implantation into a hemi-section injury model (C3 level), compared to randomly orientated nanofibre scaffolds which had almost completely degraded. Significant cell penetration and infiltration was observed into all scaffolds with an absence of neuroglial scarring. Scaffolds also supported nerve fibre sprouting. While these results show aligned nanofibres are a favourable scaffold for neural regeneration, there were some limitation with regards to the design and complexity of the scaffolds used. Firstly, the nanofibres were collected as a dense, handleable mesh. This was necessary to process the nanofibres into an

implantable form, which limited cellular infiltration within the thickness of each scaffold nanofibre layer. Secondly, by design the spiral structure contains a low cross-sectional surface area for the attachment of cells. This limited the potential of the aligned nanofibres to guide the regeneration of tissue from lesion margins. Thirdly, the incorporation of cells and/or biomolecules in combination with implanted scaffolds could have promoted regeneration to a greater extent.

Indeed, studies utilising aligned nanofibre scaffolds as part of a combinatorial repair strategy have seen significant functional improvements in hindlimb function following implantation.

Zhu, *et al.* (2010) produced a two-layered scaffold made of a PLGA/PLA blend, which was a half-cylindrical shape (4 mm length; 600 μm thickness).[130] The outer layer (500 μm) consisted of randomly orientated nanofibres, whist the inner layer was aligned in the longitudinal axis. Rolipram was immobilised to the nanofibres of some scaffolds to enhance axonal growth and suppress inflammatory mechanisms. Scaffolds were implanted into rat spinal cord hemi-sections at the T9-11 level. Three months later scaffolds containing rolipram had increased axonal growth predominantly in the inner layer of aligned nanofibres and increased blood vessel sprouting into the scaffolds. The number of astrocytes and amount of CSPGs found in the proximity of the injury site had decreased and significantly increased BBB scores were obtained.

A separate study by Rochkind, *et al.* (2006) produced a proprietary tubular scaffold (4 x 2 mm) containing a central bundle of nanofibres (ϕ <100 μm) embedded in a laminin-hyaluronic acid gel (± human nasal olfactory mucosa or embryonic spinal cord cells).[131] Three months following the induction of complete

transecting lesions (T7-T8 level) partial recovery of hindlimb function was attained according to the BBB scale. Scaffolds contained neuroglial scar tissue and blood vessels, with some evidence of axonal outgrowth and re-myelination.

Finally, Gelain, *et al.* (2011) produced a 'neural prosthetic' between 2-3 mm in length, consisting of multiple tubular, longitudinal microchannels of electrospun nanofibres (a PCL/PLGA blend; approx. ϕ 600 nm) filled with self-assembling nanofibre peptide hydrogels.[129] Some treatment groups contained ChABC and neurotrophic cytokines. Microchannelled scaffolds ($\leq$ 10 in total) were individually placed within the void space of cysts one month after contusive weight drop trauma to rat spinal cords and left during animal rehabilitation for 6 months. In biomolecule-treated scaffolds, the majority of the cyst volume was replaced by regenerated tissue consisting of both neural and stromal cells, extensive growth of nerve fibres was observed and a vascular network had formed within the scaffold. Improvements in motor function were observed that suggest successful scaffold integration and promotion of regeneration within the spinal cord. This study demonstrates the potential of using many different strategies synergistically within the same engineered bridge to promote regeneration. However, overall, the number of different material, cell and biomolecule permutations that could be used together raises important questions about the most efficacious combinations for repair and the screening of strategies in live animal SCI models. This is especially pertinent **in the absence of higher-throughput, biologically-relevant *in vitro* screening models of SCI**.[59,169]

4.1.1. Technological gap: can lesioned organotypic slice cultures be used to screen neuroregenerative materials?

There are only a few reports using organotypic slice cultures of neural tissue for screening materials ± cells or biomolecules. Overall, they were used to guide the optimisation of scaffold materials (e.g. composition, toxicity), their formulations (e.g. porosity) and provide readouts of the basic interactions with multiple neural cell types (**Table 1**). Ishihara, *et al.* (2011) used cortical motor neurons outgrowing from organotypic slice cultures of the sensorimotor cortex (dissected from coronal slices of rat brain) into adjacent Matrigel containing either Schwann cells or NIH 3T3 cells, as an axonal outgrowth assay to screen for the most promising transplant cell populations that promote nerve fibre outgrowth.[203] Nerve fibres were detected through the depth of the Matrigel structure and the co-culture system permitted the investigation of interactions between nerve fibres and transplant populations. However, the model was not used to screen regenerative properties of the Matrigel material *per se* and the Matrigel was not in direct contact over the slice body. In another study by Fabbro, *et al.* (2012), mouse embryonic (E12-13) spinal cord transverse slices were cultured with carbon nanotubes using the roller drum culture method, to examine the interactions with multilayered neural tissue.[193] The slices interfaced with nanotubes provided complex readouts of neural growth, morphology and synaptic activity following short-term culture (two weeks). Finally, Jurga, *et al.* (2011) produced rat (P7-9) hippocampal slice cultures to test the responses of either cryogelated, laminin cross-linked dextran or gelatin scaffolds in a comparative study with a live animal injury model.[204] Readouts of scaffold degradation and immunogenicity were obtained, although the degradation was significantly more rapid *in vivo*. Astrocytes were found to interact with the edges of the scaffold

Table 1: Qualitative comparison of studies utilising organotypic slice cultures of neural tissue for complex *in vitro* readouts following culture with materials, cells and/or biomolecules					
Study aim	**CNS tissue region and plane of slicing**	**Insult inflicted?**	**Material / cell / biomolecule / drug tested?**	**Results mimicked *in vivo*?**	**Ref.**
Setup a 3-D axonal outgrowth model *in vitro* to screen for neuroregenerative transplant cell populations.	Sensorimotor cortex dissected from coronal slices of rat brain.	No	Matrigel (± primary Schwann cells or NIH 3T3 fibroblast cells).	Yes	203
Study the optimal chemical and biological properties of two different scaffolds, using multicellular readouts *in vitro* and *in vivo*.	Rat hippocampal slices produced in the transverse plane.	No	Cryogelated gelatin or dextran, both cross-linked to laminin.	Yes	204
Culture slices with carbon nanotubes to establish optimal features and examine the interactions with multiple cells in a relevant tissue cytoarchitecture, including the synaptic activity of neurons.	Mouse embryonic (E12-13) spinal cord (transverse plane; roller drum culture method).	No	Carbon nanotubes	N/A (No supporting study)	193

Investigate potential neuroprotective effects of cells complexed with microparticles *in vitro* and *in vivo*, in models of ischemia.	Rat hippocampal slices (transverse plane).	Yes (via oxygen-glucose deprivation)	Fibronectin- coated PLGA microparticles (± marrow-isolated multilineage inducible cells)	Yes - where applicable	205

although no significant astroglial scarring was detected, which mimicked the results found *in vivo*. Additionally, neuroblast migration was detected in scaffolds cultured with slices, albeit at significantly higher levels than *in vivo*. This suggests that organotypic slice cultures are compatible for the robust and reproducible testing of introduced scaffolds. Importantly, the induction of cellular responses to introduced materials comparable with those in live animal injury models[206] highlights the value of the biological predictions obtained with the model. It also lends support to the use of organotypic slice culture models for screening applications with more spatial and cellular complexity. These readouts are invaluable for the development and preliminary assessment of novel neural tissue engineering strategies prior to testing *in vivo*.

However, despite their critical advantages such organotypic models have never been utilised to examine the interactions of nanomaterials (as part of combinatorial therapies) with multiple cells types in an **injury simulated environment** for the regeneration of neural tissue. Garbayo, *et al*. (2011) attempted to show protective/regenerative effects of materials (microparticles) and cells on injured slices cultures, by inducing ischemia via acute oxygen-glucose deprivation.[205] However, the use of this relevant injury model is less applicable when considering other mechanisms of primary injury to the CNS, such as contusion or penetrating lesions. Furthermore, the evaluation of the microparticles in the study was primarily as an accessory to enhance the survival and neuroprotective effects of the transplanted cells, rather than directly promote regeneration of spared tissue *per se*.

The utility of *in vitro* slice cultures to screen for materials has never been evaluated within a reproducible model of injury before. In this context, the spinal cord slice injury paradigm (Chapter 3) has the potential to act as an *in vitro* screening

model for structural bridges with more spatial and cellular complexity than other *in vitro* injury models described to-date.

4.1.2. Objectives

The aims of this chapter are to:

(i) Assess the potential of using the developed lesioned organotypic spinal cord slice culture model as a screening system for synthetic nanofibre scaffolds (specifically aligned PLLA nanofibres) intended to promote spinal cord regenerative processes post-injury.

(ii) Establish appropriate technical methods to incorporate nanofibre-bearing constructs across injury foci.

(iii) Evaluate the potential regeneration-enhancing properties of the implanted constructs using histological and morphometric analyses.

4.2. Materials and methods

4.2.1. Development of nanofibre constructs for incorporation into lesioned spinal cord slice cultures

Fluorescent and non-fluorescent nanofibres were produced using the same operational parameters as described previously (section 2.2.2). Nanofibres were desiccated overnight and sterilized in a UV chamber before use in all experiments. The line density of nanofibres used was tailored specifically for slice experiments (detailed in section 4.3.1).

4.2.1.1. Design of a portable nanofibre delivery device

Frames were made from cellulose acetate paper (**Figure 1A**), to deliver sheets of aligned nanofibres into lesioned slice cultures. The frames were designed with respect to the dimensions of the slice culture inserts and the largest slices that were generated (**Figure 1B**). The border width of the acetate frames needed to be greater than 1.5 mm, which was previously found to be too flexible (section 2.3.2.2). With a width of 2 mm there were no complications removing frames from the collector/densification tool after they were adhered to the nanofibres. No distortion was observed following storage and the frames could be accurately placed over slices. Additionally, there was insufficient room to place more than two acetate frames within the culture area of each insert, so a maximum of two slices were cultured per insert for nanofibre treatment, compared with three slices in control lesioned groups. However, for nanofibre experiments O-ring inserts developed in-

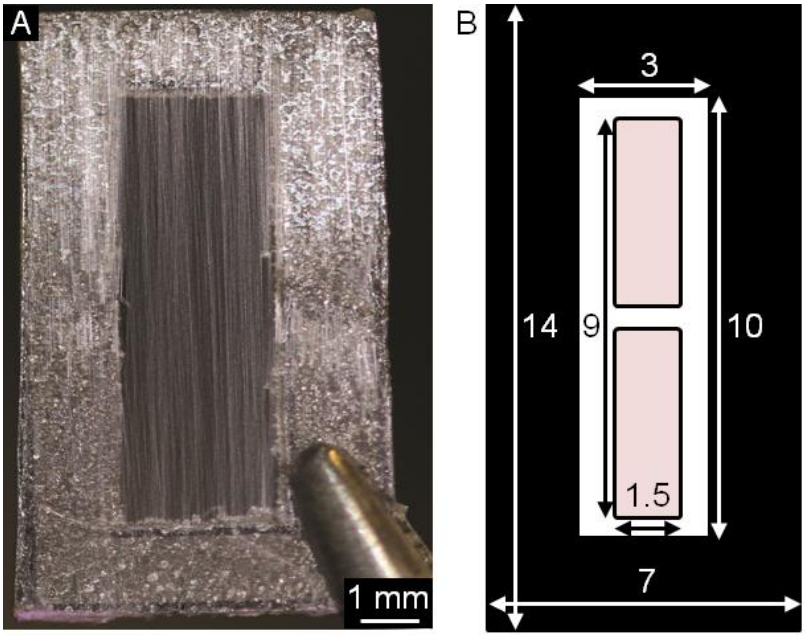

Figure 1. Portable acetate frames for the delivery of aligned fluorescent nanofibres to lesioned spinal cord slices. *(A) Photograph of aligned (vertical) fluorescent nanofibres adhered to portable acetate frames. (B) Schematic diagram showing the dimensions of the frames (black) with respect to the lesioned slices (pink) following placement (units in mm).*

---

house were only used for control lesioned slices as the final frame size was fractionally too large to place over two slices within the culture area.

When multiple nanofibre frames were stored together within a single compartment, the aligned nanofibre configuration was regularly disrupted due to adherence either together or to the bottom surface of the container, making them difficult to handle with forceps. To overcome this problem, a Petri dish with 50 individual sub-compartments was used, to keep the nanofibre frames separated and stored in an upright position.

4.2.1.2. Development of nanofibre coating procedures

A procedure to incubate multiple sterile, portable nanofibre frames sequentially with poly-D-lysine (PL; 20 µg/mL; 12 hr; RT) and laminin (LAM; 10 µg/mL; 5 hours; RT) solutions was developed. These biomolecules are widely used to coat surfaces for cell culture. The simplest method conceived involved the placement of nanofibre frames on a non-stick PTFE block (fibre side facing upwards) with the solutions then applied over the nanofibres (with three PBS washes after each incubation). However, the solutions were found to completely evaporate during incubations, which caused nanofibres to form dense bundles. This disrupted the aligned configuration and reduced the surface area for cell attachment along the width of lesion margins following the delivery of frames into lesioned slices. The use of a sealed dish and the application of PBS around the frames to maintain a humid environment during incubations prevented the coating solutions from completely evaporating. However, difficulties remained in washing the frames numerous times with PBS and picking the frames up with forceps after coating was completed. Therefore, a coating chamber was designed and produced in-house to address these issues (**Figure 2**). The solutions were added into a modified Petri dish so that levels reached the nanofibres located on the underside of each suspended acetate frame. The design of the chamber assisted the addition and removal of solutions without disturbing the nanofibres and facilitated a rapid and efficient procedure to deliver the nanofibres, as they were easy to handle with forceps when held in suspension. The use of a lid prevented the solutions from evaporating and the ability to coat up to six frames simultaneously reduced the total procedural manipulation required. Following the last wash, nanofibres were kept moist for subsequent placement (within 15 mins) over slice lesions.

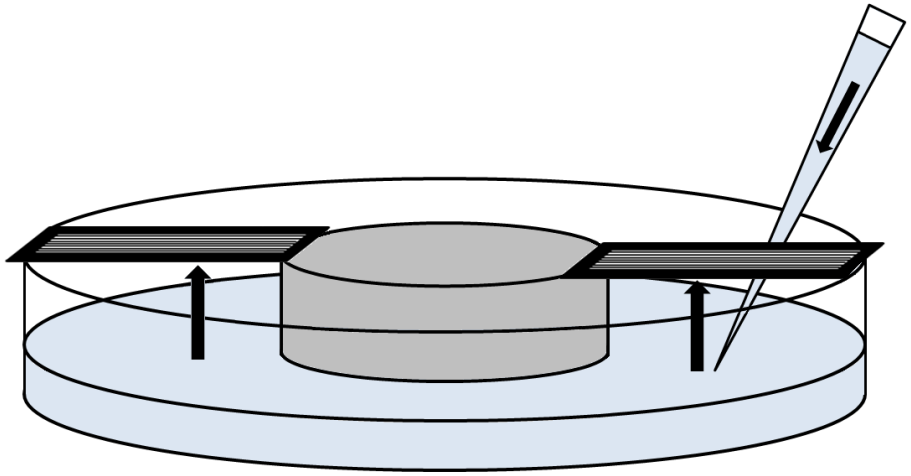

Figure 2. A chamber developed in-house to coat multiple nanofibre frames. *Schematic diagram illustrating the coating chamber, modified from a small-sized Petri dish, with a central support (grey) added to facilitate suspension of multiple acetate frames (black) simultaneously. Coating/washing solutions (light blue) were sequentially added via pipette (right) up to the level of the nanofibres (black arrows). A lid was placed on top for the duration of the coating steps (not shown).*

Fourier transform infrared (FTIR) spectroscopic analysis was conducted to verify coating procedures, using an IS50 ThermoFisher instrument fitted with a germanium single bounce ATR. Spectra were recorded at 4 cm^{-1} resolution taking an average of 128 spectra. An air background was taken immediately prior to the sample. Micrographs of nanofibres ± rhodamine B were obtained as described previously (section 2.2.6.3) and the nanofibre line density calculated (section 2.2.7.1).

4.2.1.3. Incorporation of nanofibre frames into lesioned slice cultures

The technical challenge of incorporating delicate, aligned nanofibres over lesioned slices was overcome by gently placing the nanofibres, located on the underside of the acetate frames, downwards over the slice (**Figure 3**), so that the slice was positioned within the inside edge of the frame and the frame orientated parallel to the longitudinal axis of the slice. A microscope was necessary to correctly position the frame relative to the slice and the confetti membrane. Once in place, the acetate frames were gently pushed downwards onto the confetti to ensure contact with the slice. To fix the frame in place, 50 µL of a 3 mg/mL neutralized collagen hydrogel solution was applied to the confetti, around the outside edge of the acetate frame, thus ensuring stability and that the nanofibres remained in contact with the slice during culture and post-experimental staining procedures. The area of the confetti was increased to provide sufficient space for the application of hydrogel around the frame and to prevent any hydrogel from spreading off the confetti onto the culture membrane. Additionally, the slices with attached nanofibres were easy to handle with forceps due to the elongated sections of confetti, which assisted the stability of the acetate frame during transfer to well plates and microscope slides for post-experimental processing and image analysis.

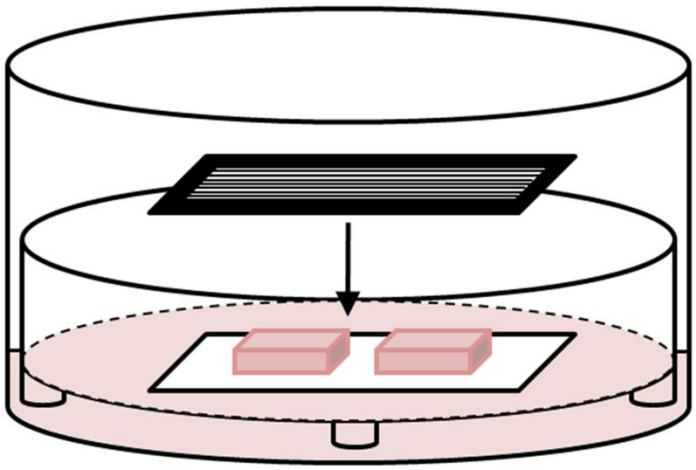

Figure 3. Method of placing aligned nanofibre frames over lesioned slices.

Schematic illustrating the placement of aligned nanofibre frames (black) over a lesioned slice (pink), within the culture area of an insert.

4.2.2. Evaluating the cellular interaction between host slice tissue and implanted constructs

To investigate the use of the injury model as a screening tool, nanofibre scaffolds ± coating were placed rapidly over slices immediately post-lesioning. Slices from both 'younger' (P0 mice: lesioned after 1 DIV; fixed 7 days later) and 'older' (P5 mice: lesioned after 8 DIV; fixed 7 days later) models of intrinsic nerve fibre outgrowth (section 3.2.2) were used. Slices bearing nanofibres were initially live/dead stained to validate nanofibre delivery procedures (section 2.2.5). Slices were immunostained (section 3.2.5) with antibodies raised against GFAP, lectin and β-III tubulin (TUJ-1), for histological and morphometric analysis of astrocytes, microglia and neurons across injury sites, respectively. Slices were co-stained with DAPI to assist with the identification of lesion margins.

4.2.2.1 Quantification of nerve fibre outgrowth

A method was conceived to quantify the average outgrowth density and variation of outgrowth density of nerve fibres across lesion sites ± nanofibres. Fluorescence micrographs of slices immunostained with TUJ-1 antibodies were used to generate OD profiles in ImageJ software of the number of TUJ-1^{+} nerve fibres parallel to the lesion margins, across the width of the slice regions demonstrating nerve fibre outgrowth. Fluorescence micrographs were generated at X 200 magnification and merged together into a single panoramic micrograph for each slice, using Kolor Autopano Giga software (version 2.6). A rectangular grid was subsequently overlaid onto each panoramic image, with marks at 18 µm intervals along the length of the lesion site. OD profiles were then generated at the level of each interval, across the width of the slice regions with nerve fibre outgrowth. The data were copied into Microsoft Office Excel software (2007) in order to distinguish within these traces the OD values (in some cases up to 2000 values) that corresponded to nerve fibres and background staining. Two conditional formulae were used to identify the number of peaks present within the trace for each interval along the lesion site:

Formula 1: [=IF(AND(A1<A2,A3<A2),A2,""]

Formula 2: [=COUNTIF(B1:B1000,">25"]

Formula 1 identified peaks within the trace for each cell (e.g. cell A2 in column ‘A’) and plotted the value in the adjacent column (e.g. ‘B2’) with the premise that each peak within the trace was defined as a cell with a value greater in magnitude than both the preceding (e.g. ‘A1’) and following (e.g. ‘A3’) cells. Formula 2 was used to count the number of peaks identified (e.g. in column ‘B’) that

were above a specified background OD value (e.g. '25'). The background value was determined for each panoramic image from a combination of: (i) the minimum threshold OD value for TUJ-1$^+$ nerve fibres; (ii) the maximum OD values obtained across acellular regions of confetti; and (iii) the maximum OD of areas where any bleed-though of red nanofibres into the green channel was apparent. To normalize the number of nerve fibres detected according to the width of slices, the total number detected at each grid interval was expressed as the total number of peaks per mm^2, by calculating the area of the 18 µm long section of the lesion site that nerve fibres extended across. The average total number of peaks per mm^2 was then calculated for each slice as a measure of the density of nerve fibre outgrowth. Control slices from both 'younger' and 'older' outgrowth models were used to compare outgrowth levels without nanofibres.

4.2.2.2. Evaluation of nerve fibre alignment

A method was conceived to quantify the alignment of TUJ-1$^+$ nerve fibres with coated and uncoated nanofibres across the lesion sites of both younger and older slice models used for outgrowth quantification. It was similar in design to the outgrowth density analysis, except the OD profiles were generated perpendicular to the lesion margins, parallel to the direction of nanofibre alignment.

It was hypothesised that the profiles would give a measure of misalignment, because the detection of a nerve fibre would indicate lateral growth perpendicular to the direction of the aligned nanofibres. Thus, a greater number of nerve fibres detected across the width of the nanofibre constructs would suggest less unidirectional outgrowth of nerve fibres. However, this method did not work

because: (i) even when the direction of nerve fibre outgrowth was distinctively unidirectional, there were still a considerable number of incidences along the length of the construct where they would deviate laterally; (ii) the high number of cells and processes growing out from lesion margins introduced variability between slices in the interaction of nerve fibres with coated nanofibres and therefore the overall alignment observed; and (iii) the line density of nanofibres used, which may have reduced the topographical influence acting on the nerve fibres in comparison with e.g. the more extreme alignment observed with astrocytes on hydrogel constructs with a single layer of nanofibres at a lower line density (section 2.3.3). Therefore a semi-quantitative method was used to assess the alignment of nerve fibres. Two subjects that were blinded to the slice model and nanofibre treatment groups estimated the percentage of TUJ-1^{+} nerve fibres within the micrographs that were orientated vertically ($n \geq 3$ per group). Five bins, each with a range of 20%, were used to classify any potential alignment observed.

4.2.3. Statistical analysis

Data were analysed using GraphPad Prism statistical analysis software (version 5.0). All data are expressed as mean ± S.E.M. The number of experiments (n) refers to the number of slices obtained across different animals and litters. **Nanofibre line density analysis:** Data were square-root transformed and a Student's t-test (two-tailed) was used to quantify differences in nanofibre line density between nanofibres ± rhodamine B. **Nerve fibre outgrowth density analysis**: A one-way ANOVA with Bonferroni's post-hoc tests was used to compare differences in

outgrowth density between control lesioned slices without nanofibres and those with nanofibres incorporated into lesion sites (± coating; $n \geq 3$ per group).

4.3. Results

4.3.1. Optimisation of nanofibre line density

A pilot study was performed to establish the optimal nanofibre density for slice experiments. Nanofibres were collected either from a single unit operation between 5-10 mins in duration and directly transferred to acetate frames, or from one or more unit operations over a total duration between 10-15 mins and processed onto a densification tool. Using a fluorescence microscope for visualisation, the optimal density of nanofibres was from a single ten minute unit operation processed onto the densification tool (**Figure 4A**). Using these parameters, densities were great enough to provide sufficient nanofibre surfaces for cells to interact with along the width of the slice, but not so dense as to obscure the visualisation of cellular events in lesions and reduce the effect of the aligned scaffold topography on the direction of outgrowth. As the total area of nanofibres on the densification tool was far greater than the area of an individual frame it was considered that a grid consisting of two rows of five frames would cover the majority of the area (**Figure 4B**). This improved the ease with which the frames could be detached from the tool and increased the throughput of nanofibre frames fabricated per unit operation. No problems were experienced cutting each frame from the grid following the application of adhesive and the alignment of the nanofibres was maintained after this process (**Figure 4C).**

The average mass of individual acetate frames with attached nanofibres was 11.2 ± 0.8 mg. No significant difference was found between the line density of fluorescent and non-fluorescent nanofibres (498 ± 85 nanofibres/mm versus 493 ± 102 nanofibres/mm), respectively, with representative SEM micrographs shown in **Figure 5**.

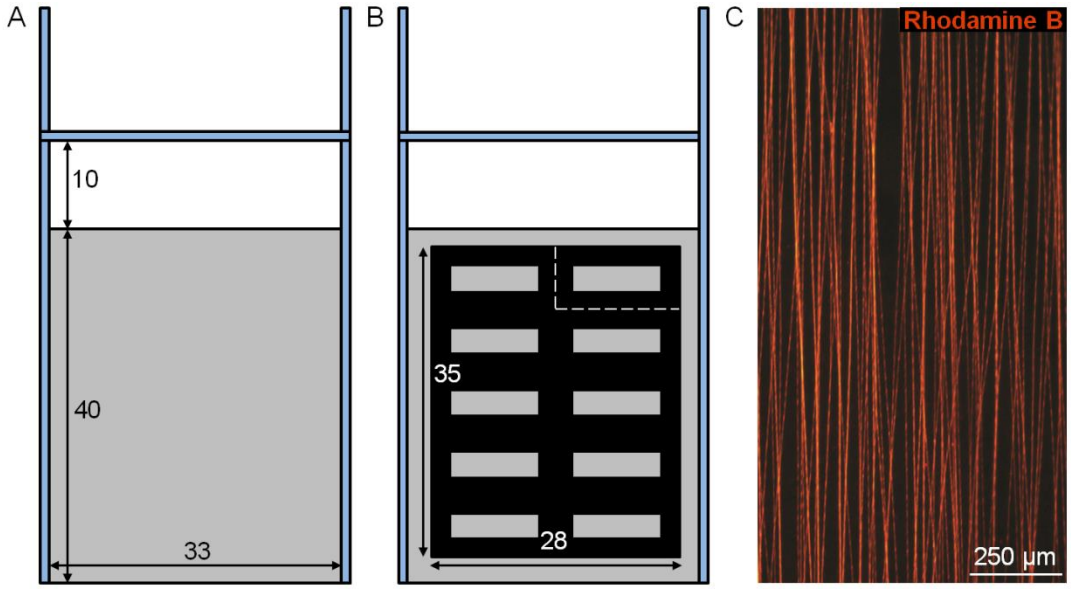

Figure 4. Nanofibre processing for the production of acetate frames containing nanofibres with an optimal line density. *(A) Schematic showing the dimensions of the densification tool (blue) with nanofibres (grey) attached from a single 10 min unit operation. (B) The placement of a grid of 10 acetate frames (black) across the area of nanofibres on the tool (white dashed lines demarcate a single frame). (C) Representative fluorescence micrograph showing the alignment of fluorescent nanofibres is maintained following attachment to portable acetate frames.*

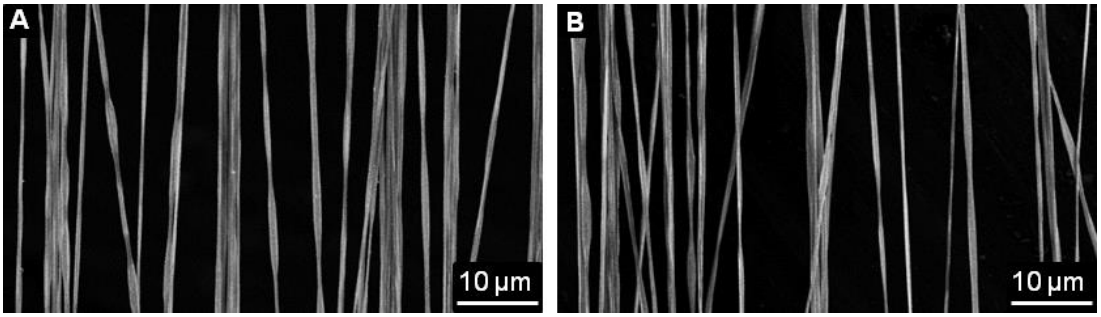

Figure 5. Representative SEM micrographs showing the line density of nanofibres used in lesioned slice experiments. *(A) Non-fluorescent nanofibres. (B) Fluorescent nanofibres.*

4.3.2. Evaluation of nanofibre coating procedures

There was no difference observed in the overall appearance and stability of the coated nanofibre frames compared to the uncoated nanofibre frames. FTIR spectroscopic analysis (conducted by Dr. Paul Roach, Keele University) confirmed the presence of protein on the surface of treated nanofibres, verifying surface coating procedures. Peaks corresponding to laminin are apparent in the amide region, with amide I (~1640 cm^{-1} centre) and II (1535 cm^{-1}) clearly present on fibres treated with laminin (**Figure 6A**) and not on untreated fibres (**Figure 6B**). The free carboxyl of the poly-L,D-lactic acid backbone can be observed at 1754 cm^{-1} in both samples. Aliphatic C-H stretch (2990-2840 cm^{-1}) is also much more apparent in laminin treated samples. The band in the O-H stretching region (3640-3030 cm^{-1}) is also more distinct in the laminin treated samples, indicating the presence of water within the adsorbed protein structure.

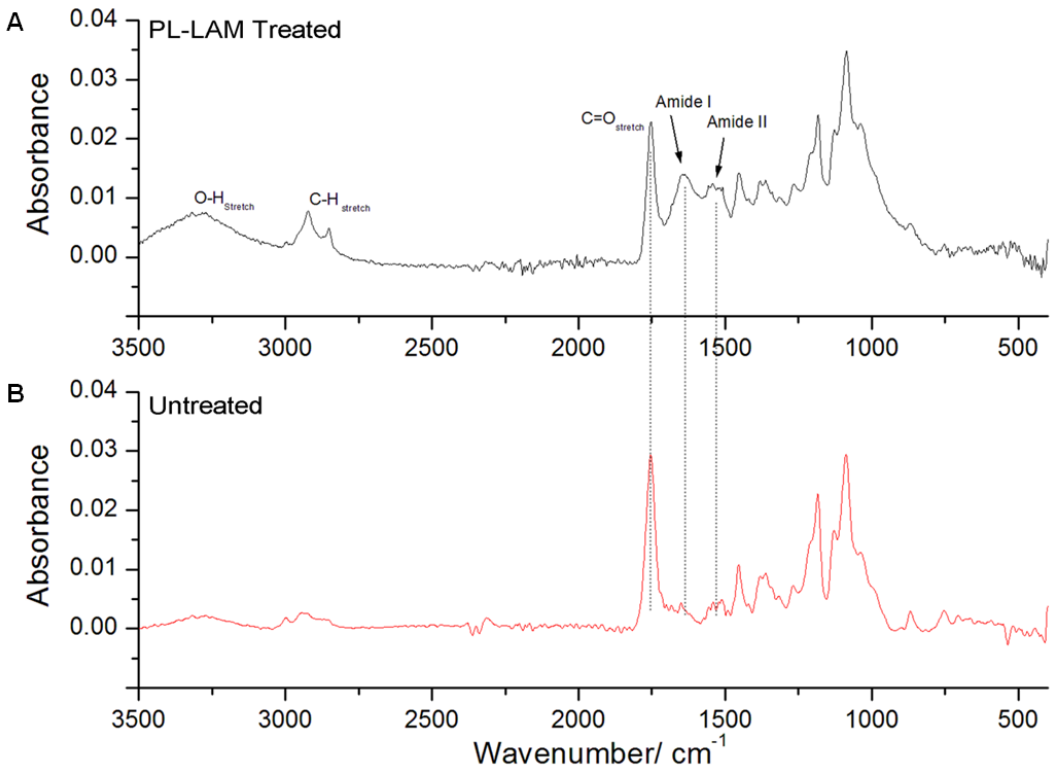

Figure 6. Verifying nanofibre coating procedures. (A) FTIR ATR spectrum of PDL-laminin treated nanofibres. (B) FTIR ATR spectrum of untreated poly-L,D-lactic acid nanofibres. (Both spectra generated by Dr. Paul Roach, Keele University).

4.3.3. Incorporation of nanofibres into lesioned slices

The overall viability after incorporation of uncoated nanofibre scaffolds over lesioned slices (**Figure 7A**) remained high, with comparatively few dead cells present around the lesion site and within the body of the slice. Some evidence of cellular attachment to nanofibres across the lesion was also demonstrated (**Figure 7B**; white arrow heads), indicating nanofibre-slice contact over the culture period. No leaching of rhodamine B was detected at the concentration used.

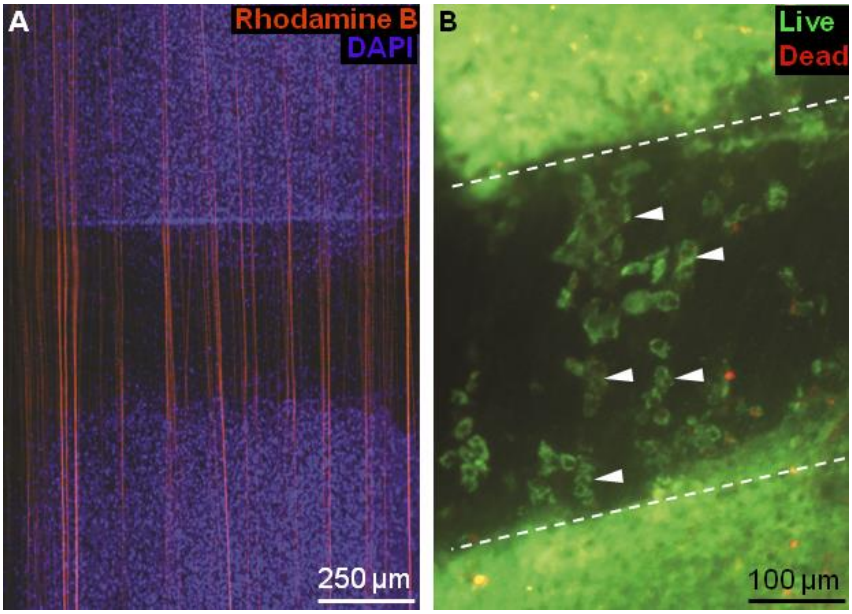

Figure 7. Incorporation of nanofibres into lesioned slice cultures. *(A) Fluorescence micrograph showing placement of portable, aligned, uncoated nanofibres over a lesioned slice. (B) Live/dead staining of a lesioned slice 3 days after placement of aligned uncoated nanofibres, verifying safe nanofibre-placement procedures (white arrowheads mark cells likely to be in contact with nanofibres across the lesion).*

4.3.4. Interactions of astrocytes with nanofibres (± coating)

Evaluation of the topographical influence of the nanofabricated scaffolds ± coating ($n \geq 3$ slices in each treatment group) on cells in lesion sites showed that gliotic scar formation occurred similar to control slices (without nanofibres), with an intense region of GFAP expression at the first 100 µm of lesion margins. Following incorporation of uncoated nanofibres, no evidence of astrocyte attachment/alignment was observed (**Figure 8A**). In striking contrast, PL-LAM coating of nanofibres

induced extensive alignment of astrocytes, notably extending long thin processes (c.a. 100-200 µm) across the lesion site (**Figure 8B**).

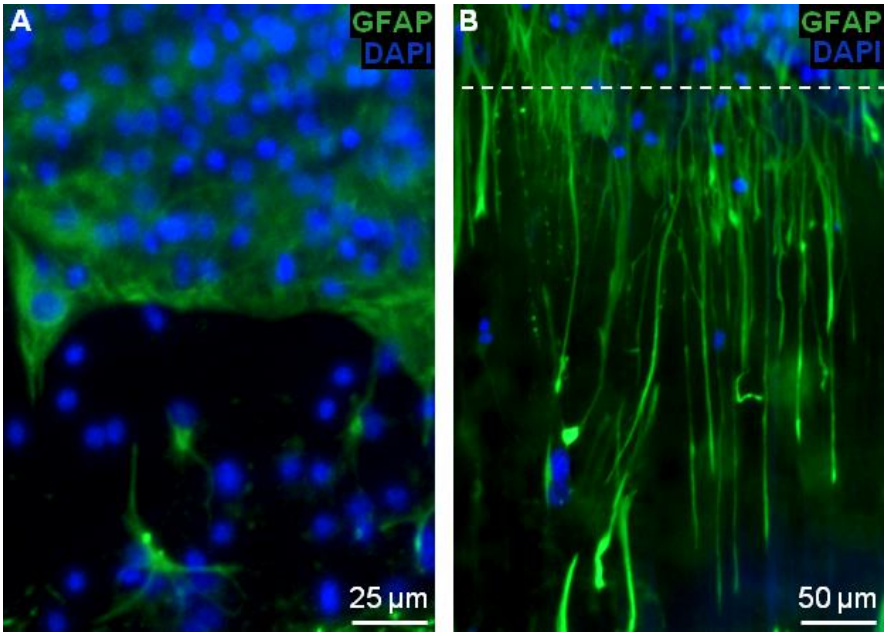

Figure 8. The coating of nanofibres with poly-lysine and laminin is necessary for the attachment and elongation of astrocytes. *(A) Representative fluorescence micrograph of GFAP$^+$ scar-forming astrocytes shows no interaction with aligned uncoated nanofibres. (B) Representative fluorescence micrograph showing the attachment, outgrowth and alignment of scar-forming GFAP$^+$ astrocytes on poly-lysine/laminin coated nanofibres across slice lesions.*

4.3.5. Interactions of microglia with nanofibres (± coating)

Extensive attachment of microglia to both uncoated (**Figure 9**) and coated nanofibres was observed over lesion sites. Notably, elongated microglia were visible over the entire area of the slice in contact with nanofibres.

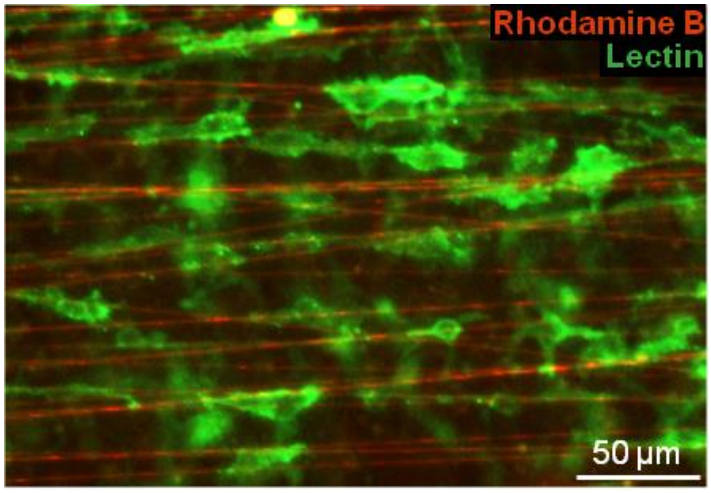

Figure 9. The interaction of microglia with nanofibres occurred regardless of nanofibre coating or proximity to the lesion site. *Representative fluorescence micrograph showing attachment and alignment of lectin^{+} microglia to uncoated nanofibres across the body of a slice. Similar cellular profiles were observed with coated nanofibres.*

4.3.6. Nerve fibre outgrowth across lesion sites

Limited attachment of TUJ-1^{+} nerve fibres was observed from the margins of lesions with uncoated aligned nanofibres (**Figure 10A**). By contrast, the incorporation of coated nanofibres appeared to result in the extensive outgrowth of TUJ-1^{+} nerve fibres from lesion margins (**Figure 10B**). The effects were most evident within the 'older' lesion model, with more limited intrinsic regeneration compared to the 'young' model.

The quantification of nerve fibre outgrowth performed in both models of intrinsic regeneration showed no significant effect following incorporation of uncoated nanofibres, whereas coated nanofibres enhanced nerve fibre outgrowth (**Figure 11A**). The coefficients of variation (**Figure 11B**) suggest fairly consistent outgrowth ± nanofibres across the young lesion model, whereas the outgrowth is significantly more variable in the older lesion model ± uncoated nanofibres, compared to slices with coated nanofibres.

Some slices were double-immunostained, with non-fluorescent nanofibres incorporated into lesion sites. Occasionally evidence was seen of nerve fibre extension that was coincident with elongated astrocytes (**Figure 12**). This suggests that a component of nerve fibre elongation may occur secondary to topographical cues from aligned astrocytes.

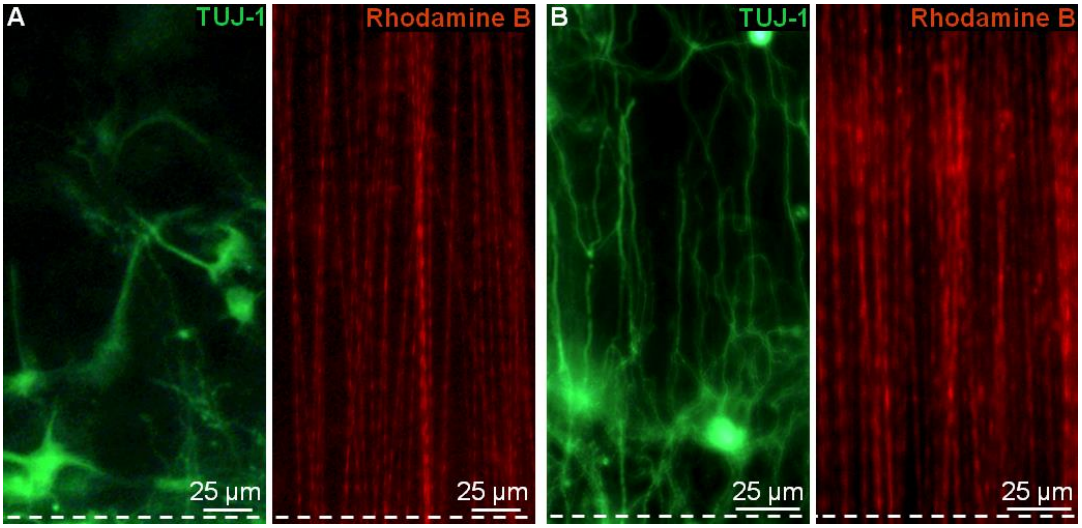

Figure 10. Nanofibres coated with poly-lysine and laminin are necessary for the outgrowth and alignment of TUJ-1$^+$ nerve fibres from the lesion margins of slices. *(A) Representative fluorescence micrographs of the same field showing limited attachment and alignment of TUJ-1$^+$ nerve fibres (left-hand panel) to uncoated aligned nanofibres (right-hand panel) in an 'older' lesion model displaying limited intrinsic regeneration (P5 slices; lesioning and nanofibre placement after 8 DIV; fixed 7 days later). (B) Representative fluorescence micrographs of the same field showing extensive outgrowth and alignment of TUJ-1$^+$ nerve fibres (left-hand panel) on aligned coated nanofibres (right-hand panel) in the same lesion model as in (A).*

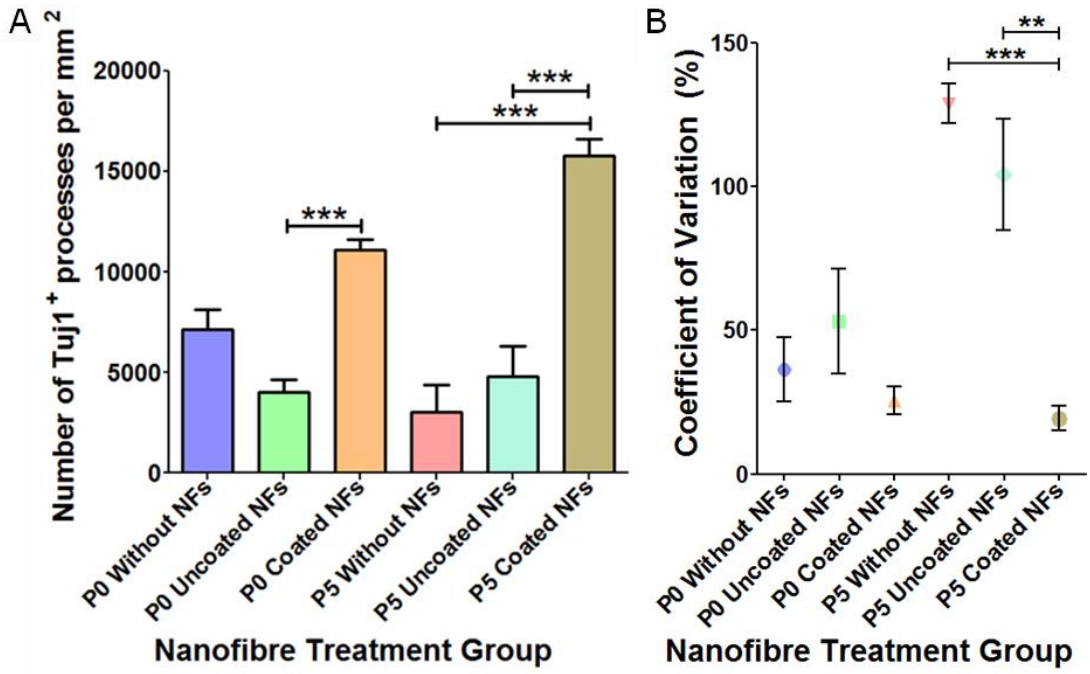

Figure 11. Quantification of nerve fibre outgrowth across lesioned slices. *(A) Bar chart quantifying TUJ-1^{+} nerve fibre outgrowth density across lesions with uncoated and coated nanofibre (NF) treatment groups, compared to controls without nanofibres, in both 'younger' (P0 slices; lesioned after 1 DIV) and 'older' (P5 slices; lesioned after 8 DIV) slice models (one-way ANOVA with Bonferroni's post-tests; ***p < 0.001). (B) Line graph quantifying the variation in the outgrowth density across the lesions for the same treatment groups as (A).*

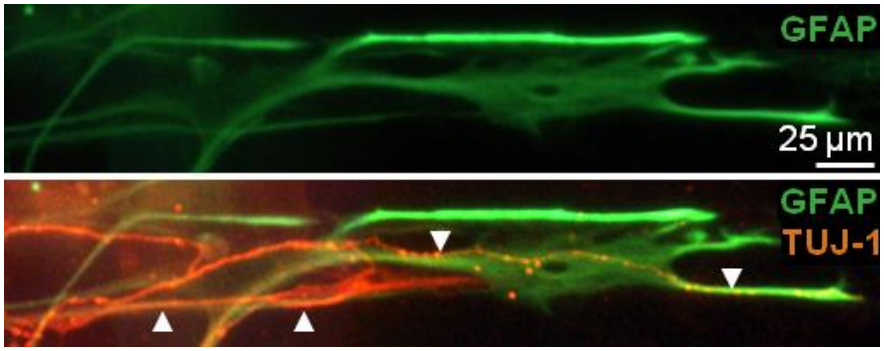

Figure 12. Multiple mechanisms of nerve fibre outgrowth on coated nanofibres.

Fluorescence micrograph showing incidences of TUJ-1$^+$ nerve fibre contact-guidance with aligned GFAP$^+$ astrocytes (white arrowheads) in lesions with coated nanofibers (P5; lesioned at 8 DIV; stained 3 days later).

4.3.7. Nerve fibre alignment across lesion sites

A semi-quantitative analysis of nerve fibre alignment across lesioned slices with nanofibres (**Figure 13**) revealed a greater proportion of aligned nerve fibres in the presence of coated nanofibres than uncoated nanofibres. The distribution of scores also shows a greater percentage of alignment in the younger (P0) model of nerve fibre outgrowth than the older (P5) model.

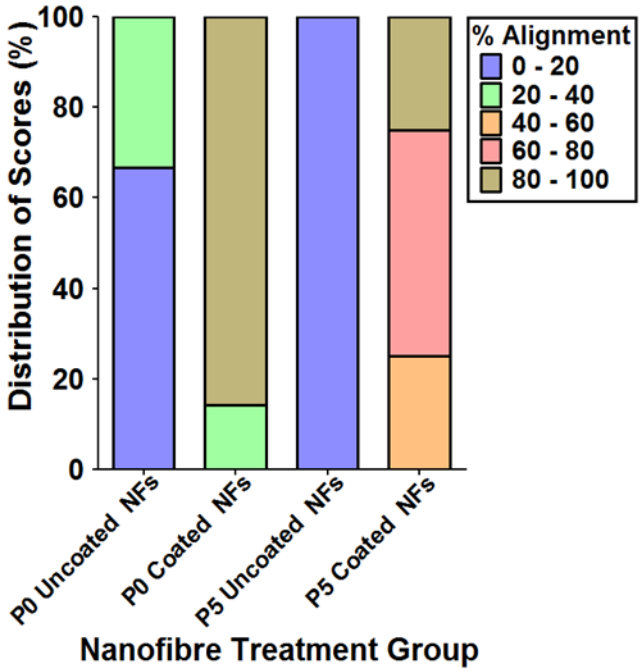

Figure 13. The alignment of nerve fibres outgrowth across the lesions is greater with coated nanofibres (semi-quantitative assessment). *Bar graph showing the distributions in scores of TUJ-1^{+} nerve fibre alignment for both uncoated and coated nanofibre treatment groups in both younger and older models.*

4.4. Discussion

This is the first report of a 3-D *in vitro* model of SCI used to screen the pro-regenerative properties of nanomaterials. Technical methods were successfully developed to deliver sheets of aligned nanofibres (± coating with biologically relevant molecules) into slice lesions. Interactions of neural cells with the delivered nanofibres could be evaluated using standard microscopy, with methods established to quantify parameters such as axonal outgrowth. The striking similarity of histopathological responses observed compared with live animal models of SCI confirm the value of the *in vitro* model as a biologically relevant predictive tool.

4.4.1. Development of a strategy to incorporate aligned nanofibres into lesioned slices

The utility of portable acetate frames for the delivery of aligned nanofibre sheets in multiple applications was demonstrated by the incorporation of nanofibre frames into lesioned slice cultures. In this regard, the portable acetate frames were an ideal delivery device because they: provided mechanical stability to the nanofibres; permitted a choice of nanofibre density; were relatively straightforward to place over lesioned slices; and maintained nanofibre alignment throughout culture. Additionally, with respect to the use of the model for screening, the acetate frames obviated the requirement for including a supporting substrate (e.g. a hydrogel) into the scaffold design. This would have added complexity to the construct and increased the difficulty of interpreting the basic pro-regenerative readout of different nanofibre materials and surface treatments on multiple neural populations across injury sites.

Importantly, the viability and sterility of lesioned slice cultures was unaffected following the incorporation of nanofibre frames into slices, despite the additional time and manipulation required following the lesioning procedure. This also suggests that the nanofibre frame were lightweight and no additional compressive effect was exerted on the slices. No leaching of rhodamine B was detected from nanofibres over the culture period and following storage for two years post-culture, in concurrence with the previous (3-D) collagen hydrogel experiments using the same concentration of dye. The development of a coating chamber for these studies permits the sequential coating and washing of multiple nanofibre frames in suspension with different biomolecules.

The nerve fibre outgrowth analysis developed to characterise the density and extent of growth across the lesion was a fast and accurate method. In this context, the use of the formulae to identify TUJ-1^{+} nerve fibres above background levels of fluorescent staining was crucial. Despite the problems encountered trying to quantify nerve fibre alignment across lesions, there is an opportunity to develop a quantitative analysis based on existing image processing techniques that have been used to characterise the randomness, alignment and periodicity of nerve fibre outgrowth, by analysing Fourier transforms of the fluorescent micrographs generated.[207]

4.4.2. Potential of nanofibre-based bridges to promote repair

The cellular responses observed in slice lesions following incorporation of PLA scaffolds or laminin-coated scaffolds are comparable to published reports *in vivo*, using a complete transecting injury model. In this regard, PLA is approved for clinical use by the FDA as it creates non-toxic waste products and has been widely

used as a scaffolding material in the tissue engineering research community. Uncoated, hydrophobic PLA scaffolds generally exhibit low levels of host neuronal regeneration and typically result in the formation of a gliotic scar at the interface between host tissue and the implant.[208–211] By contrast, the incorporation of laminin (or a suitable hydrogel e.g. fibrin)[125] into bridges increases axon regeneration and disrupts gliotic scar formation *in vivo.*[212–215] PL has additional effects in promoting neuronal cell adhesion.[100] The decision to use both coatings in this study was based on reports in the literature that suggest the attachment and extension of neuronal processes is enhanced on PL-LAM coated surfaces, compared to PL alone.[216]

The nanofibre-induced alignment of scar-forming astrocytes and the concurrent outgrowth of nerve fibres from lesion margins highlight the potential of aligned nanofibres to direct the growth of multiple neural cell types across lesion sites. Such potential to promote and support tissue growth has only been demonstrated before in scaffolds containing aligned nanofibres arranged in tubular structures, surrounding a central core of SANPs.[129] For the studies utilising purely nanofibre-based scaffolds, a relatively high density of nanofibres was used, which was necessary in order to process the nanofibres collected into an implantable form. This is likely to have reduced the extent of cellular infiltration and growth within the 3-D scaffolds compared to the density of nanofibres used in this study.[217,218]

Additionally, biological coronas have been shown to form around materials that come into contact with components from culture media.[219] It is possible that the surface of the PL-LAM nanofibres were coated by biomolecules from the serum used in the slice culture medium, which could have contributed to the extent of cellular attachment observed. In this regard, a mass spectrometry analysis of the nanofibres used in lesioned culture experiments with and without the PL-LAM

coating would identify the presence of any additional components associated with the nanofibres.

4.4.3. Applicability of the lesioned slice model for screening studies

The observation that cells in the 3-D slices can distinguish between different surface coatings suggests that they are able to make sophisticated choices regarding material interactions, within a complex environment *in vitro*. This highlights the utility of the lesioned spinal cord slice cultures in acting as a reliable predictor of *in vivo* neural cell behaviours in response to various materials and surface chemistries, and hence its value as a bio-screening method. In this context the morphological reorganization of scar forming astrocytes, which normally form a critical barrier to nerve fibre regeneration, highlights the potential screening application of the injury model. Thus, efficacious molecules and strategies that aim to disrupt the neuroglial scar via the re-organization of reactive astrocyte morphology can be screened. The extensive attachment of microglia to nanofibres resembles the activity of microglia *in vivo* following transplantation of nanofibre scaffolds into SCI sites.[129] Such attachment provides an *in vitro* readout for the optimization and testing of biocompatible materials and coatings that evoke minimal inflammatory responses. It also demonstrates the potential for long-term studies, where preliminary examination of the material degradation properties and breakdown mechanisms may be assessed.

The increased outgrowth and alignment of nerve fibres in response to coated nanofibres (and the distinct absence of such responses of neural cells to the uncoated fibres) suggests that the model can enable comparative investigations of various combinatorial strategies to enhance nerve fibre outgrowth and alignment. These

include: different polymer formulations and other potentially efficacious substrates with an aligned topography; fibre densities and diameters; scaffold functionalization with therapeutic biomolecules (promoting growth or targeting major CNS inhibitors) and therapeutic stem/progenitor cell populations. In addition, the ability to simultaneously examine the response of multiple cell types (e.g. scar-forming astrocytes and outgrowing nerve fibres) within the same complex injury environment will allow for the design and development of more efficacious growth-promoting strategies for repair of SCI *in vivo*. In this regard, the incidences of nerve fibre contact-guidance with aligned astrocytes lend support to the use of scaffolds containing aligned astrocytes as a favourable biological substrate for nerve fibre outgrowth.[60,138–140]

The readouts of outgrowth and alignment from the younger and older models of regeneration highlight their use in examination of different aspects of scaffold design. The extensive, random nerve fibre outgrowth in younger slices is suited to the examination of axonal outgrowth on bioengineered substrates with an aligned topography. By contrast, the older slices that recapitulate cardinal neural features of traumatic injury in the adult CNS such as limited nerve fibre outgrowth are suited to the examination of the regeneration-enhancing properties of novel biomaterials. Both models are suitable for studying the responses of the non-neuronal, (supporting) glial cells in lesions. Further functional assessments of regeneration i.e. electrophysiological recordings may provide a more detailed readout of scaffold regeneration-enhancing properties within this model.[178]

The full potential of combinatorial strategies utilising aligned nanofibres with combinations of cells, and biomolecules has yet to be elucidated, due in part to a heavy reliance on *in vivo* SCI models, in the absence of high-throughput,

biologically-relevant *in vitro* screening models of SCI.[59,169] It can be predicted that the screening model presented here will allow for the identification of novel pro-regenerative materials, whilst significantly reducing reliance on live animal experimentation in keeping with the 3 R's principles of Reduction, Refinement and Replacement, thereby accelerating the rate of discovery of nanotherapeutic agents for neural tissue engineering, as summarised in **Figure 14**.

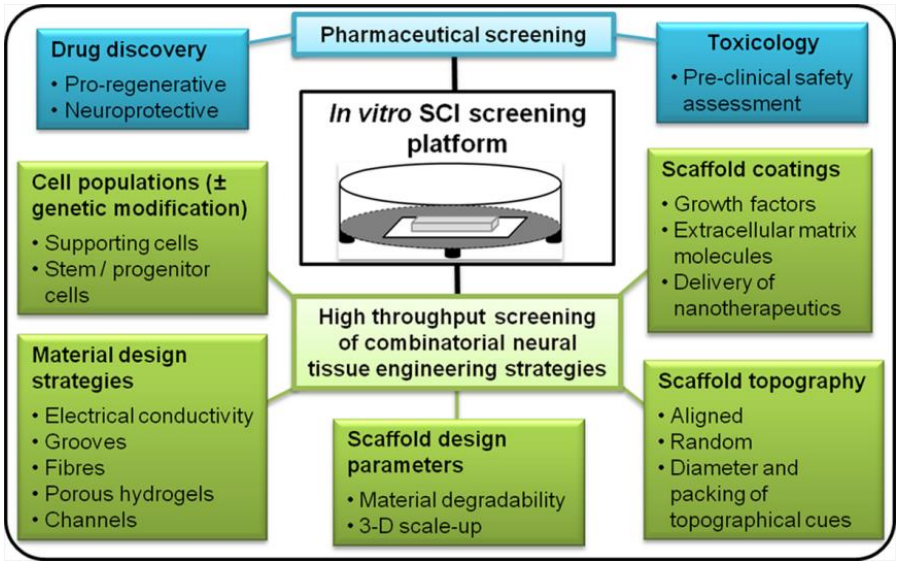

Figure 14. Schematic diagram illustrating the potential screening utility of a 'neural injury-nanomaterial' interface paradigm.

4.4.4. Conclusions

A method to coat and place portable sheets of aligned nanofibres into lesioned slices was developed. Functionalised nanofibres were able to induce dramatic responses in multiple cell types in the injury sites; these are comparable to those induced in live animal models. This study demonstrates the high potential of the

slice lesion model to function as a prototype screening system for promising nanotherapeutic interventions, either in isolation, or as part of a combinatorial treatment strategy. The use of higher-throughput *in vitro* models of SCI such as the one described here can aid in overcoming a growing bottleneck in the therapeutic testing of promising new materials and combinatorial therapies, whilst reducing the high current reliance on live animal testing.[c]

[c] Most of the data in this chapter has been published. The main article is included here as Appendix 3 and features in an article included as Appendix 4.

Chapter 5: Conclusions and general discussion

5.1. Summary of thesis findings

It has been shown in this thesis that the complexity of neural tissue engineering platforms may be increased, towards the production of both more advanced nanofibre-based strategies for spinal cord repair, and higher-throughput *in vitro* screening models to test the regeneration-promoting capacity of such strategies *ex vivo*. The findings obtained in this thesis can be summarised as follows:

- The assembly process of single layer nanofibre-hydrogel constructs was successfully optimised for the culture, attachment and elongation of astrocytes or OPCs.
- Astrocytes, OPCs and microglia derived from the same primary source were co-cultured together on hydrogel constructs containing a single layer of nanofibres.
- A bed layer of pre-aligned astrocytes was necessary for the survival and elongation of OPCs on nanofibre-hydrogel constructs. The aspect ratios of astrocytes and OPCs aligned to the nanofibres were considerably greater in magnitude than previous reports.
- The nanofibre-hydrogel constructs facilitated the proliferation and maturation of OPCs in co-culture with astrocytes.
- Increasing the spatial complexity of constructs was addressed by aligning astrocytes over three nanofibre mesh layers, towards the production of an implantable device containing a complete supporting system of neuroglia that can be used to reconstruct the complex glial circuitry in injury sites.
- The production and handling of organotypic spinal cord slice cultures were successfully optimised for the induction of reproducible, complete transecting lesions with a tool designed in-house.

- Slice lesions displayed three cardinal pathological features of SCI *in vivo*: post-traumatic astrogliosis, infiltration of lesions by activated microglia and limited random outgrowth of nerve fibres from the lesion margins of slices derived from older animals, demonstrating the tissue-mimetic capacity of the model in replicating neural injury.
- A method has been developed to coat portable sheets of aligned nanofibres with poly-D-lysine and laminin and place them into lesioned slices.
- Functionalisation of nanofibres was necessary in order for the attachment of astrocytes and neurons, although microglia attached to both treated and untreated nanofibres.
- A method to quantitatively assess the outgrowth of nerve fibres from lesion margins was developed and revealed significant differences between the coated and uncoated treatment groups.

A detailed discussion of the implications directly surrounding these findings may be found in each respective chapter. Discussed below are future directions for further development of the platforms, in the context of complexity, testing and promoting repair in neurological injury.

5.2. Future directions

Prior to further nanofibre-hydrogel construct development, an opportunity exists to assess the potential of the aligned glial cell co-cultures to enhance nerve fibre outgrowth by culturing isolated DRG explants on top. The distances of nerve fibre growth could be quantified compared to control constructs without glial cells. Furthermore, electrophysiological and electron microscopic studies could also

provide important information with regards to the integration of the neurons with the supporting glial cell circuitry e.g. intercellular signaling and the myelination of nerve fibres. However, to generate more clinically relevant readouts of repair, the constructs require processing into an implantable form for delivery into an injury environment. Strategically, the line density of the nanofibre meshes needs to be reduced to target the infiltration of spared host tissue and the seeding protocol of the glial cell co-cultures requires optimisation to scale-up over multiple nanofibre mesh layers. The assembled constructs then need to undergo a plastic compression step to reduce the construct volume and the viability of cells within the construct will require verification. Finally, a safe delivery method is required to surgically implant constructs with the correct dimensions in sites of injury.

The potential of strategies utilising aligned nanofibres to promote regeneration has been demonstrated both in the literature and here in the lesioned spinal cord slice culture model. However, the nanofibre frames delivered in lesioned slice experiments lack the spatial and cellular complexity of the nanofibre-hydrogel constructs developed. Therefore, the next proposed stage in construct testing is the delivery of more complex nanofibre-hydrogel constructs into the lesion sites of slices, to test the potential of the proposed strategy to enhance repair in a 3-D injury environment, using anatomical readouts from multiple cell types. Furthermore, the complex readout *in vitro* facilitates the identification of any potential problems and any necessary optimisation work required before the use of live animal neurological injury models.

The final stages of testing would involve a rat model of complete or partial transecting injury to evaluate constructs over a period of 4-6 months. This could be followed up with a comparative study in primates, as a more clinically relevant

model. In the first instance, fundamental questions need to be addressed with regards to the stability of the constructs in the lesions sites over this time period, such as the correct surgical placement of the scaffolds upon implantation and whether they remain in position or dislodge over time. Further physical properties to investigate include: characterising scaffold degradation and any undesirable accumulation of breakdown products at the injury site; whether the topography of the aligned nanofibres is maintained over time to facilitate neural regeneration of host tissue; and if there appears to be a mismatch in mechanical properties between the construct and the host tissue, which usually results in the formation of scar tissue at the interface.

With respect to anatomical repair, a detailed investigation is required into the effects on neuronal growth enhancement, myelin sheath formation, the interactions of host and implanted immune-competent cells with the scaffolds, the reactivity of surrounding scar-forming astrocytes and the formation of new microvascular networks to connect cell populations within the constructs with the host circulatory system. Readouts of functional regeneration may be obtained by assessing hindlimb motor function by means of BBB score analysis from e.g. a footprint assay or gridwalk test. This may be used in combination with electrophysiological investigation to evaluate transmission of electrical impulses across lesion sites, through both ascending and descending pathways.

The complexity of the constructs and therefore their regenerative properties could be enhanced further through functionalisation of the nanofibres and/or hydrogel. This could be accomplished using spatiotemporal gradients of biomolecules such as growth factors, ECM molecules and/or suppressors of inhibitory molecules, and genetic modification of the seeded cell populations. The use of human-derived glial cells could be used to characterise any differences in the

response to the constructs following *in vitro* culture and will be required before the constructs can be implanted into sites of human SCI in the clinic. Additionally, the approach described here has a range of further applications in both basic research and in clinical product translation. For example, this approach provides an *in vitro* paradigm of increased complexity to study glial interactions in normal culture and injury-simulated conditions, and may be used as a model for drug screening and evaluation of neurotoxicity in safety assessments of novel pharmaceutical agents.

In order to determine the extent that the lesioned spinal cord slices mimic SCI *in vivo*, a systematic study is required to compare and contrast all of the known pathophysiological responses following injury. This includes the use of sophisticated mass spectrometry analyses to generate genomic and proteomic profiles from the cells surrounding the injury sites of slices and examine cellular changes at the genetic and molecular level e.g. regeneration-associated genes and expression of CSPGs, respectively. Preliminary findings from the experiments performed suggest that a multi-electrode array would be a more practical and informative method of generating an electrophysiological readout of functional repair from the slices, than the use of individual stimulating and recording electrodes.

To seek ways of further increasing the clinical relevance of the model the generation of lesioned organotypic spinal cord slice cultures from human cadavers or non-human primates could be undertaken as a comparative study.[175] Furthermore, the induction of compressive trauma via weight-drop could produce a paradigm for screening strategies that mimics the most common type of injury found in the clinic. Finally, work has been published with the aim of producing customised surfaces that permit the long-term culture of organotypic slices of adult neural tissue.[220] This could be adapted and optimised to produce lesioned slice cultures of adult spinal

cord tissue and compared with the ‘older’ lesion model described here, which was found to mimic features of axonal regeneration following injury in adults.

The successful production of a lesioned organotypic spinal cord slice culture model with biologically-relevant readouts following delivery of structural bridges demonstrates the significant potential of organotypic slice cultures to serve as highly versatile bio-screening systems for the identification of pro-regenerative materials for a wide range of tissue applications. In the context of SCI, given the biologically-relevant predictions of the model in response to the introduction of nanofibres coated with widely-used cell adhesion and guidance molecules, a systematic study should be undertaken of all the materials and coatings that have been shown to promote repair following injury. This includes the screening of more complex combinatorial strategies utilising cells, materials and multiple biomolecules synergistically. The data obtained could be compared with results from comparative studies *in vivo* to further validate the predictive utility of the model. Additionally, it could provide feedback for the improved design of neural tissue engineering strategies for repair e.g. monitor the release profile of biomolecules from the scaffold (e.g. burst-release) during culture to determine the effectiveness of the delivery strategy and the efficacy of the concentrations used (although the injury paradigm here may be too simplistic as the material would lie at the interface between air and medium, limiting the mimicry of the *in vivo* environment). Finally, high resolution pictures of the slices (e.g. SEM) could provide a more comprehensive method of visualising anatomical interactions and regenerative events between cells and bridges introduced into the lesion sites of slices. It is hoped that this work will demonstrate the feasibility of increasing the complexity of neural tissue engineering platforms for the repair of neurological injury.

Appendix 1: Article published by Nanomedicine (NBM).

The article in this appendix contains data from Chapter 2.

Weightman AP, Jenkins SI, Pickard MR, Chari DM, Yang Y

Alignment of multiple glial cell populations in 3D nanofiber scaffolds: Toward the development of multicellular implantable scaffolds for repair of neural injury

Nanomedicine vol. 10, no. 2, 291-295, 2014

Appendix 2: Biomedical picture of the day

An image from the study in Chapter 2 (not included in this thesis) published online as *'biomedical picture of the day'* on the 4th April 2014 by the MRC (http://bpod.mrc.ac.uk/archive/2014/4/4).

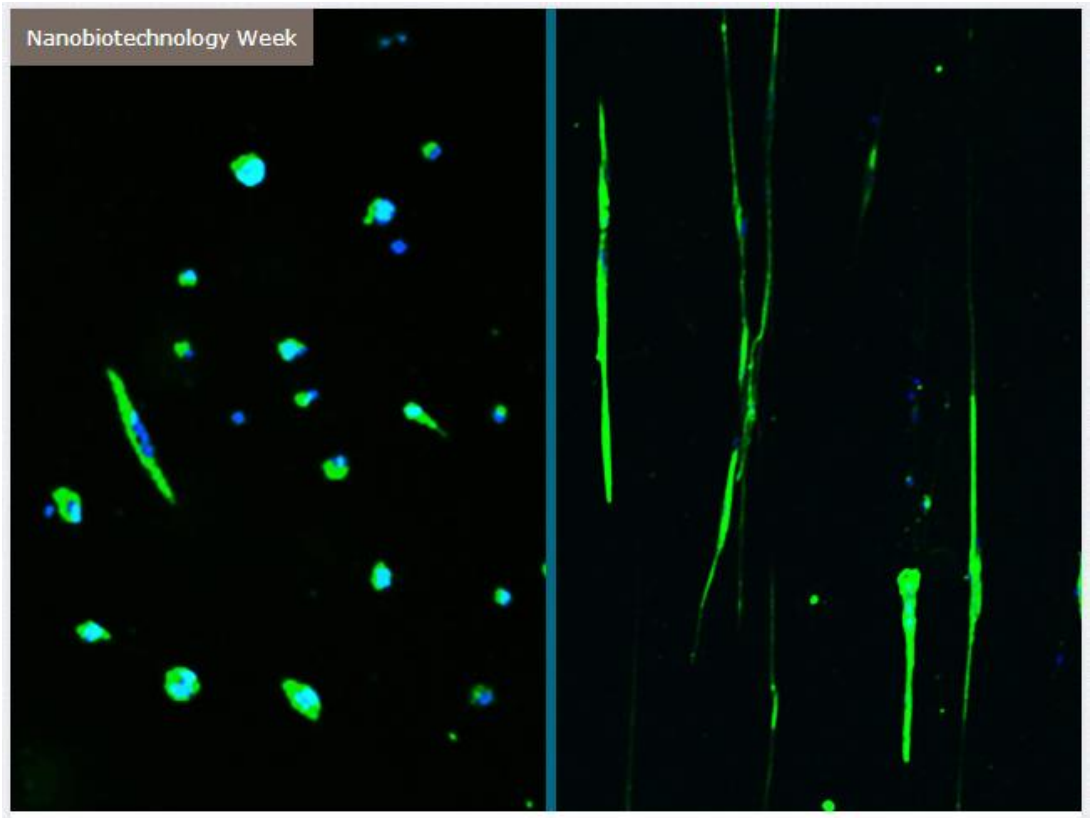

04 April 2014

Growing the Distance

Spinal injury can leave rips and tears in the delicate bundles of nerve cells (**neurons**) of the central nervous system. Often this trauma is so great that the **glial cells** that nurture our neurons' natural growth are unable to bridge the gaps. Pictured in green with their nuclei stained blue, these glial cells have been grown outside of the human body. The cells on the right were given manmade nanofibres as scaffolding and, like a garden vine climbing along a fence (only 10,000 times smaller), have stretched out as they might along the spine. Such growth guidance could be an important first step to healing complex spinal injuries. In the future, meshes of different types of glial cells designed and grown outside the patient, could be transplanted to encourage neurons to knit back into damaged areas.

Written by John Ankers

Appendix 3: Article published by Biomaterials.

The article in this appendix contains data from Chapter 3 and 4.

Weightman AP, Pickard MR, Yang Y, Chari DM

An *in vitro* spinal cord injury model to screen neuroregenerative materials

Biomaterials vol. 35, no. 12, 3756-3765, 2014

Appendix 4: Article feature published by Alternatives to Laboratory Animals.

The article in this appendix was published on the work from Chapter 3 and 4 and the article in Appendix 3.

Spinal cord injury model

Alternatives to Laboratory Animals vol. 42, 3-5, 2014

References

(1) Grundy, G.; Swain, A. *ABC of Spinal Cord Injury*; 1st ed.; BMJ Books: London, UK, **2002**; Vol. 41.

(2) Adams, M.; Cavanagh, J. F. R. International Campaign for Cures of Spinal Cord Injury Paralysis (ICCP): Another Step Forward for Spinal Cord Injury Research. *Spinal Cord* **2004**, *42*, 273–280.

(3) Dobkin, B. H.; Havton, L. A. Basic Advances and New Avenues in Therapy of Spinal Cord Injury. *Annu. Rev. Med.* **2004**, *55*, 255–282.

(4) Sofroniew, M. V; Vinters, H. V. Astrocytes: Biology and Pathology. *Acta Neuropathol.* **2010**, *119*, 7–35.

(5) Tremblay, M.-È.; Stevens, B.; Sierra, A.; Wake, H.; Bessis, A.; Nimmerjahn, A. The Role of Microglia in the Healthy Brain. *J. Neurosci.* **2011**, *31*, 16064–16069.

(6) Shibuya, S.; Yamamoto, T.; Itano, T. Glial and Axonal Regeneration Following Spinal Cord Injury. *Cell Adh. Migr.* **2009**, *3*, 99–106.

(7) Richardson, W. D.; Kessaris, N.; Pringle, N. Oligodendrocyte Wars. *Nat. Rev. Neurosci.* **2006**, *7*, 11–18.

(8) Mekhail, M.; Almazan, G.; Tabrizian, M. Oligodendrocyte-Protection and Remyelination Post-Spinal Cord Injuries: A Review. *Prog. Neurobiol.* **2012**, *96*, 322–339.

(9) Verkhratsky, A.; Butt, A. *Glial Neurobiology: A Textbook*; 1st ed.; John Wiley & Sons: Chichester, **2007**.

(10) Crossman, A. R.; Neary, D. *Neuroanatomy: An Illustrated Colour Text*; 4th ed.; Churchill Livingstone, **2010**.

(11) Robins, S. L.; Fehlings, M. G. Models of Experimental Spinal Cord Injury: Translational Relevance and Impact. *Drug Discov. Today Dis. Model.* **2008**, *5*, 5–11.

(12) Blesch, A.; Tuszynski, M. H. Spinal Cord Injury: Plasticity, Regeneration and the Challenge of Translational Drug Development. *Trends Neurosci.* **2009**, *32*, 41–47.

(13) Varma, A. K.; Das, A.; Wallace IV, G.; Barry, J.; Vertegel, A. A.; Ray, S. K.; Banik, N. L. Spinal Cord Injury: A Review of Current Therapy, Future Treatments, and Basic Science Frontiers. *Neurochem. Res.* **2013**, *38*, 895–905.

(14) Kwon, B. K.; Sekhon, L. H.; Fehlings, M. G. Emerging Repair, Regeneration, and Translational Research Advances for Spinal Cord Injury. *Spine (Phila. Pa. 1976).* **2010**, *35*, S263–70.

(15) Schnell, L.; Schwab, M. E. Axonal Regeneration in the Rat Spinal Cord Produced by an Antibody against Myelin-Associated Neurite Growth Inhibitors. *Nature* **1990**, *343*, 269–272.

(16) Mukhopadhyay, G.; Doherty, P.; Walsh, F. S.; Crocker, P. R.; Filbin, M. T. A Novel Role for Myelin-Associated Glycoprotein as an Inhibitor of Axonal Regeneration. *Neuron* **1994**, *13*, 757–767.

(17) Wang, K. C.; Koprivica, V.; Kim, J. A.; Sivasankaran, R.; Guo, Y.; Neve, R. L.; He, Z. Oligodendrocyte-Myelin Glycoprotein Is a Nogo Receptor Ligand That Inhibits Neurite Outgrowth. *Nature* **2002**, *417*, 941–944.

(18) Tator, C. H.; Fehlings, M. G. Review of the Secondary Injury Theory of Acute Spinal Cord Trauma with Emphasis on Vascular Mechanisms. *J. Neurosurg.* **1991**, *75*, 15–26.

(19) Kwon, B. K.; Tetzlaff, W. Spinal Cord Regeneration: From Gene to Transplants. *Spine (Phila. Pa. 1976).* **2001**, *26*, S13–22.

(20) Sobani, Z. A.; Quadri, S. A.; Enam, S. A. Stem Cells for Spinal Cord Regeneration: Current Status. *Surg. Neurol. Int.* **2010**, *1*, 93.

(21) Neumann, H.; Kotter, M. R.; Franklin, R. J. M. Debris Clearance by Microglia: An Essential Link between Degeneration and Regeneration. *Brain* **2009**, *132*, 288–295.

(22) Loane, D. J.; Byrnes, K. R. Role of Microglia in Neurotrauma. *Neurotherapeutics* **2010**, *7*, 366–377.

(23) Wehrle, R.; Camand, E.; Chedotal, A.; Sotelo, C.; Dusart, I. Expression of Netrin-1, Slit-1 and Slit-3 but not of Slit-2 after Cerebellar and Spinal Cord Lesions. *Eur. J. Neurosci.* **2005**, *22*, 2134–2144.

(24) Kitayama, M.; Ueno, M.; Itakura, T.; Yamashita, T. Activated Microglia Inhibit Axonal Growth through RGMa. *PLoS One* **2011**, *6*, e25234.

(25) Ridet, J. L.; Malhotra, S. K.; Privat, A.; Gage, F. H. Reactive Astrocytes: Cellular and Molecular Cues to Biological Function. *Trends Neurosci.* **1997**, *20*, 570–577.

(26) Yiu, G.; He, Z. Glial Inhibition of CNS Axon Regeneration. *Nat. Rev. Neurosci.* **2006**, *7*, 617–627.

(27) Faulkner, J. R.; Herrmann, J. E.; Woo, M. J.; Tansey, K. E.; Doan, N. B.; Sofroniew, M. V. Reactive Astrocytes Protect Tissue and Preserve Function after Spinal Cord Injury. *J. Neurosci.* **2004**, *24*, 2143–2155.

(28) Fawcett, J. W.; Asher, R. A. The Glial Scar and Central Nervous System Repair. *Brain Res. Bull.* **1999**, *49*, 377–391.

(29) Silver, J.; Miller, J. H. Regeneration beyond the Glial Scar. *Nat. Rev. Neurosci.* **2004**, *5*, 146–156.

(30) Hulsebosch, C. E. Recent Advances in Pathophysiology and Treatment of Spinal Cord Injury. *Adv. Physiol. Ed.* **2002**, *26*, 238–255.

(31) David, S.; Aguayo, A. J. Axonal Elongation into Peripheral Nervous System "bridges" after Central Nervous System Injury in Adult Rats. *Science.* **1981**, *214*, 931–933.

(32) Woolhead, C. L.; Zhang, Y.; Lieberman, A. R.; Schachner, M.; Emson, P. C.; Anderson, P. N. Differential Effects of Autologous Peripheral Nerve Grafts to the Corpus Striatum of Adult Rats on the Regeneration of Axons of Striatal and Nigral Neurons and on the Expression of GAP-43 and the Cell Adhesion Molecules N-CAM and L1. *J. Comp. Neurol.* **1998**, *391*, 259–273.

(33) Chen, D. F.; Jhaveri, S.; Schneider, G. E. Intrinsic Changes in Developing Retinal Neurons Result in Regenerative Failure of Their Axons. *Proc. Natl. Acad. Sci. U. S. A.* **1995**, *92*, 7287–7291.

(34) Fernandes, K. J.; Fan, D. P.; Tsui, B. J.; Cassar, S. L.; Tetzlaff, W. Influence of the Axotomy to Cell Body Distance in Rat Rubrospinal and Spinal Motoneurons: Differential Regulation of GAP-43, Tubulins, and Neurofilament-M. *J. Comp. Neurol.* **1999**, *414*, 495–510.

(35) Chen, M. S.; Huber, A. B.; van der Haar, M. E.; Frank, M.; Schnell, L.; Spillmann, A. A.; Christ, F.; Schwab, M. E. Nogo-A Is a Myelin-Associated Neurite Outgrowth Inhibitor and an Antigen for Monoclonal Antibody IN-1. *Nature* **2000**, *403*, 434–439.

(36) Tuinstra, H. M.; Aviles, M. O.; Shin, S.; Holland, S. J.; Zelivyanskaya, M. L.; Fast, A. G.; Ko, S. Y.; Margul, D. J.; Bartels, A. K.; Boehler, R. M.; et al. Multifunctional, Multichannel Bridges That Deliver Neurotrophin Encoding Lentivirus for Regeneration Following Spinal Cord Injury. *Biomaterials* **2012**, *33*, 1618–1626.

(37) Gruner, J. A. A Monitored Contusion Model of Spinal Cord Injury in the Rat. *J. Neurotrauma* **1992**, *9*, 123–6; discussion 126–8.

(38) Stokes, B. T. Experimental Spinal Cord Injury: A Dynamic and Verifiable Injury Device. *J. Neurotrauma* **1992**, *9*, 129–31; discussion 131–4.

(39) Tator, C. H. Acute Spinal Cord Injury in Primates Produced by an Inflatable Extradural Cuff. *Can. J. Surg.* **1973**, *16*, 222–231.

(40) Rivlin, A. S.; Tator, C. H. Effect of Duration of Acute Spinal Cord Compression in a New Acute Cord Injury Model in the Rat. *Surg. Neurol.* **1978**, *10*, 38–43.

(41) Kim, H. J.; Park, J. W.; Byun, J. H.; Vahidi, B.; Rhee, S. W.; Jeon, N. L. Integrated Microfluidics Platforms for Investigating Injury and Regeneration of CNS Axons. *Ann. Biomed. Eng.* **2012**, *40*, 1268–1276.

(42) Vahidi, B.; Park, J. W.; Kim, H. J.; Jeon, N. L. Microfluidic-Based Strip Assay for Testing the Effects of Various Surface-Bound Inhibitors in Spinal Cord Injury. *J. Neurosci. Methods* **2008**, *170*, 188–196.

(43) Crain, S. M.; Peterson, E. R. Bioelectric Activity in Long-Term Cultures of Spinal Cord Tissues. *Science* **1963**, *141*, 427–429.

(44) Bonnici, B.; Kapfhammer, J. P. Spontaneous Regeneration of Intrinsic Spinal Cord Axons in a Novel Spinal Cord Slice Culture Model. *Eur. J. Neurosci.* **2008**, *27*, 2483–2492.

(45) Langer, R.; Vacanti, J. P. Tissue Engineering. *Science.* **1993**, *260*, 920–926.

(46) Xie, J.; MacEwan, M. R.; Schwartz, A. G.; Xia, Y. Electrospun Nanofibers for Neural Tissue Engineering. *Nanoscale* **2010**, *2*, 35–44.

(47) Wong, D. Y.; Leveque, J.-C.; Brumblay, H.; Krebsbach, P. H.; Hollister, S. J.; Lamarca, F. Macro-Architectures in Spinal Cord Scaffold Implants Influence Regeneration. *J. Neurotrauma* **2008**, *25*, 1027–1037.

(48) Nisbet, D. R.; Forsythe, J. S.; Shen, W.; Finkelstein, D. I.; Horne, M. K. A Review of the Cellular Response on Electrospun Nanofibers for Tissue Engineering. *J. Biomater. Appl.* **2009**, *24*, 7–29.

(49) Okano, H. Neural Stem Cells and Strategies for the Regeneration of the Central Nervous System. *Proc. Japan Acad. Ser. B* **2010**, *86*, 438–450.

(50) Bradbury, E. J.; Moon, L. D. F.; Popat, R. J.; King, V. R.; Bennett, G. S.; Patel, P. N.; Fawcett, J. W.; McMahon, S. B. Chondroitinase ABC Promotes Functional Recovery after Spinal Cord Injury. *Nature* **2002**, *416*, 636–640.

(51) Wang, M.; Zhai, P.; Chen, X.; Schreyer, D. J.; Sun, X.; Cui, F. Bioengineered Scaffolds for Spinal Cord Repair. *Tissue Eng. Part B* **2011**, *17*, 177–194.

(52) Rooney, G. E.; Vaishya, S.; Ameenuddin, S.; Currier, B. L.; Schiefer, T. K.; Knight, A.; Chen, B.; Mishra, P. K.; Spinner, R. J.; Macura, S. I.; et al. Rigid Fixation of the Spinal Column Improves Scaffold Alignment and Prevents Scoliosis in the Transected Rat Spinal Cord. *Spine (Phila Pa 1976)* **2008**, *33*, E914–9.

(53) Reynolds, L. F.; Bren, M. C.; Wilson, B. C.; Gibson, G. D.; Shoichet, M. S.; Murphy, R. J. Transplantation of Porous Tubes Following Spinal Cord

Transection Improves Hindlimb Function in the Rat. *Spinal Cord* **2008**, *46*, 58–64.

(54) Kubinová, S.; Syková, E. Biomaterials Combined with Cell Therapy for Treatment of Spinal Cord Injury. *Regen. Med.* **2012**, *7*, 207–224.

(55) Madigan, N. N.; McMahon, S.; O'Brien, T.; Yaszemski, M. J.; Windebank, A. J. Current Tissue Engineering and Novel Therapeutic Approaches to Axonal Regeneration Following Spinal Cord Injury Using Polymer Scaffolds. *Respir. Physiol. Neurobiol.* **2009**, *169*, 183–199.

(56) Ramakrishna, S.; Fujihara, K.; Wee-Eong, T.; Teik-Cheng, L.; Zuwei, M. *An Introduction to Electrospinning and Nanofibers*; 1st ed.; World Scientific Publishing Co. Pte. Ltd, **2005**.

(57) Matthews, J. A.; Wnek, G. E.; Simpson, D. G.; Bowlin, G. L. Electrospinning of Collagen Nanofibers. *Biomacromolecules* **2002**, *3*, 232–238.

(58) Houweling, D. A.; Lankhorst, A. J.; Gispen, W. H.; Bär, P. R.; Joosten, E. A. Collagen Containing Neurotrophin-3 (NT-3) Attracts Regrowing Injured Corticospinal Axons in the Adult Rat Spinal Cord and Promotes Partial Functional Recovery. *Exp. Neurol.* **1998**, *153*, 49–59.

(59) Straley, K. S.; Foo, C. W. P.; Heilshorn, S. C. Biomaterial Design Strategies for the Treatment of Spinal Cord Injuries. *J. Neurotrauma* **2010**, *27*, 1–19.

(60) East, E.; de Oliveira, D. B.; Golding, J. P.; Phillips, J. B. Alignment of Astrocytes Increases Neuronal Growth in Three-Dimensional Collagen Gels and Is Maintained Following Plastic Compression to Form a Spinal Cord Repair Conduit. *Tissue Eng. Part A* **2010**, *16*, 3173–3184.

(61) Augst, A. D.; Kong, H. J.; Mooney, D. J. Alginate Hydrogels as Biomaterials. *Macromol. Biosci.* **2006**, *6*, 623–633.

(62) Moroni, L.; Seliktar, D.; Elisseeff, J. Biomimetics of the Extracellular Matrix: An Integrated Three- Dimensional Fiber-Hydrogel Composite for Cartilage Tissue Engineering. *Smart Struct. Syst.* **2012**, *7*, 213–222.

(63) Belkas, J. S.; Munro, C. A; Shoichet, M. S.; Johnston, M.; Midha, R. Long-Term in Vivo Biomechanical Properties and Biocompatibility of poly(2-Hydroxyethyl Methacrylate-Co-Methyl Methacrylate) Nerve Conduits. *Biomaterials* **2005**, *26*, 1741–1749.

(64) Dalton, P. D.; Flynn, L.; Shoichet, M. S. Manufacture of poly(2-Hydroxyethyl Methacrylate-Co-Methyl Methacrylate) Hydrogel Tubes for Use as Nerve Guidance Channels. *Biomaterials* **2002**, *23*, 3843–3851.

(65) Gunatillake, P. A.; Adhikari, R. Biodegradable Synthetic Polymers for Tissue Engineering. *Eur. Cell. Mater.* **2003**, *20*, 1–16; discussion 16.

(66) Prabhakaran, M. P.; Venugopal, J. R.; Chyan, T. T.; Hai, L. B.; Chan, C. K.; Lim, A. Y.; Ramakrishna, S. Electrospun Biocomposite Nanofibrous Scaffolds for Neural Tissue Engineering. *Tissue Eng. Part A* **2008**, *14*, 1787–1797.

(67) Ghasemi-Mobarakeh, L.; Prabhakaran, M. P.; Morshed, M.; Nasr-Esfahani, M.-H.; Ramakrishna, S. Electrospun Poly(epsilon-Caprolactone)/gelatin Nanofibrous Scaffolds for Nerve Tissue Engineering. *Biomaterials* **2008**, *29*, 4532–4539.

(68) Schnell, E.; Klinkhammer, K.; Balzer, S.; Brook, G.; Klee, D.; Dalton, P.; Mey, J. Guidance of Glial Cell Migration and Axonal Growth on Electrospun Nanofibers of Poly-Epsilon-Caprolactone and a Collagen/poly-Epsilon-Caprolactone Blend. *Biomaterials* **2007**, *28*, 3012–3025.

(69) Kim, T. G.; Park, T. G. Biomimicking Extracellular Matrix: Cell Adhesive RGD Peptide Modified Electrospun poly(D,L-Lactic-Co-Glycolic Acid) Nanofiber Mesh. *Tissue Eng.* **2006**, *12*, 221–233.

(70) Yucel, D.; Kose, G. T.; Hasirci, V. Tissue Engineered, Guided Nerve Tube Consisting of Aligned Neural Stem Cells and Astrocytes. *Biomacromolecules* **2010**, *11*, 3584–3591.

(71) Moore, M. J.; Friedman, J. A; Lewellyn, E. B.; Mantila, S. M.; Krych, A. J.; Ameenuddin, S.; Knight, A. M.; Lu, L.; Currier, B. L.; Spinner, R. J.; et al. Multiple-Channel Scaffolds to Promote Spinal Cord Axon Regeneration. *Biomaterials* **2006**, *27*, 419–429.

(72) Stokols, S.; Sakamoto, J.; Breckon, C.; Holt, T.; Weiss, J.; Tuszynski, M. H. Templated Agarose Scaffolds Support Linear Axonal Regeneration. *Tissue Eng.* **2006**, *12*, 2777–2787.

(73) Krych, A. J.; Rooney, G. E.; Chen, B.; Schermerhorn, T. C.; Ameenuddin, S.; Gross, L.; Moore, M. J.; Currier, B. L.; Spinner, R. J.; Friedman, J. A; et al. Relationship between Scaffold Channel Diameter and Number of Regenerating Axons in the Transected Rat Spinal Cord. *Acta Biomater.* **2009**, *5*, 2551–2559.

(74) Chen, Z.; Palmer, T. D. Cellular Repair of CNS Disorders: An Immunological Perspective. *Hum. Mol. Genet.* **2008**, *17*, R84–92.

(75) Fitch, M. T.; Silver, J. CNS Injury, Glial Scars, and Inflammation: Inhibitory Extracellular Matrices and Regeneration Failure. *Exp. Neurol.* **2008**, *209*, 294–301.

(76) Ho, A. D. Kinetics and Symmetry of Divisions of Hematopoietic Stem Cells. *Exp. Hematol.* **2005**, *33*, 1–8.

(77) Keirstead, H. S.; Nistor, G.; Bernal, G.; Totoiu, M.; Cloutier, F.; Sharp, K.; Steward, O. Human Embryonic Stem Cell-Derived Oligodendrocyte

Progenitor Cell Transplants Remyelinate and Restore Locomotion after Spinal Cord Injury. *J. Neurosci.* **2005**, *25*, 4694–4705.

(78) Lu, P.; Jones, L. L.; Snyder, E. Y.; Tuszynski, M. H. Neural Stem Cells Constitutively Secrete Neurotrophic Factors and Promote Extensive Host Axonal Growth after Spinal Cord Injury. *Exp. Neurol.* **2003**, *181*, 115–129.

(79) Zhang, L.; Zhang, H.-T.; Hong, S.-Q.; Ma, X.; Jiang, X.-D.; Xu, R.-X. Cografted Wharton's Jelly Cells-Derived Neurospheres and BDNF Promote Functional Recovery after Rat Spinal Cord Transection. *Neurochem. Res.* **2009**, *34*, 2030–2039.

(80) Li, Y. Repair of Adult Rat Corticospinal Tract by Transplants of Olfactory Ensheathing Cells. *Science.* **1997**, *277*, 2000–2002.

(81) Takami, T.; Oudega, M.; Bates, M. L.; Wood, P. M.; Kleitman, N.; Bunge, M. B. Schwann Cell but Not Olfactory Ensheathing Glia Transplants Improve Hindlimb Locomotor Performance in the Moderately Contused Adult Rat Thoracic Spinal Cord. *J. Neurosci.* **2002**, *22*, 6670–6681.

(82) Lu, P.; Jones, L. L.; Snyder, E. Y.; Tuszynski, M. H. Neural Stem Cells Constitutively Secrete Neurotrophic Factors and Promote Extensive Host Axonal Growth after Spinal Cord Injury. *Exp. Neurol.* **2003**, *181*, 115–129.

(83) Kocsis, J. D.; Lankford, K. L.; Sasaki, M.; Radtke, C. Unique in Vivo Properties of Olfactory Ensheathing Cells That May Contribute to Neural Repair and Protection Following Spinal Cord Injury. *Neurosci. Lett.* **2009**, *456*, 137–142.

(84) Eiselt, P.; Kim, B. S.; Chacko, B.; Isenberg, B.; Peters, M. C.; Greene, K. G.; Roland, W. D.; Loebsack, A. B.; Burg, K. J.; Culberson, C.; et al. Development of Technologies Aiding Large-Tissue Engineering. *Biotechnol. Prog.* ***1998***, *14*, 134–140.

(85) Schmidt, C. E.; Leach, J. B. Neural Tissue Engineering: Strategies for Repair and Regeneration. *Annu. Rev. Biomed. Eng.* **2003**, *5*, 293–347.

(86) Tang, X.; Davies, J. E.; Davies, S. J. A. Changes in Distribution, Cell Associations, and Protein Expression Levels of NG2, V2, and Tenascin-C During Acute to Chronic Maturation of Spinal Cord Scar Tissue. *Neurosci Res.* **2003**, *444*, 427–444.

(87) Yamagata, T.; Saito, H.; Habuchi, O.; Suzuki, S. Purification and Properties of Bacterial Chondroitinases and Chondrosulfatases. *J. Biol. Chem.* **1968**, 243, 1523-1535.

(88) Mueller, B. K.; Mack, H.; Teusch, N. Rho Kinase, a Promising Drug Target for Neurological Disorders. *Nat. Rev. Drug Discov.* **2005**, *4*, 387–398.

(89) Liebscher, T.; Schnell, L.; Schnell, D.; Scholl, J.; Schneider, R.; Gullo, M.; Fouad, K.; Mir, A.; Rausch, M.; Kindler, D.; et al. Nogo-A Antibody Improves Regeneration and Locomotion of Spinal Cord-Injured Rats. *Ann. Neurol.* **2005**, *58*, 706–719.

(90) Freund, P.; Wannier, T.; Schmidlin, E.; Bloch, J.; Mir, A.; Schwab, M. E.; Rouiller, E. M. Anti-Nogo-A Antibody Treatment Enhances Sprouting of Corticospinal Axons Rostral to a Unilateral Cervical Spinal Cord Lesion in Adult Macaque Monkey. *J. Comp. Neurol.* **2007**, *659*, 644–659.

(91) McKerracher, L.; Higuchi, H. Targeting Rho to Stimulate Repair after Spinal Cord Injury. *J. Neurotrauma.* **2006**. *23*, 309–317.

(92) Dubreuil, C. I.; Winton, M. J.; McKerracher, L. Rho Activation Patterns after Spinal Cord Injury and the Role of Activated Rho in Apoptosis in the Central Nervous System. *J. Cell Biol.* **2003**, *162*, 233–243.

(93) Dergham, P.; Ellezam, B.; Essagian, C.; Avedissian, H.; Lubell, W. D.; McKerracher, L. Rho Signaling Pathway Targeted to Promote Spinal Cord Repair. *J. Neurosci.* **2002**, *22*, 6570–6577.

(94) Silva, N. A; Salgado, A. J.; Sousa, R. A; Oliveira, J. T.; Pedro, A. J.; Leite-Almeida, H.; Cerqueira, R.; Almeida, A.; Mastronardi, F.; Mano, J. F.; et al. Development and Characterization of a Novel Hybrid Tissue Engineering-Based Scaffold for Spinal Cord Injury Repair. *Tissue Eng. Part A* **2010**, *16*, 45–54.

(95) Gros, T.; Sakamoto, J. S.; Blesch, A.; Havton, L. A; Tuszynski, M. H. Regeneration of Long-Tract Axons through Sites of Spinal Cord Injury Using Templated Agarose Scaffolds. *Biomaterials* **2010**, *31*, 6719–6729.

(96) Chen, B. K.; Knight, A. M.; Ruiter, G. C. W. De; Spinner, R. J.; Yaszemski, M. J.; Currier, B. L.; Windebank, A. J. Axon Regeneration through Scaffold into Distal Spinal Cord after Transection. J. Neurotrauma. **2009**, *1771*, 1759–1771.

(97) Prang, P.; Müller, R.; Eljaouhari, A.; Heckmann, K.; Kunz, W.; Weber, T.; Faber, C.; Vroemen, M.; Bogdahn, U.; Weidner, N. The Promotion of Oriented Axonal Regrowth in the Injured Spinal Cord by Alginate-Based Anisotropic Capillary Hydrogels. *Biomaterials* **2006**, *27*, 3560–3569.

(98) Fan, J.; Zhang, H.; He, J.; Xiao, Z.; Chen, B.; Xiaodan, J.; Dai, J.; Xu, R. Neural Regrowth Induced by PLGA Nerve Conduits and Neurotrophin-3 in Rats with Complete Spinal Cord Transection. *J. Biomed. Mater. Res. B. Appl. Biomater.* **2011**, *97*, 271–277.

(99) Chen, G.; Hu, Y.; Wan, H.; Xia, L.; Li, J.; Yang, F.; Qu, X.; Wang, S.; Wang, Z. Functional Recovery Following Traumatic Spinal Cord Injury Mediated by a Unique Polymer Scaffold Seeded with Neural Stem Cells and Schwann Cells. *Chin. Med. J. (Engl).* **2010**, *123*, 2424–2431.

(100) Wei, Y.-T.; He, Y.; Xu, C.-L.; Wang, Y.; Liu, B.-F.; Wang, X.-M.; Sun, X.-D.; Cui, F.-Z.; Xu, Q.-Y. Hyaluronic Acid Hydrogel Modified with Nogo-66 Receptor Antibody and Poly-L-Lysine to Promote Axon Regrowth after Spinal Cord Injury. *J. Biomed. Mater. Res. B. Appl. Biomater.* **2010**, *95*, 110–117.

(101) Li, S.; Liu, B. P.; Budel, S.; Li, M.; Ji, B.; Walus, L.; Li, W.; Jirik, A.; Rabacchi, S.; Choi, E.; et al. Blockade of Nogo-66, Myelin-Associated Glycoprotein, and Oligodendrocyte Myelin Glycoprotein by Soluble Nogo-66 Receptor Promotes Axonal Sprouting and Recovery after Spinal Injury. *J. Neurosci.* **2004**, *24*, 10511–10520.

(102) Han, Q.; Jin, W.; Xiao, Z.; Ni, H.; Wang, J.; Kong, J.; Wu, J.; Liang, W.; Chen, L.; Zhao, Y.; et al. The Promotion of Neural Regeneration in an Extreme Rat Spinal Cord Injury Model Using a Collagen Scaffold Containing a Collagen Binding Neuroprotective Protein and an EGFR Neutralizing Antibody. *Biomaterials* **2010**, *31*, 9212–9220.

(103) Koprivica, V.; Cho, K.-S.; Park, J. B.; Yiu, G.; Atwal, J.; Gore, B.; Kim, J. A.; Lin, E.; Tessier-Lavigne, M.; Chen, D. F.; et al. EGFR Activation Mediates Inhibition of Axon Regeneration by Myelin and Chondroitin Sulfate Proteoglycans. *Science* **2005**, *310*, 106–110.

(104) Yang, F.; Murugan, R.; Wang, S.; Ramakrishna, S. Electrospinning of Nano/Micro Scale Poly(L-Lactic Acid) Aligned Fibers and Their Potential in Neural Tissue Engineering. *Biomaterials* **2005**, *26*, 2603–2610.

(105) Stevens, M. M.; George, J. H. Exploring and engineering the cell surface interface. *Science* **2005**, 310, 1135-1138.

(106) Fu, X.; Matsuyama, H.; Teramoto, M.; Nagai, H. Preparation of Hydrophilic Poly(vinyl Butyral) Hollow Fiber Membrane via Thermally Induced Phase Separation. *Sep. Purif. Technol.* **2005**, *45*, 200–207.

(107) Ondarçuhu, T.; Joachim, C. Drawing a Single Nanofibre over Hundreds of Microns. *Europhys. Lett.* **1998,** *42*, 215–220.

(108) Ma, Z.; Kotaki, M.; Inai, R.; Ramakrishna, S. Potential of Nanofiber Matrix as Tissue-Engineering Scaffolds. *Tissue Eng.* **2005**, *11*, 101–109.

(109) Toh, Y.-C.; Ng, S.; Khong, Y. M.; Zhang, X.; Zhu, Y.; Lin, P.-C.; Te, C.-M.; Sun, W.; Yu, H. Cellular Responses to a Nanofibrous Environment. *Nano Today.* **2006**, *1*, 34–43.

(110) Jayaraman, K.; Kotaki, M.; Zhang, Y.; Mo, X.; Ramakrishna, S. Recent Advances in Polymer Nanofibers. *J. Nanosci. Nanotechnol.* **2004,** *4*, 52–65.

(111) Xie, J.; Macewan, M. R.; Li, X.; Sakiyama-Elbert, S. E.; Xia, Y. Neurite Outgrowth on Nanofiber Scaffolds with Different Orders. ACS Nano. **2009**, *3*, 1151–1159.

(112) Chew, S. Y.; Wen, J.; Yim, E. K. F.; Leong, K. W. Sustained Release of Proteins from Electrospun Biodegradable Fibers. *Biomacromolecules* **2005**, *6*, 2017–2024.

(113) Li, D.; Wang, Y.; Xia, Y. Electrospinning of Polymeric and Ceramic Nanofibers as Uniaxially Aligned Arrays. *Nano Lett.* **2003**, *3*, 1167–1171.

(114) Katta, P.; Alessandro, M.; Ramsier, R. D.; Chase, G. G. Continuous Electrospinning of Aligned Polymer Nanofibers onto a Wire Drum Collector. *Nano Lett.* **2004**, *4*, 2215–2218.

(115) Teo, W. E.; Ramakrishna, S. Electrospun Fibre Bundle Made of Aligned Nanofibres over Two Fixed Points. *Nanotechnology.* **2005**, *16*, 1878–1884.

(116) Bosworth, L. A; Turner, L. A.; Cartmell, S. H. State of the Art Composites Comprising Electrospun Fibres Coupled with Hydrogels: A Review. *Nanomedicine.* **2013**, *9*, 322–335.

(117) Wang, H. B.; Mullins, M. E.; Cregg, J. M.; Hurtado, A.; Oudega, M.; Trombley, M. T.; Gilbert, R. J. Creation of Highly Aligned Electrospun Poly-L-Lactic Acid Fibers for Nerve Regeneration Applications. *J. Neural Eng.* **2009**, *6*, 016001.

(118) Saracino, G. A. A.; Cigognini, D.; Silva, D.; Caprini, A.; Gelain, F. Nanomaterials Design and Tests for Neural Tissue Engineering. *Chem. Soc. Rev.* **2013**, *42*, 225–262.

(119) Chen, B. K.; Knight, A. M.; Madigan, N. N.; Gross, L.; Dadsetan, M.; Nesbitt, J. J.; Rooney, G. E.; Currier, B. L.; Yaszemski, M. J.; Spinner, R. J.; et al. Comparison of Polymer Scaffolds in Rat Spinal Cord: A Step toward Quantitative Assessment of Combinatorial Approaches to Spinal Cord Repair. *Biomaterials* **2011**, *32*, 8077–8086.

(120) Kubinová, S.; Syková, E. Nanotechnologies in Regenerative Medicine. *Minim. Invasive Ther. Allied Technol.* **2010**, *19*, 144–156.

(121) Pêgo, A. P.; Kubinova, S.; Cizkova, D.; Vanicky, I.; Mar, F. M.; Sousa, M. M.; Sykova, E. Regenerative Medicine for the Treatment of Spinal Cord Injury: More than Just Promises? *J. Cell. Mol. Med.* **2012**, *16*, 2564–2582.

(122) Subramanian, A.; Krishnan, U. M.; Sethuraman, S. Development of Biomaterial Scaffold for Nerve Tissue Engineering: Biomaterial Mediated Neural Regeneration. *J. Biomed. Sci.* **2009**, *16*, 108.

(123) Cao, H.; Liu, T.; Chew, S. Y. The Application of Nanofibrous Scaffolds in Neural Tissue Engineering. *Adv. Drug Deliv. Rev.* **2009**, *61*, 1055–1064.

(124) Ashammakhi, N.; Ndreu, A.; Nikkola, L.; Wimpenny, I.; Yang, Y. Advancing Tissue Engineering by Using Electrospun Nanofibers. *Regen. Med.* **2008**, *3*, 547–574.

(125) Hurtado, A.; Cregg, J. M.; Wang, H. B.; Wendell, D. F.; Oudega, M.; Gilbert, R. J.; McDonald, J. W. Robust CNS Regeneration after Complete Spinal Cord Transection Using Aligned Poly-L-Lactic Acid Microfibers. *Biomaterials* **2011**, *32*, 6068–6079.

(126) Liu, T.; Houle, J. D.; Ph, D.; Xu, J.; Eng, M.; Chan, B. P.; Chew, S. Y. Nanofibrous Collagen Nerve Conduits for Spinal Cord Repair. *Tissue Eng. Part A* **2012**, *18*.

(127) Gerardo-Nava, J.; Klinkhammer, K.; Seiler, N.; Klee, D.; Dalton, P. D.; Brook, G. A. Human Neural Cell Interactions with Orientated Electrospun Nanofibers in Vitro. *Nanomed*. **2009**, 4, 11–30.

(128) Corey, J. M.; Lin, D. Y.; Mycek, K. B.; Chen, Q.; Samuel, S.; Feldman, E. L.; Martin, D. C. Aligned Electrospun Nanofibers Specify the Direction of Dorsal Root Ganglia Neurite Growth. **2007**, 10–15.

(129) Gelain, F.; Panseri, S.; Antonini, S.; Cunha, C.; Donega, M.; Lowery, J.; Taraballi, F.; Cerri, G.; Montagna, M.; Baldissera, F.; et al. Transplantation of Nanostructured Composite Scaffolds Results in the Regeneration of Chronically Injured Spinal Cords. *ACS Nano* **2011**, *5*, 227–236.

(130) Zhu, Y.; Wang, A.; Shen, W.; Patel, S.; Zhang, R.; Young, W.; Li, S. Nanofibrous Patches for Spinal Cord Regeneration. *Adv. Funct. Mater.* **2010**, *20*, 1433–1440.

(131) Rochkind, S.; Shahar, A; Fliss, D.; El-Ani, D.; Astachov, L.; Hayon, T.; Alon, M.; Zamostiano, R.; Ayalon, O.; Biton, I. E.; et al. Development of a Tissue-Engineered Composite Implant for Treating Traumatic Paraplegia in Rats. *Eur. Spine J.* **2006**, *15*, 234–245.

(132) Přádný, M.; Lesný, P.; Martinová, L.; Michálek, J. S. E. Nonwoven Polymeric Nanofiber Scaffolds Utilizable for Spinal Cord Injury Repair. *Drugs Futur.* **2007**, *32*.

(133) Yang, Y.; Wimpenny, I.; Ahearne, M. Portable Nanofiber Meshes Dictate Cell Orientation throughout Three-Dimensional Hydrogels. *Nanomedicine.* **2011**, *7*, 131–136.

(134) Guimarães, A.; Martins, A.; Pinho, E. D.; Faria, S.; Reis, R.L.; Neves, N.M. Solving Cell Infiltration Limitations of Electrospun Nanofiber Meshes for Tissue Engineering Applications. *Nanomedicine (Lond).* **2010**, *5*, 539–554.

(135) Nisbet, D. R.; Forsythe, J. S.; Shen, W.; Finkelstein, D. I.; Horne, M. K. A Review of the Cellular Response on Electrospun Nanofibers for Tissue Engineering. *J. Biomater. Appl.* **2009**, *24*, 7–29.

(136) Tsai, H.-H.; Li, H.; Fuentealba, L. C.; Molofsky, A. V; Taveira-Marques, R.; Zhuang, H.; Tenney, A.; Murnen, A. T.; Fancy, S. P. J.; Merkle, F.; et al.

Regional Astrocyte Allocation Regulates CNS Synaptogenesis and Repair. *Science* **2012**, *337*, 358–362.

(137) Pfrieger, F. W. Roles of Glial Cells in Synapse Development. *Cell. Mol. Life Sci.* **2009**, *66*, 2037–2047.

(138) Biran, R.; Noble, M. D.; Tresco, P. A. Directed Nerve Outgrowth Is Enhanced by Engineered Glial Substrates. *Exp. Neurol.* **2003**, *184*, 141–152.

(139) Deumens, R.; Koopmans, G. C.; Den Bakker, C. G. J.; Maquet, V.; Blacher, S.; Honig, W. M.; Jérôme, R.; Pirard, J. P.; Steinbusch, H. W.; Joosten, E. A. Alignment of Glial Cells Stimulates Directional Neurite Growth of CNS Neurons in Vitro. *Neuroscience* **2004**, *125*, 591–604.

(140) Meng, F.; Hlady, V.; Tresco, P. A. Inducing Alignment in Astrocyte Tissue Constructs by Surface Ligands Patterned on Biomaterials. *Biomaterials* **2012**, *33*, 1323–1335.

(141) Ruff, C.A.; Fehlings, M. G. Neural Stem Cells in Regenerative Medicine: Bridging the Gap. *Panminerva Med.* **2010**, *52*, 125–147.

(142) Ginhoux, F.; Greter, M.; Leboeuf, M.; Nandi, S.; See, P.; Mehler, M. F.; Conway, S. J.; Ng, L. G.; Stanley, E. R.; Igor, M.; et al. Fate Mapping Analysis Reveals That Adult Microglia Derive from Primitive Macrophages. *Science* **2010**, *330*, 841–845.

(143) McMahon, R. E.; Qu, X.; Jimenez-Vergara, A. C.; Bashur, C. A.; Guelcher, S. A.; Goldstein, A. S.; Hahn, M. S. Hydrogel–Electrospun Mesh Composites for Coronary Artery Bypass Grafts. *Tissue Eng. Part C. Methods* **2011**, *17*, 451–461.

(144) Xu, W.; Ma, J.; Jabbari, E. Material Properties and Osteogenic Differentiation of Marrow Stromal Cells on Fiber-Reinforced Laminated Hydrogel Nanocomposites. *Acta Biomater.* **2010**, *6*, 1992–2002.

(145) Hsieh, A.; Zahir, T.; Lapitsky, Y.; Amsden, B.; Wan, W.; Shoichet, M. S. Hydrogel/Electrospun Fiber Composites Influence Neural Stem/Progenitor Cell Fate. *Soft Matter.* **2010**, *6*, 2227.

(146) McCarthy, K. D.; de Vellis, J. Preparation of separate astroglial and oligodendroglial cell cultures from rat cerebral tissue. *J. Cell Biol.* **1980**, *85*, 890-902.

(147) Lee, S.; Leach, M. K.; Redmond, S. A.; Chong, S. Y. C.; Mellon, H.; Tuck, S. J.; Feng, Z.; Corey, J. M.; Chan, J. R. A Culture System to Study Oligodendrocyte Myelination-Processes Using Engineered Nanofibers. *Nat. Methods.* **2012**, *9*, 917–922.

(148) Li, Y.; Ceylan, M.; Shrestha, B.; Wang, H.; Lu, Q. R.; Asmatulu, R.; Yao, L. Nanofibers Support Oligodendrocyte Precursor Cell Growth and Function as a

Neuron-Free Model for Myelination Study. *Biomacromolecules* **2013**, *15*, 319–326.

(149) Georges, P. C.; Miller, W. J.; Meaney, D. F.; Sawyer, E. S.; Janmey, P. A. Matrices with Compliance Comparable to that of Brain Tissue Select Neuronal over Glial Growth in Mixed Cortical Cultures. *Biophys. J.* **2006**, *90*, 3012–3018.

(150) Yu, L. M. Y.; Leipzig, N. D.; Shoichet, M. S. Promoting Neuron Adhesion and Growth. **2008**, *11*, 36–43.

(151) Jagielska, A.; Norman, A. L.; Whyte, G.; Vliet, K. J.; Guck, J.; Franklin, R. J. M. Mechanical Environment Modulates Biological Properties of Oligodendrocyte Progenitor Cells. *Stem Cells Dev.* **2012**, *21*, 2905–2914.

(152) Wang, D. D.; Bordey, A. The Astrocyte Odyssey. *Prog. Neurobiol.* **2008**, *86*, 342–367.

(153) Gard, A. L.; Burrell, M. R.; Pfeiffer, S. E.; Rudge, J. S.; Williams, W. C. Astroglial Control of Oligodendrocyte Survival Mediated by PDGF and Leukemia Inhibitory Factor-like Protein. *Development* **1995**, *121*, 2187–2197.

(154) Chernausek, S. D. Insulin-like Growth Factor-I (IGF-I) Production by Astroglial Cells: Regulation and Importance for Epidermal Growth Factor-Induced Cell Replication. *J. Neurosci. Res.* **1993**, *34*, 189–197.

(155) Sendtner, M.; Kreutzberg, G. W.; Thoenen, H. Ciliary Neurotrophic Factor Prevents the Degeneration of Motor Neurons after Axotomy. *Nature* **1990**, *345*, 440–441.

(156) Barres, B. A; Schmid, R.; Sendnter, M.; Raff, M. C. Multiple Extracellular Signals Are Required for Long-Term Oligodendrocyte Survival. *Development* **1993**, *118*, 283–295.

(157) Daud, M. F. B.; Pawar, K. C.; Claeyssens, F.; Ryan, A. J.; Haycock, J. W. An Aligned 3D Neuronal-Glial Co-Culture Model for Peripheral Nerve Studies. *Biomaterials* **2012**, *33*, 5901–5913.

(158) Brown, R. A.; Wiseman, M.; Chuo, C.-B.; Cheema, U.; Nazhat, S. N. Ultrarapid Engineering of Biomimetic Materials and Tissues: Fabrication of Nano- and Microstructures by Plastic Compression. *Adv. Funct. Mater.* **2005**, *15*, 1762–1770.

(159) Wang, L.; Hu, B.; Wong, W. M.; Lu, P.; Wu, W.; Xu, X.-M. Glial and Axonal Responses in Areas of Wallerian Degeneration of the Corticospinal and Dorsal Ascending Tracts after Spinal Cord Dorsal Funiculotomy. *Neuropathology* **2009**, *29*, 230–241.

(160) Zhou, F. Q.; Snider, W. D. Intracellular Control of Developmental and Regenerative Axon Growth. *Philos. Trans. R. Soc. Lond. B Bio. Sci.* **2006**, *361*, 1575–1592.

(161) Allen, A. R. Surgery of Experimental Lesion of Spinal Cord Equivalent to Crush Injury of Fracture Dislocation of Spinal Column. *J. Am. Med. Assoc.* **1911**, *57*, 878–880.

(162) Hwang, D. H.; Kim, H. M.; Kang, Y. M.; Joo, I. S.; Cho, C.-S.; Yoon, B.-W.; Kim, S. U.; Kim, B. G. Combination of Multifaceted Strategies to Maximize the Therapeutic Benefits of Neural Stem Cell Transplantation for Spinal Cord Repair. *Cell Transplant.* **2011**, *20*, 1361–1379.

(163) Svensson, L. G.; Crawford, E. S.; Hess, K. R.; Coselli, J. S.; Safi, H. J. Experience with 1509 Patients Undergoing Thoracoabdominal Aortic Operations. *J. Vasc. Surg.* **1993**, *17*, 357–68; discussion 368–70.

(164) Talac, R.; Friedman, J. A.; Moore, M. J.; Lu, L.; Jabbari, E.; Windebank, A. J.; Currier, B. L.; Yaszemski, M. J. Animal Models of Spinal Cord Injury for Evaluation of Tissue Engineering Treatment Strategies. *Biomaterials* **2004**, *25*, 1505–1510.

(165) Morrison, B.; Saatman, K. E.; Meaney, D. F.; McIntosh, T. K. In Vitro Central Nervous System Models of Mechanically Induced Trauma: A Review. *J. Neurotrauma* **1998**, *15*, 911–928.

(166) Krassioukov, A. V.; Ackery, A.; Schwartz, G.; Adamchik, Y.; Liu, Y.; Fehlings, M. G. An in Vitro Model of Neurotrauma in Organotypic Spinal Cord Cultures from Adult Mice. *Brain Res. Protoc.* **2002**, *10*, 60–68.

(167) Russell, W. M. S.; Burch, R. L. *The Principles of Humane Experimental Technique*; Methuen & Co. Ltd: London, 1959.

(168) East, E.; Golding, J. P.; Phillips, J. B. Engineering an Integrated Cellular Interface in Three-Dimensional Hydrogel Cultures Permits Monitoring of Reciprocal Astrocyte and Neuronal Responses. *Tissue Eng. Part C Meth.***2012**, *18*, 13–17.

(169) Boomkamp, S. D.; Riehle, M. O.; Wood, J.; Olson, M. F.; Barnett, S. C. The Development of a Rat in Vitro Model of Spinal Cord Injury Demonstrating the Additive Effects of Rho and ROCK Inhibitors on Neurite Outgrowth and Myelination. *Glia* **2012**, *60*, 441–456.

(170) Cho, S.; Wood, A.; Bowlby, M. R. Brain Slices as Models for Neurodegenerative Disease and Screening Platforms to Identify Novel Therapeutics. *Curr. Neuropharmacol.* **2007**, *5*, 19–33.

(171) Ardelt, A. A.; Flaris, N. A.; Roth, K. A. Neurotrophin-4 Selectively Promotes Survival of Striatal Neurons in Organotypic Slice Culture. *Brain Res.* **1994**, *647*, 340–344.

(172) Lohmann, C.; Ehrlich, I.; Friauf, E. Axon Regeneration in Organotypic Slice Cultures from the Mammalian Auditory System Is Topographic and Functional. *J. Neurobiol.* **1999**, *41*, 596–611.

(173) Lee, Y. B., Baratta, J., Yu, J., Lin, V. W., Robertson, R. T. aFGF Promotes Axonal Growth in Rat Spinal Cord Organotypic Slice Co-Cultures. *J. Neurotrauma* **2002**, *19*, 357–367.

(174) Coltman, B. W.; Earley, E. M.; Shahar, A.; Dudek, F. E.; Ide, C. F. Factors Influencing Mossy Fiber Collateral Sprouting in Organotypic Slice Cultures of Neonatal Mouse Hippocampus. *J .Comp. Neurol.* **1995**, *362*, 209–222.

(175) Jeong, D. K.; Taghavi, C. E.; Song, K. J.; Lee, K. B.; Kang, H. W. Organotypic Human Spinal Cord Slice Culture as an Alternative to Direct Transplantation of Human Bone Marrow Precursor Cells for Treating Spinal Cord Injury. *World neurosurg.* **2011**, *75*, 533–539.

(176) Kosuge, Y.; Sekikawa-Nishida, K.; Negi, H.; Ishige, K.; Ito, Y. Characterization of Chronic Glutamate-Mediated Motor Neuron Toxicity in Organotypic Spinal Cord Culture Prepared from ALS Model Mice. *Neurosci. Lett.* **2009**, *454*, 165–169.

(177) Duff, K.; Noble, W.; Gaynor, K.; Matsuoka, Y. Organotypic Slice Cultures from Transgenic Mice as Disease Model Systems. *J. Mol. Neurosci.* **2002**, *19*, 317–320.

(178) Dong, H. W.; Buonomano, D. V. A Technique for Repeated Recordings in Cortical Organotypic Slices. *J. Neurosci. Methods* **2005**, *146*, 69–75.

(179) Marsh, D. R.; Dekaban, G. A.; Tan, W.; Strathdee, C. A.; Weaver, L. C. Herpes Simplex Viral and Amplicon Vector-Mediated Gene Transfer into Glia and Neurons in Organotypic Spinal Cord and Dorsal Root Ganglion Cultures. *Mol .Ther.* **2000**, *1*, 464–478.

(180) Seidl, A. H.; Rubel, E. W. A Simple Method for Multi-Day Imaging of Slice Cultures. *Microsc. Res. Tech.* **2010**, *73*, 37–44.

(181) Hailer, N. P.; Vogt, C.; Korf, H.-W.; Dehghani, F. Interleukin-1beta Exacerbates and Interleukin-1 Receptor Antagonist Attenuates Neuronal Injury and Microglial Activation after Excitotoxic Damage in Organotypic Hippocampal Slice Cultures. *Eur. J. Neurosci.* **2005**, *21*, 2347–2360.

(182) Cho, J. S.; Park, H. W.; Park, S. K.; Roh, S.; Kang, S. K.; Paik, K. S.; Chang, M. S. Transplantation of Mesenchymal Stem Cells Enhances Axonal Outgrowth and Cell Survival in an Organotypic Spinal Cord Slice Culture. *Neurosci. Lett.* **2009**, *454*, 43–48.

(183) Balentine, J. D.; Greene, W. B.; Bornstein, M. In Vitro Spinal Cord Trauma. *Lab Invest.* **1988**, *58*, 93–99.

(184) Stoppini, L.; Buchs, P. A.; Muller, D. A Simple Method for Organotypic Cultures of Nervous Tissue. *J. Neurosci. Methods* **1991**, *37*, 173–182.

(185) Gähwiler, B. H.; Capogna, M.; Debanne, D.; McKinney, R. A.; Thompson, S. M. Organotypic Slice Cultures: A Technique Has Come of Age. *Trends Neurosci.* **1997**, *20*, 471–477.

(186) Cooper, J. A. Background Subtraction to Obtain Total Fluorescence per Cell, using ImageJ and Excel http://www.cooperlab.wustl.edu/LabMethodsReagentsOperations/Background Subtract Total Fluor per Cell/Instructions.pdf (accessed Feb 4, 2013).

(187) Jenkins, S. I.; Koller, C. J.; Furness, D. N.; Chari, D. M. Magnetic Nanoparticle Labeling of Astrocytes Derived for Neural Transplantation. *Tissue Eng Part C Methods*. **2011**, *17*, 89-99.

(188) Sofroniew, M. V. Molecular Dissection of Reactive Astrogliosis and Glial Scar Formation. *Trends Neurosci.* **2009**, *32*, 638–647.

(189) Jin, X.; Ishii, H.; Bai, Z.; Itokazu, T.; Yamashita, T. Temporal Changes in Cell Marker Expression and Cellular Infiltration in a Controlled Cortical Impact Model in Adult Male C57BL/6 Mice. *PLoS One* **2012**, *7*, e41892.

(190) Beck, K. D.; Nguyen, H. X.; Galvan, M. D.; Salazar, D. L.; Woodruff, T. M.; Anderson, A. J. Quantitative Analysis of Cellular Inflammation after Traumatic Spinal Cord Injury: Evidence for a Multiphasic Inflammatory Response in the Acute to Chronic Environment. *Brain* **2010**, *133*, 433–447.

(191) Foran, D. R.; Peterson, A. C. Myelin Acquisition in the Central Nervous System of the Mouse Revealed by an MBP-Lac Z Transgene. *J. Neurosci.* **1992**, *12*, 4890–4897.

(192) Zhang, H.; Jarjour, A. A; Boyd, A.; Williams, A. Central Nervous System Remyelination in Culture--a Tool for Multiple Sclerosis Research. *Exp. Neurol.* **2011**, *230*, 138–148.

(193) Fabbro, A.; Villari, A.; Laishram, J.; Scaini, D.; Toma, F. M.; Turco, A.; Prato, M.; Ballerini, L. Spinal Cord Explants Use Carbon Nanotube Interfaces to Enhance Neurite Outgrowth and to Fortify Synaptic Inputs. *ACS Nano* **2012**, *6*, 2041–2055.

(194) Fehlings, M. G.; Nashmi, R. A New Model of Acute Compressive Spinal Cord Injury in Vitro. *J. Neurosci. Methods* **1997**, *71*, 215–224.

(195) Viktorov, I. V.; Sharonova, I. N. Formation of Functional Synaptic Connections between Heterogeneous Brain Formations in Organotypic Nerve Tissue Culture. *Neurophysiology* **1980**, *12*, 311–317.

(196) Heidemann, M.; Streit, J.; Tscherter, A. Functional Regeneration of Intraspinal Connections in a New in Vitro Model. *Neuroscience* **2014**, *262*, 40–52.

(197) Czarnecki, A.; Magloire, V.; Streit, J. Local Oscillations of Spiking Activity in Organotypic Spinal Cord Slice Cultures. *Eur. J. Neurosci.* **2008**, *27*, 2076–2088.

(198) Kadoya, K.; Tsukada, S.; Lu, P.; Coppola, G.; Geschwind, D.; Filbin, M. T.; Blesch, A.; Tuszynski, M. H. Combined Intrinsic and Extrinsic Neuronal Mechanisms Facilitate Bridging Axonal Regeneration One Year after Spinal Cord Injury. *Neuron* **2009**, *64*, 165–172.

(199) Ruff, C. A.; Wilcox, J. T.; Fehlings, M. G. Cell-Based Transplantation Strategies to Promote Plasticity Following Spinal Cord Injury. *Exp. Neurol.* **2012**, *235*, 78–90.

(200) Lu, P.; Yang, H.; Jones, L. L.; Filbin, M. T.; Tuszynski, M. H. Combinatorial Therapy with Neurotrophins and cAMP Promotes Axonal Regeneration beyond Sites of Spinal Cord Injury. *J. Neurosci.* **2004**, *24*, 6402–6409.

(201) Bradbury, E. J.; McMahon, S. B. Spinal Cord Repair Strategies: Why Do They Work? *Nat. Rev. Neurosci.* **2006**, *7*, 644–653.

(202) Nomura, H.; Tator, C. H.; Shoichet, M. S. Bioengineered Strategies for Spinal Cord Repair. *J. Neurotrauma* **2006**, *23*, 496–507.

(203) Ishihara, M.; Mochizuki-Oda, N.; Iwatsuki, K.; Kishima, H.; Iwamoto, Y.; Ohnishi, Y.; Umegaki, M.; Yoshimine, T. A New Three-Dimensional Axonal Outgrowth Assay for Central Nervous System Regeneration. *J. Neurosci. Methods* **2011**, *198*, 181–186.

(204) Jurga, M.; Dainiak, M. B.; Sarnowska, A.; Jablonska, A.; Tripathi, A.; Plieva, F. M.; Savina, I. N.; Strojek, L.; Jungvid, H.; Kumar, A.; et al. The Performance of Laminin-Containing Cryogel Scaffolds in Neural Tissue Regeneration. *Biomaterials* **2011**, *32*, 3423–3434.

(205) Garbayo, E.; Raval, A. P.; Curtis, K. M.; Della-Morte, D.; Gomez, L. A; D'Ippolito, G.; Reiner, T.; Perez-Stable, C.; Howard, G. A; Perez-Pinzon, M. A.; et al. Neuroprotective Properties of Marrow-Isolated Adult Multilineage-Inducible Cells in Rat Hippocampus Following Global Cerebral Ischemia Are Enhanced When Complexed to Biomimetic Microcarriers. *J. Neurochem.* **2011**, *119*, 972–988.

(206) Daviaud, N.; Garbayo, E.; Schiller, P. C.; Perez-Pinzon, M.; Montero-Menei, C. N. Organotypic Cultures as Tools for Optimizing Central Nervous System Cell Therapies. *Exp. Neurol.* **2013**, *248*, 429–440.

(207) Lee, K. L.; Chen, L. H. A New Method for Coarse Classification of Textures and Class Weight Estimation for Texture Retrieval. *Pattern Recognit. image Anal.* **2002**, *12*, 400–410.

(208) Patist, C. M.; Mulder, M. B.; Gautier, S. E.; Maquet, V.; Jérôme, R.; Oudega, M. Freeze-Dried Poly(d,l-Lactic Acid) Macroporous Guidance Scaffolds Impregnated with Brain-Derived Neurotrophic Factor in the Transected Adult Rat Thoracic Spinal Cord. *Biomaterials* **2004**, *25*, 1569–1582.

(209) Oudega, M.; Gautier, S. E.; Chapon, P.; Fragoso, M.; Bates, M. L.; Parel, J. M.; Bunge, M. B. Axonal Regeneration into Schwann Cell Grafts within Resorbable Poly(alpha-Hydroxyacid) Guidance Channels in the Adult Rat Spinal Cord. *Biomaterials* **2001**, *22*, 1125–1136.

(210) Maquet, V.; Martin, D.; Scholtes, F.; Franzen, R.; Schoenen, J.; Moonen, G.; Jérome, R. Poly(D,L-Lactide) Foams Modified by Poly(ethylene Oxide)-Block-poly(D,L-Lactide) Copolymers and a-FGF: In Vitro and in Vivo Evaluation for Spinal Cord Regeneration. *Biomaterials* **2001**, *22*, 1137–1146.

(211) Hurtado, A.; Moon, L. D. F.; Maquet, V.; Blits, B.; Jérôme, R.; Oudega, M. Poly (D,L-Lactic Acid) Macroporous Guidance Scaffolds Seeded with Schwann Cells Genetically Modified to Secrete a Bi-Functional Neurotrophin Implanted in the Completely Transected Adult Rat Thoracic Spinal Cord. *Biomaterials* **2006**, *27*, 430–442.

(212) Liesi, P. Do Neurons in the Vertebrate CNS Migrate on Laminin? *EMBO J.* **1985**, *4*, 1163–1170.

(213) Menezes, K.; de Menezes, J. R.; Nascimento, M. A.; Santos Rde. S.; Coelho-Sampaio, T. Polylaminin, a Polymeric Form of Laminin, Promotes Regeneration after Spinal Cord Injury. *FASEB J.* **2010**, *24*, 4513–4522.

(214) Tsai, E. C.; Dalton, P. D.; Shoichet, M. S.; Tator, C. H. Matrix Inclusion within Synthetic Hydrogel Guidance Channels Improves Specific Supraspinal and Local Axonal Regeneration after Complete Spinal Cord Transection. *Biomaterials* **2006**, *27*, 519–533.

(215) Cheng, H.; Huang, Y.-C.; Chang, P.-T.; Huang, Y.-Y. Laminin-Incorporated Nerve Conduits Made by Plasma Treatment for Repairing Spinal Cord Injury. *Biochem. Biophys. Res. Commun.* **2007**, *357*, 938–944.

(216) Rogers, S. L.; Letourneau, P. C.; Palm, S. L.; McCarthy, J.; Furcht, L. T. Neurite Extension by Peripheral and Central Nervous System Neurons in Response to Substratum-Bound Fibronectin and Laminin. *Dev. Biol.* **1983**, *98*, 212–220.

(217) Ekaputra, A. K.; Prestwich, G. D.; Cool, S. M.; Hutmacher, D. W. Combining Electrospun Scaffolds with Electrosprayed Hydrogels Leads to Three-Dimensional Cellularization of Hybrid Constructs. *Biomacromolecules* **2008**, *9*, 2097–2103.

(218) Li, W.-J.; Laurencin, C. T.; Caterson, E. J.; Tuan, R. S.; Ko, F. K. Electrospun Nanofibrous Structure: A Novel Scaffold for Tissue Engineering. *J. Biomed. Mater. Res.* **2002**, *60*, 613–621.

(219) Monopoli, M. P.; Walczyk, D.; Campbell, A.; Elia, G.; Lynch, I.; Bombelli, F. B.; Dawson, K. A. Physical-Chemical Aspects of Protein Corona: Relevance to in Vitro and in Vivo Biological Impacts of Nanoparticles. *J. Am. Chem. Soc.* **2011**, *133*, 2525–2534.

(220) Dallacasagrande, V.; Zink, M.; Huth, S.; Jakob, A.; Müller, M.; Reichenbach, A.; Käs, J. A; Mayr, S. G. Tailoring Substrates for Long-Term Organotypic Culture of Adult Neuronal Tissue. *Adv. Mater.* **2012**, *24*, 2399–2403.